UNITED STATES DEPARTMENT OF TRANSPORTATION

GLOBAL POSITIONING SYSTEM (GPS)

ADJACENT BAND COMPATIBILITY ASSESSMENT

FINAL REPORT

DECEMBER 2017

EXECUTIVE SUMMARY

The goal of the U.S. Department of Transportation (DOT) Global Positioning System (GPS) Adjacent Band Compatibility Assessment is to evaluate the maximum transmitted power levels of adjacent band radiofrequency (RF) systems that can be tolerated by GPS and Global Navigation Satellite System (GNSS) receivers. The results of this effort advance the Department's understanding of the extent to which such adjacent band transmitters impact GPS/GNSS devices used for transportation safety purposes, among numerous other civil applications. The assessment described in this report addresses transmitters in bands adjacent to the 1559-1610 MHz radionavigation satellite service (RNSS) band used for GPS Link 1 (L1) signals that are centered at 1575.42 MHz.

The assessment includes two primary components:

- One component, led by the DOT Office of the Assistant Secretary for Research and Technology (OST-R), focused on all civilian GPS devices and their applications, apart from certified aviation. Through this component of the Study, categories of receivers were evaluated that included aviation (non-certified), cellular, general location/navigation, high precision, timing, and space-based receivers. An element of this effort was to determine equipment susceptibility to adjacent band interference to support analyses for deriving compatible power levels.

- The other component, led by the Federal Aviation Administration (FAA), focused on certified GPS avionics, and was conducted by analysis to determine the adjacent band power levels that conform to existing certified GPS aviation equipment standards.

The DOT GPS Adjacent Band Study is the product of an extensive process to gather stakeholder views and input. OST-R and FAA benefited significantly from feedback received via governmental and public outreach on equipment use cases, interaction scenarios, propagation models, and transmitter characteristics.

Certified GPS avionics meet their performance requirements when operating within the RF interference (RFI) environment defined in appropriate FAA Technical Standard Orders (TSOs). For civil GPS/GNSS receivers other than certified avionics, receiver testing needed to be conducted to determine the Interference Tolerance Masks (ITMs) for various categories of receivers. ITM defines, for a particular receiver, the maximum received aggregate interference power that can be tolerated by the corresponding tested GPS/GNSS receiver.

To accomplish this testing, OST-R sought to include a broad range of devices used in rail, aviation, motor vehicle, maritime, and space applications, among a number of other civil uses of GPS/GNSS including timing, surveying, precision agriculture, weather forecasting, earthquake monitoring, and emergency response. The GPS/GNSS receivers for this test effort were provided by U.S. Government and industry partners and represented the diverse nature of GPS/GNSS applications and services.

GPS/GNSS receiver testing, led by the OST-R/Volpe Center, was conducted at the U.S. Army Research Laboratory (ARL) at the White Sands Missile Range (WSMR) facility in New Mexico in April of 2016 with 80 civil GPS and GNSS receivers tested, as shown in Figure ES-1. The Air Force GPS Directorate conducted testing of military GPS receivers the week prior to the civil receivers being tested.

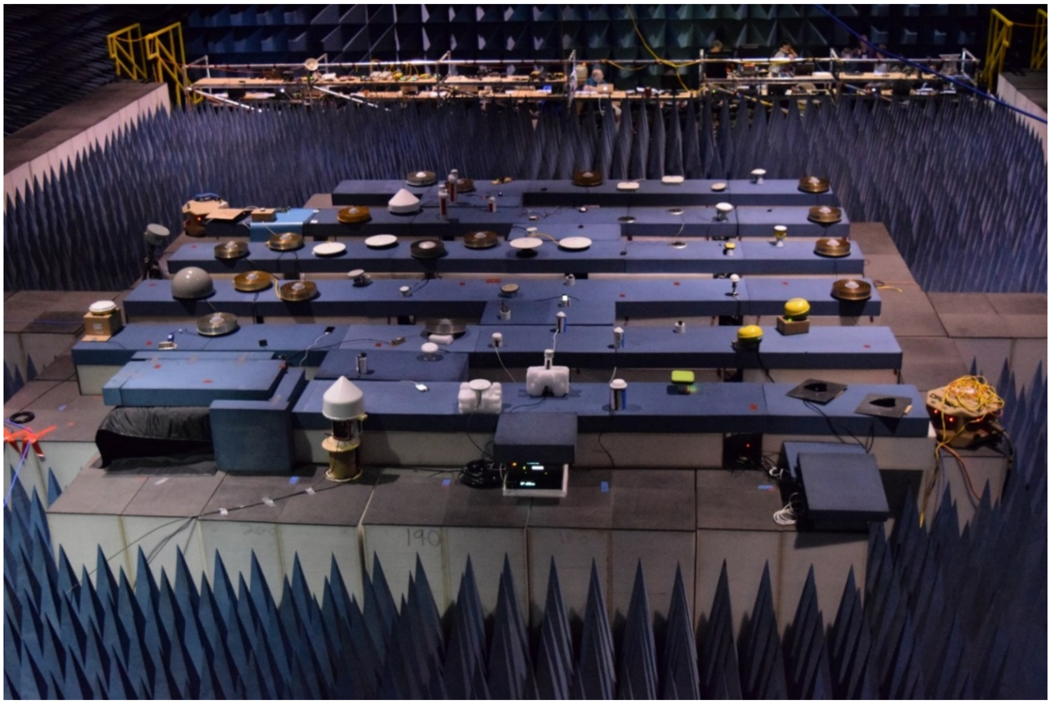

Figure ES-1: GPS/GNSS Receivers in WSMR Anechoic Chamber

In determining the transmit power level analysis, it is important to understand real-world scenarios and the proximity those applications of GPS/GNSS may come to adjacent band transmitters. A graphic of various emergency response uses is shown in Figure ES-2. First responders are increasingly using GPS/GNSS to locate patients both during emergencies and as a normal course of duty. As shown in the figure, there are multiple uses of GPS/GNSS for navigation of emergency service response vehicles, as well as asset tracking, including increased situational awareness of where response personnel and vehicles are located. An unmanned aircraft system (UAS) or drone, which also has a GPS/GNSS receiver incorporated also plays a role in this scenario, supporting the response effort. Drones are becoming of increasing importance in collecting imagery and sensor data in response to natural disasters and other incidents.

This scenario illustrates that use of a GPS/GNSS receiver can be quite close in distance -- within tens of meters of a base station transmitter and potentially very close to a handset as well transmitting in the adjacent band. The GPS/GNSS receiver also could be located vertically above the base station.

Figure ES-2: Emergency Response Use Case

Results for the high precision receiver category for an emitter at 1530 MHz based on results of analysis and testing are presented in Figure ES-3. These results are for a typical cellular base station power level of 29 dBW (794 watts) with the base station antenna 25 m above the ground. In this figure, the horizontal axis is the lateral distance between the GPS/GNSS receiver and the base station. The vertical axis is the height of the GPS/GNSS receiver above the ground. Note the high precision category of receiver exceeds a 1 dB signal-to-noise density (C/N_0) interference protection criteria at a distance beyond 14 km from the transmitter. When this occurs, the behavior of the GPS/GNSS receiver can become unpredictable in its ability to meet the accuracy, availability, and integrity requirements of its intended application and a receiver in a mobile application may not be able to reacquire GPS positioning as the mobile application encounters multiple, closely-spaced emitters in an urban scenario. Furthermore, this category of receiver experiences loss of lock for low elevation GPS/GNSS satellites at distances up to 3 km with loss of lock on all satellites at approximately 1 km from the transmitter.

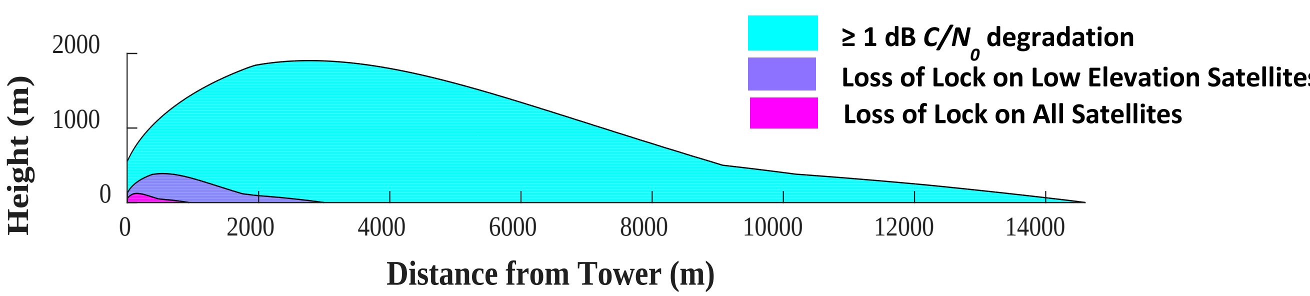

Figure ES-3: Impact of a 29 dBW Cellular Base Station Transmitting at 1530 MHz on a High Precision GPS/GNSS Receiver

Further analysis was performed to determine the maximum tolerable power levels for various categories of civil GPS/GNSS receivers for deployments of a macro urban and micro urban cellular network at frequencies within 100 MHz of GPS L1 (1475 – 1675 MHz). As an example, the results for 1530 MHz are shown in Table ES-1 for general location and navigation (GLN), high precision (HPR), Timing (TIM), and cellular (CEL) receivers. The transmit power level as quantified by the effective isotropic radiated power (EIRP) that can be tolerated is a function of distance from the transmitter. Two distances were chosen for evaluation (10 m and 100 m). The results demonstrate that other than the cellular devices, the other categories of GPS/GNSS receivers are sensitive to adjacent band power and can tolerate levels in the milliwatts or microwatts range as described below, depending on the separation distance to the transmitter.

Table ES-1: Maximum Tolerable Power Level for GPS/GNSS Receivers at 1530 MHz

Deployment	Stand off distance (m)	Max Tolerable EIRP (dBW)			
		GLN	HPR	TIM	CEL
Macro Urban	10	-31.0	-41.9	-20.6	10.9
	100	-11.0	-21.9	-0.6	31
Micro Urban	10	-29.8	-41.2	-20.1	10.7
	100	-9.8	-21.1	-0.1	30.8

Deployment	Stand off distance (m)	Max Tolerable EIRP			
		GLN	HPR	TIM	CEL
Macro Urban	10	0.8 mW	64 μW	8.7 mW	12.3 W
	100	79.4 mW	6.5 mW	0.9 W	1.26 kW
Micro Urban	10	1 mW	76 μW	9.8 mW	11.7 W
	100	104 mW	7.8 mW	1 W	1.2 kW

Table ES-2 depicts the maximum tolerable power levels of space-based receivers used for performing scientific measurements. A future NASA mission, COSMIC-2, fitted with a TriG receiver built by NASA/Jet Propulsion Laboratory, was modeled, simulated, and analyzed using various cellular network deployment scenarios. The COSMIC-2 mission will be operating at an orbit of 800 km.

Table ES-2: Maximum Tolerable Power Level for Space-Based Receivers at 1530 MHz

Deployment Scenario	Number of Base Stations	Max Tolerable Power	
		dBW	EIRP
Macro Cell	184,500	11	12.6 W
Macro Cell	67,240	16	39.8 W
Macro Cell	44,850	17	50.1 W
Macro Cell	24,140	21	125.9 W
Macro + Micro Cell	282,186	8	6.3 W
Macro + Micro Cell	102,841	12	15.8 W
Macro + Micro Cell	69,477	14	25.1 W
Macro + Micro Cell	39,695	16	39.8 W

For certified GPS avionics, the FAA analyzed a number of scenarios including:

1) Inflight Aircraft with a Ground-based Handset
2) Inflight Aircraft with a Ground Base Station
3) Inflight Aircraft with an Onboard Handset
4) Aircraft on the ground with an Onboard Handset
5) Aircraft at Gate / Single Handset Source on or near Boarding Stairs or Jetway
6) Aircraft at Gate/Users Inside Airport
7) Terrain Awareness Warning System (TAWS) / Helicopter TAWS (HTAWS) Scenarios with Ground-based Mobile Broadband Handsets
8) TAWS and HTAWS Scenarios with Broadband Base Station

The analysis for certified avionics is based on the concept of an "assessment zone" (see Figure ES-4) inside of which GPS performance may be compromised or unavailable and GPS-based safety systems will be impacted accordingly due to the elevated levels of RFI. Under the described engineering and operational assumptions, helicopter operations are the limiting factor in the analysis. These analyses indicate that protection of certified avionics, operating under the assumption of the described 250 foot (76.2 m) radius assessment zone, requires that the ground station transmission not exceed 9.8 dBW (10W) (cross-polarized) at 1531 MHz. This limit is obtained from the HTAWS scenario which was found to be the most restrictive of the certified aviation scenarios examined.

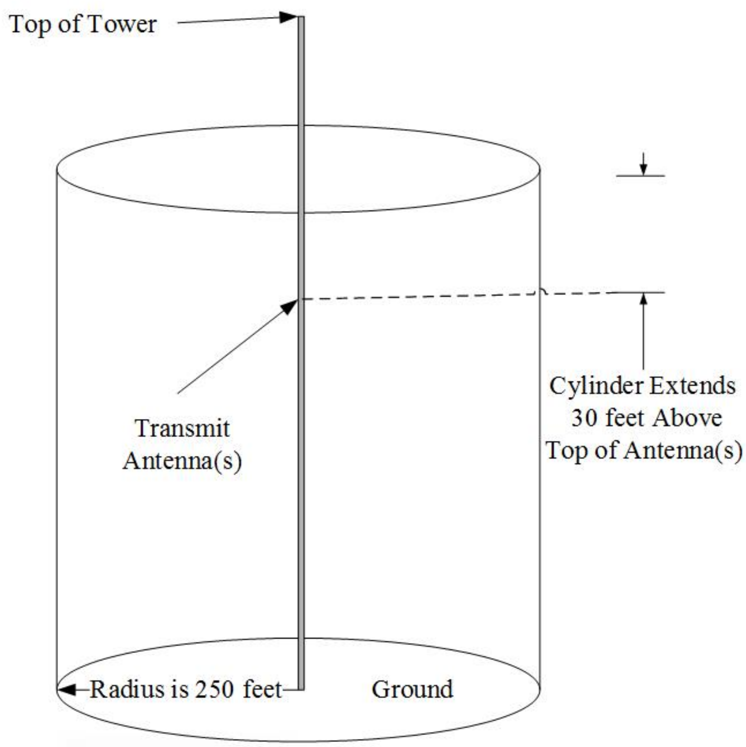

Figure ES-4: Candidate Assessment Zone (Not to Scale)

This concept generated a number of comments and questions from the aviation community when vetted through RTCA, Inc. One rotorcraft operator stated that its pilots use visual reference within the assessment zone and the assessment zone would have no negative impact on their operation. However, there were unresolved concerns expressed by several, though not all, operators about the assessment zone and its impacts to aviation operations and safety.

These concerns include: technical and human factors issues associated with re-initialization of GPS after loss of the signal or when the signal reception is intermittent; workload and human factors impacts on pilots to monitor and track assessment zone locations; the possibility that pilot workload, confusion, or error could lead to aircraft inadvertently entering an assessment zone and losing needed GPS functionality; and impacts to onboard and ground systems that are dependent upon GPS, such as Automatic Dependent Surveillance (ADS) Broadcast/Contract (B/C), or fixed-wing and helicopter terrain awareness warning system including obstacle alerting.

The FAA has not completed an exhaustive evaluation of the operational scenarios in developing this assessment zone. Further, the current analyses do not include an operational assessment of the impact of the assessment zone in densely populated areas, which may present additional variables, including the risk posed to people and property for operations such as UAS using certified avionics which may be required to operate within the assessment zone.

However, based on the results of the OST-R testing and analysis of the other categories of receivers, the transmitter power level that can be tolerated by certified aviation may cause interference with, or degradation to, most other categories of GPS/GNSS receivers including those used for General Aviation and drones, as detailed in the results set forth in this report.

The U.S. Department of Transportation would like to thank all of the Federal departments and agencies for their participation in this effort, including the National Telecommunications and Information Administration (NTIA) and Federal Communications Commission (FCC), as well the GPS/GNSS receiver manufacturers who participated in the testing, and all of the stakeholders who attended the public workshops and RTCA meetings and provided valuable feedback during this effort.

TABLE OF CONTENTS

LIST OF FIGURES

LIST OF TABLES

1. INTRODUCTION

The goal of the U.S. Department of Transportation (DOT) Global Positioning System (GPS) Adjacent Band Compatibility Assessment is to evaluate the maximum transmitted power levels of adjacent band radiofrequency (RF) systems that can be tolerated by GPS and Global Navigation Satellite System (GNSS) receivers. The results of this effort advance the Department's understanding of the extent to which such adjacent band transmitters impact GPS/GNSS devices used for transportation safety purposes, among numerous other civil applications. The assessment described in this report addresses transmitters in bands adjacent to the 1559-1610 MHz radionavigation satellite service (RNSS) band used for GPS Link 1 (L1) signals that are centered at 1575.42 MHz.

The assessment had two primary components:

- One component, led by the DOT Office of the Assistant Secretary for Research and Technology (OST-R), focused on all civilian GPS devices and their applications, apart from certified aviation. Through this component of the Study, categories of receivers were evaluated that included aviation (non-certified), cellular, general location/navigation, high precision, timing, and space-based receivers. An element of this effort was to determine equipment susceptibility to adjacent band interference to support analyses for deriving compatible power levels.

- The other component, led by the Federal Aviation Administration (FAA), focused on certified GPS avionics, and was conducted by analysis to determine the adjacent band power levels that conform to existing certified GPS aviation equipment standards.

The DOT GPS Adjacent Band Study is the product of an extensive process to gather stakeholder views and input. OST-R and FAA benefited significantly from feedback received via governmental and public outreach. This feedback was important to ensure broad agreement and understanding of equipment use cases, interaction scenarios, propagation models, and transmitter characteristics.

For the OST-R component of the effort, the first public workshop was held in September 2014 at DOT's Volpe Center in Cambridge, MA. Five subsequent workshops were held at locations on both coasts of the United States (Los Angeles, CA and Washington, DC) to obtain broad stakeholder participation. These workshops presented the elements of the OST-R assessment: equipment susceptibility testing, development of use cases and interaction scenarios, transmitter characteristics, and propagation modeling assumptions, and finally, the analysis and assessment results. Initial planning of the DOT GPS Adjacent Band Compatibility Assessment focused on testing receivers that only process GPS signals. However, based upon feedback from public outreach, the assessment was expanded to include widely available equipment that also processes GNSS signals from other satellite navigation constellations in the 1559-1610 MHz band.

While the compatibility assessment is intended to be generally applicable in terms of the type of adjacent band system, the main focus for this L1 band assessment was on Long Term Evolution (LTE) signals. The OST-R effort included extensive equipment testing to derive interference tolerance masks (ITMs). The ITM defines, for a given frequency, the maximum power allowed to ensure the tested GPS/GNSS receiver did not experience more than a 1 dB reduction in carrier-to-noise density ratio (CNR) for various categories of GPS/GNSS receivers. The receiver ITMs were derived from radiofrequency equipment testing, both radiated and conducted, for frequencies ranging from 1475 MHz to 1675 MHz (GPS L1 +/- 100 MHz). These ITMs were then used with appropriate use cases and interaction scenarios to determine maximum transmitter EIRP levels that could be tolerated from adjacent band transmitters.

The equipment susceptibility testing involved 80 GPS/GNSS receivers tested in an anechoic chamber in April 2016. The GPS/GNSS receivers for this test effort were provided by U.S. Government (USG) partners and industry and represented the diverse nature of GPS/GNSS applications and services. In addition to this primary test effort, more focused testing on a subset of equipment was conducted with wired testing in a laboratory setting and antenna characterizations in a different anechoic chamber. The receiver test data from the primary test effort was analyzed to develop ITMs, based on a 1 dB CNR degradation, which provided bounding performance for each GPS/GNSS receiver category.

These bounding ITMs and GPS/GNSS antenna characteristics were the primary inputs to use case scenario assessments to determine the maximum Effective Isotropic Radiated Power (EIRP) that could be tolerated in the adjacent radiofrequency bands for each GPS/GNSS receiver category. Space-based applications are different from other GPS/GNSS applications considered, primarily due to the need to account for aggregation effects of multiple transmitters visible in orbit. Although OST-R derived ITMs for space-based receivers, along with other GPS/GNSS receiver types, OST-R deferred to the National Aeronautics and Space Administration (NASA) for assessing adjacent-band transmitter power levels that can be tolerated for this receiver category.

The FAA’s public outreach for their component of the GPS Adjacent Band Compatibility Assessment was initiated in early 2014 with RTCA Inc., an aviation advisory body. This outreach was followed in October 2014 with a document detailing the FAA’s approach to the assessment for certified aviation and the request to RTCA to vet assumptions and respond to specific questions. These questions ranged from receiver/antenna characteristics and their applicability to fixed- and rotary-winged aircraft to specific propagation modes to be used and interaction scenarios.

RTCA also was requested to comment on use of an exclusion zone concept and its implications for operations and flight safety. RTCA completed the review and provided comments to FAA in 2015. The FAA was approached starting in 2016 by one entrant with an analysis approach for certified aviation that included a specific transmitter network and exclusion zone. This proposal was reviewed by RTCA and was considered with the material originally vetted by them in FAA’s assessment of maximum tolerable EIRP for certified aviation.

The FAA effort did not require receiver and antenna equipment testing because certified aviation receiver standards specify the maximum tolerable interference environment to ensure all receiver functions are protected. The FAA effort also considered use cases based upon one specific, proposed adjacent-band LTE network.

This report is organized as follows. Section 2 provides background information to the study. Section 3 discusses the radiated and wired tests performed and provides results for all civil receiver categories with the exception of the certified aviation receiver category. Section 4 presents the analysis to determine the tolerable transmit power levels, including use cases for applications other than certified aviation. Analysis of aggregate effects for on-orbit space applications is provided by the National Aeronautics and Space Administration (NASA). Section 5 discusses the analysis approach and presents the results for the certified aviation receiver category. Section 6 provides an overall summary of the report. Additional information on test results and analyses are included in the appendices.

2. BACKGROUND

Over the past three decades, GPS has grown into a global utility providing multi-use service integral to U.S. national security, economic growth, transportation safety, and homeland security, and as an essential element of the worldwide economic infrastructure. GPS affects the lives of the American public every day, ranging from its use in all modes of transportation to incorporation of GPS timing into the electric grid, communications networks, point of sale transactions, banking and finance, as well as applications of GPS for surveying, precision agriculture, weather forecasting, earthquake monitoring, and emergency response. The range of commercial and civil applications of GPS continues to expand and the importance of many GPS and GNSS applications has significantly increased.

Private sector innovations in the use of GPS greatly exceed any originally envisioned or imagined applications. However, unlike communication systems where performance improvements are enabled by coordinated changes to both the transmitting and receiving systems, GPS has shown that user processing innovations can significantly improve performance without changing the transmitted GPS signals. These innovations have enabled the civil community to develop and implement new GPS antenna/receiver technologies and applications, with minimal dependency on government actions. As the economic and security importance of positioning, navigation, and timing (PNT) gained international recognition, other countries have initiated or renewed their commitments to provide satellite navigation systems, fueling further development of new user-based GPS/GNSS technologies.

The framework for GPS policy is defined by Presidential Policy. Title 10 United States Code, Section 2281 (b) states that the GPS Standard Positioning Service shall be provided for peaceful civil, commercial and scientific uses on a continuous worldwide basis. The 2010 National Space Policy sustains the overall radiofrequency environment in which critical U.S. space systems such as GPS operate and calls for continued U.S. leadership in the service, provision, and use of GNSS.

This policy reaffirms existing U.S. commitments under National Security Presidential Directive (NSPD)-39, U.S. Space-Based Positioning, Navigation, and Timing Policy (15 December 2004) to provide continuous, worldwide access to civil GPS, free of direct user fees; pursue international GNSS cooperation including use of foreign PNT to augment and strengthen the resiliency of GPS; operate and maintain GPS to meet published standards; and take steps to detect and mitigate GPS interference. Per NSPD-39, DOT serves as the civil lead for GPS.

At the direction of the DOT Deputy Secretary, FAA and OST-R developed the GPS Adjacent Band Compatibility Assessment Plan to provide a means to advance the Department's understanding of the adjacent radiofrequency band power levels that would be compatible for GPS civil applications. The plan identifies the processes to: (a) derive adjacent-band transmitter power limit criteria for assumed new applications necessary to ensure continued operation of GPS services, and (b) determine similar levels for future GPS receivers utilizing modernized GPS and interoperable GNSS signals [1]. This document provided the framework for the processes and assumptions that resulted in the testing and analysis conducted during the effort and presented in this report.

3. CIVIL RECEIVER TESTING

3.1 Anechoic/Radiated Testing

In planning and preparation for receiver testing, OST-R held multiple public workshops to discuss plans for the Study and to foster the exchange of information among interested parties. These workshops took place on September 18, 2014 (see 79 Fed. Reg. 47171), December 4, 2014 (see 79 Fed. Reg. 68345), March 12, 2015 (see 80 Fed. Reg. 8125), and October 2, 2015 (see 80 Fed. Reg. 57915). Representatives from NTIA, FCC, and NIST, and other Space-Based PNT EXCOM departments and agencies participated in the public workshops.

A draft test plan was issued for public comment on September 9, 2015 (see 80 Fed. Reg. 54368). There were six organizations and individuals who provided written comments on the draft of the test plan: Ligado, GPS Innovation Alliance, Greenwood Telecom, Alliance for Telecommunications Industry Solutions (ATIS), General Motors, and Logan Scott. The Department carefully reviewed and considered the comments that were submitted in devising a final test plan, as well as other information that was offered in the course of the public workshops. In addition, DOT made public its Nondisclosure Agreement (NDA) for the protection of certain confidential or proprietary information that may be offered by companies that participated in the Study (see 81 Fed. Reg. 12564). DOT executed five NDAs with Deere & Company, GM Global Technology Operations LLC, Novatel Inc., Trimble Navigation Limited, and u-Blox AG.

After the Test Plan was finalized and published (see 81 Fed. Reg. 12564), GPS/GNSS receiver testing, led by the OST-R/Volpe Center, was conducted at the U.S. Army Research Laboratory (ARL) at the White Sands Missile Range (WSMR) facility in New Mexico in April of 2016. Results from the testing described in this section were presented at public workshops held on October 14, 2016 (see 81 Fed. Reg. 68105) and on March 30, 2017 (see 82 Fed. Reg. 13924). Information from all of the public workshops that were held can be found at a website hosted by the National Space-Based PNT Coordination Office (NCO) at http://www.gps.gov/spectrum/ABC/.

3.1.1 Devices Under Test (DUTs)

DOT sought to include a broad range of devices used in rail, aviation, motor vehicle, maritime, and space applications, among a number of other civil uses of GPS/GNSS including timing, surveying, precision agriculture, weather forecasting, earthquake monitoring, and emergency response. The GPS/GNSS receivers for this test effort were provided by USG partners and industry.

Six categories of GPS/GNSS receivers were considered for the OST-R portion of the effort, which are identified in Table 3-1. High precision (HPR) and the differential Network (NET) receivers are grouped together into one category since HPR receivers are commonly used in differential networks. General aviation receivers include non-certified receivers and are separate from certified aviation receivers which did not require testing since existing certified aviation receiver standards specify the maximum tolerable interference environment to ensure all receiver functions are protected. Space-based receivers were included with assistance from NASA.

Table 3-1: GPS/GNSS Receiver Categories

Number	Category	Abbreviation
1	General Aviation (Non-Certified)	GAV
2	General Location/Navigation	GLN
3	High Precision/Networks	HPR/NET
4	Timing	TIM
5	Cellular	CEL
6	Space Based	SPB

3.1.1.1 GPS/GNSS Receivers Tested

During the WSMR anechoic radiated chamber testing in April 2016, DOT and other participants tested 80 GPS/GNSS receivers listed along with the associated antennas in Table 3-2. Duplicated entries in Table 3-2 indicate that two identical receiver/antenna model pairings were tested, which occurred in three instances. In addition, 14 (out of the 80) were subsequently subjected to additional conducted/wired testing at Zeta Associates as indicated by an asterisk next to the receiver name in Table 3-2. The Air Force GPS Directorate conducted testing of military GPS receivers the week prior to the civil receivers being tested.

Table 3-2: List of GPS/GNSS Receivers Tested at WSMR

Receiver	Antenna
Android S5*	Integrated
Android S6	Integrated
Android S7	Integrated
Arbiter Systems 1088B-Satellite Control Clock	Arbiter AS0087800
Arbiter Systems 1094B-GPS Substation Clock	Arbiter AS0087800
Ashtech uZ-CGRS	Choke Ring
Ashtech Z-12	Choke Ring
Dual Electronics - SkyPro XGPS 150	Integrated
Dynon 2020	Integrated
Dynon 250	Integrated
EVA-7M EVK-7EVA-0	AeroAntenna Technology Inc AT2775-41-TNCF

EVA-M8M EVK-M8EVA-0	AeroAntenna Technology Inc AT2775-41-TNCF
EVK-6n	Passive patch
EVK-7P	Passive patch
EVK-M8N*	Passive patch
EVK-M8T	Passive patch
Furuno GP-33	GPA017/19
Garmin - Area 560	AeroAntenna Technology Inc AT2775-41-TNCF
Garmin - GLOGPS (GPS & GLONASS)	Integrated
Garmin - GPSMap 696*	AeroAntenna Technology Inc AT2775-41-TNCF
Garmin EDGE 1000	Integrated
Garmin ETREX 20x	Integrated
Garmin GPSMap 295	AeroAntenna Technology Inc AT2775-41-TNCF
Garmin GPSMAP 64	Integrated
Garmin GPSMAP 741	Garmin GA 38 GPS/GLONASS antenna
Hemisphere R330	Hemisphere A42
Javad Delta II*	JAVAD JAVRINGANT_DM
Javad Delta-3	Choke Ring
Javad EGGDT-160	Choke Ring
JAVAD Triumph-1	Integrated
LEA-M8F EVK-M8F-0	AeroAntenna Technology Inc AT2775-41-TNCF
LEA-M8S EVK-M8N-0	AeroAntenna Technology Inc AT2775-41-TNCF
Leica GR10	TRM59800.00
Leica GRX1200GGPRO	Leica AX1202GG
Leica GRX1200GGPRO*	LEIAT504
MAX-7C EVK-7C-0	AeroAntenna Technology Inc AT2775-41-TNCF
MAX-7Q EVK-7N-0	AeroAntenna Technology Inc AT2775-41-TNCF
MAX-M8Q	Passive patch
MAX-M8Q EVK-M8N-0	AeroAntenna Technology Inc AT2775-41-TNCF
NAVCOM SF3050*	NAVCOM ANT-3001R
NovAtel 628 Card w/ Flex pack	703GG
Novatel OEM628V-G1S-B0G-TTN-H installed in Development board	Patch
Schweitzer Eng. Labs SEL-2401-Satellite Synchronized Clock	SEL 235-0209
Septentrio PolaRx4Pro*	AERO AERAT1675_120
Septentrio PolaRx4TR Pro	Choke Ring

Septentrio PolaRx5TR Pro*	TRM59800.00
Septentrio PolaRx5TR Pro*	TRM59800.00
SF3000	Integrated
SF3000	Integrated
SiRF III	AeroAntenna Technology Inc AT2775-41-TNCF
Supercruise "VCP"	Shark Fin
Supercruise "VCP"	Shark Fin
Symmetricom SyncServer S350	AeroAntenna AT575-142
Symmetricom Xli	Symmetricom Antenna 1
Symmetricom Xli	AeroAntenna AT575-142
Symmetricom-GPS	Symmetricom Antenna 2
Topcon Net-G3A Sigma	Topcon CR-G3
TriG	Choke Ring
TriG V2	Choke Ring
Trimble 5700*	Trimble TRM41249.00
Trimble Acutime 360	Integrated
Trimble Ag-382	Integrated
Trimble Ag-382	Integrated
Trimble Bison III	Trimble 70229-52
Trimble Geo 7X	Integrated
Trimble NETR5	Trimble TRM55971.00
Trimble NETR5	Trimble Zephyr Geodetic Model 2
Trimble NETR5*	Trimble Zephyr 59800-00
Trimble NETR9	TRM59800.00
Trimble NETR9*	Trimble TRM29659.00
Trimble NETRS	Ant com Active L1/L2
Trimble NETRS	Trimble Zephyr Geodetic
Trimble NetRS	TRM59800.00
Trimble NETRS*	Ashtech ASH701945B_M
Trimble R8	Integrated
Trimble SMT360 GPS receiver*	Trimble SMT-360 Antenna
Trimble SPS461	GA530 Ruggedized
Trimble SPS855	Trimble Zephyr 2
Trimble SPS985	Integrated
uBlox EVU-6P-0-001	AeroAntenna Technology Inc AT2775-41-TNCF

*Subsequently subjected to additional conducted/wired testing at Zeta Associates

3.1.1.2 Antennas Tested

In addition to the antennas listed in Table 3-11, that were subjected to radiated testing at WSMR while connected to the corresponding receivers listed in this table, a subset of these antennas and some additional antennas were subsequently characterized in a smaller anechoic chamber at MITRE in Bedford, MA. See Section 3.3.1.

3.1.2 Anechoic Chamber

The radiated adjacent band testing was performed at the Army Research Laboratory (ARL) Anechoic Chamber located at WSMR. The test configuration and approximate dimensions for the Electromagnetic Vulnerability Assessment Facility (EMVAF) are shown in Figure 3-1.

The GNSS equipment test area was approximately 24' × 24' and was radiated from above using two separate antennas. One antenna radiated the interference signals while the other radiated GNSS signals with both approximately 25' above the center of the test area. The signal generation equipment was located on the mezzanine platform while participant collection and support equipment was located at the opposite end of the chamber. To emulate standard field operation of each particular receiver as closely as possible, some receivers were located in the participant area and RF cables were run to their respective antennas. Receivers with integrated antennas were placed directly in the test area with data collection/control cables typically routed to the participant area.

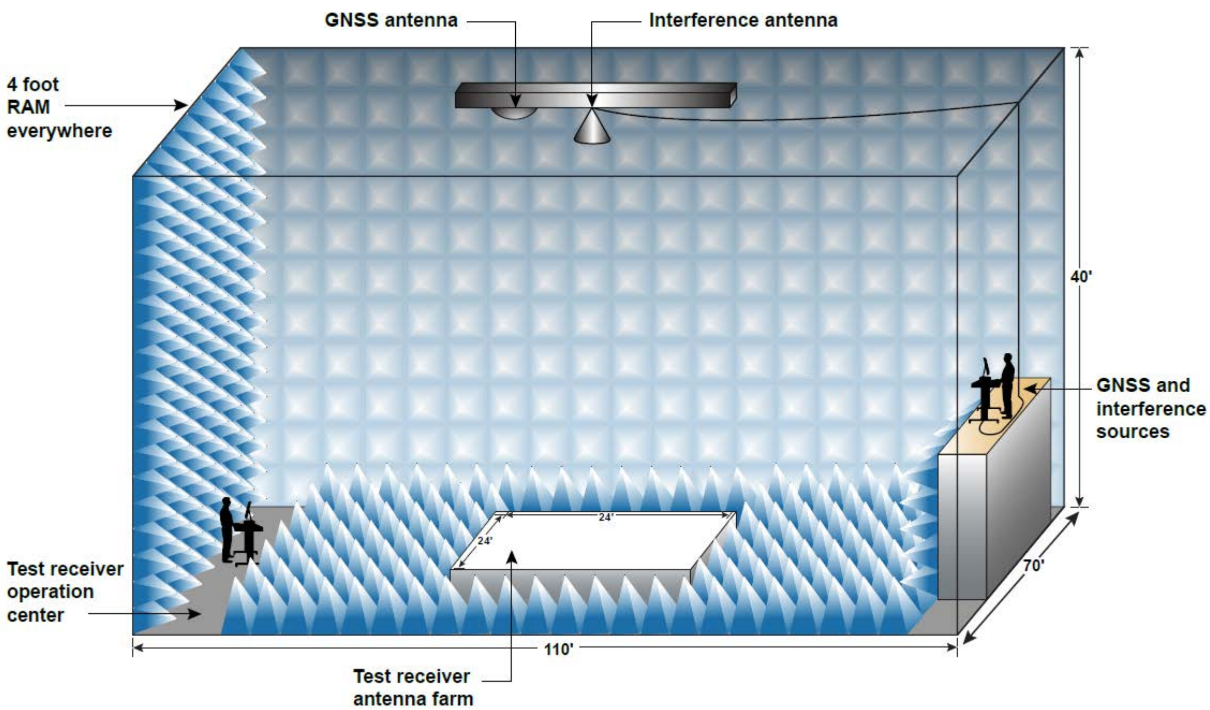

Figure 3-1: Chamber Dimensions and Layout

3.1.3 Location in Chamber

During the radiated testing, there were 12 participating organizations including DOT's Federal partners and agencies, and GPS/GNSS receiver manufacturers. The organizations included: 1) United States Coast Guard (USCG), 2) NASA, 3) National Oceanic and Atmospheric Administration (NOAA), 4) United States Geological Survey (USGS), 5) FAA, 6) U.S. DOT, 7) General Motors (GM), 8) u-blox, 9) NovAtel, 10) Trimble, 11) John Deere, and 12) UNAVCO, a non-profit university-governed consortium that facilitates geoscience research and education using geodesy sponsored by NASA and the National Science Foundation. The participating organizations, number of receivers and location on the test grid can be found in Figure 3-2. A cavity backed spiral antenna used for signal calibration and chamber mapping was placed at the edge of the test grid between locations E0 and G0. This antenna was connected to a spectrum analyzer and used for continuous signal and interference monitoring. In addition, a horn antenna connected to a spectrum analyzer was setup in the middle of the test grid (E7) for signal and interference monitoring and situational awareness for participants.

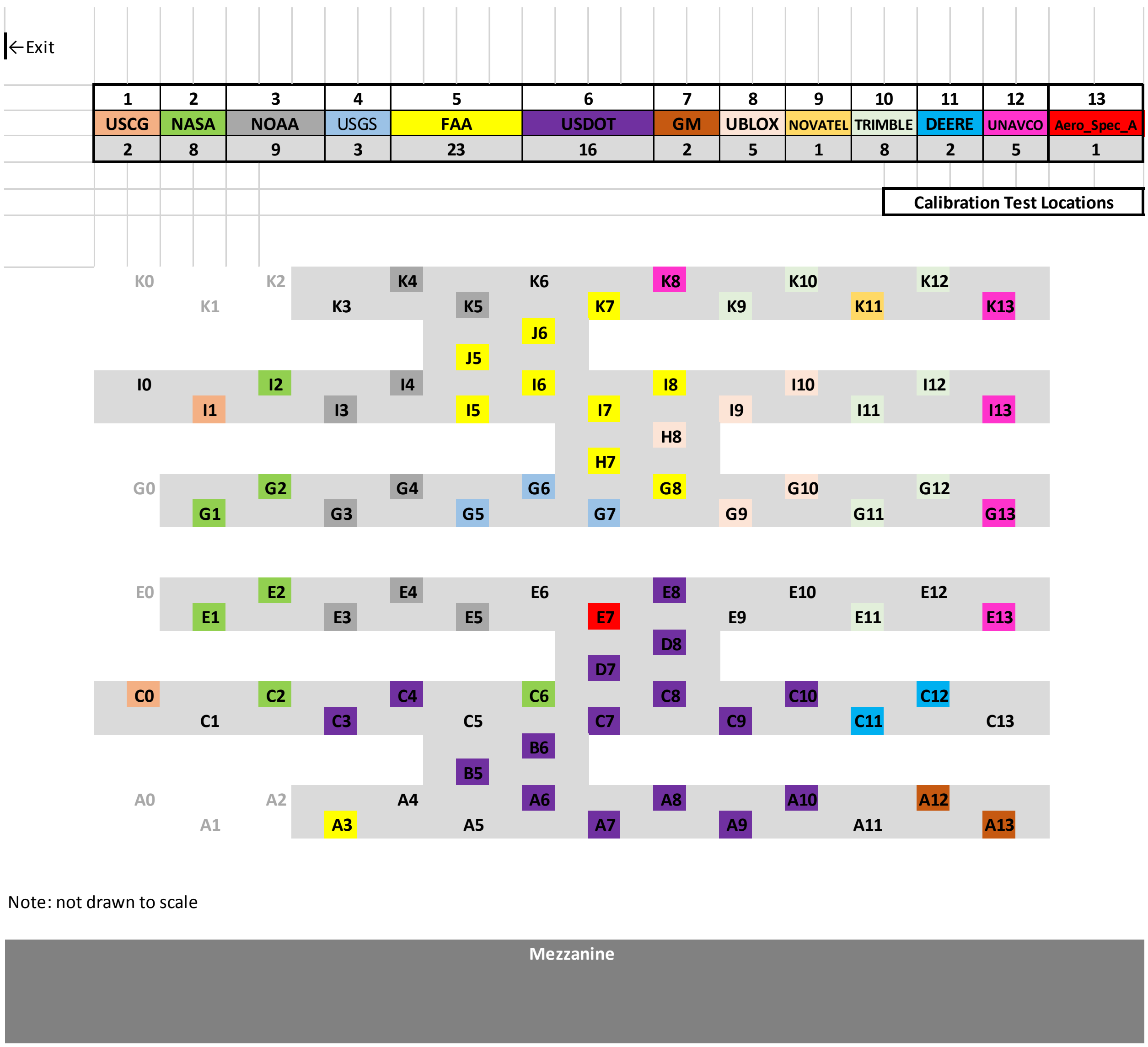

Figure 3-2: DUT and Calibration Grid Locations

Figure 3-3 is a photo of the DUTs during the anechoic chamber testing.

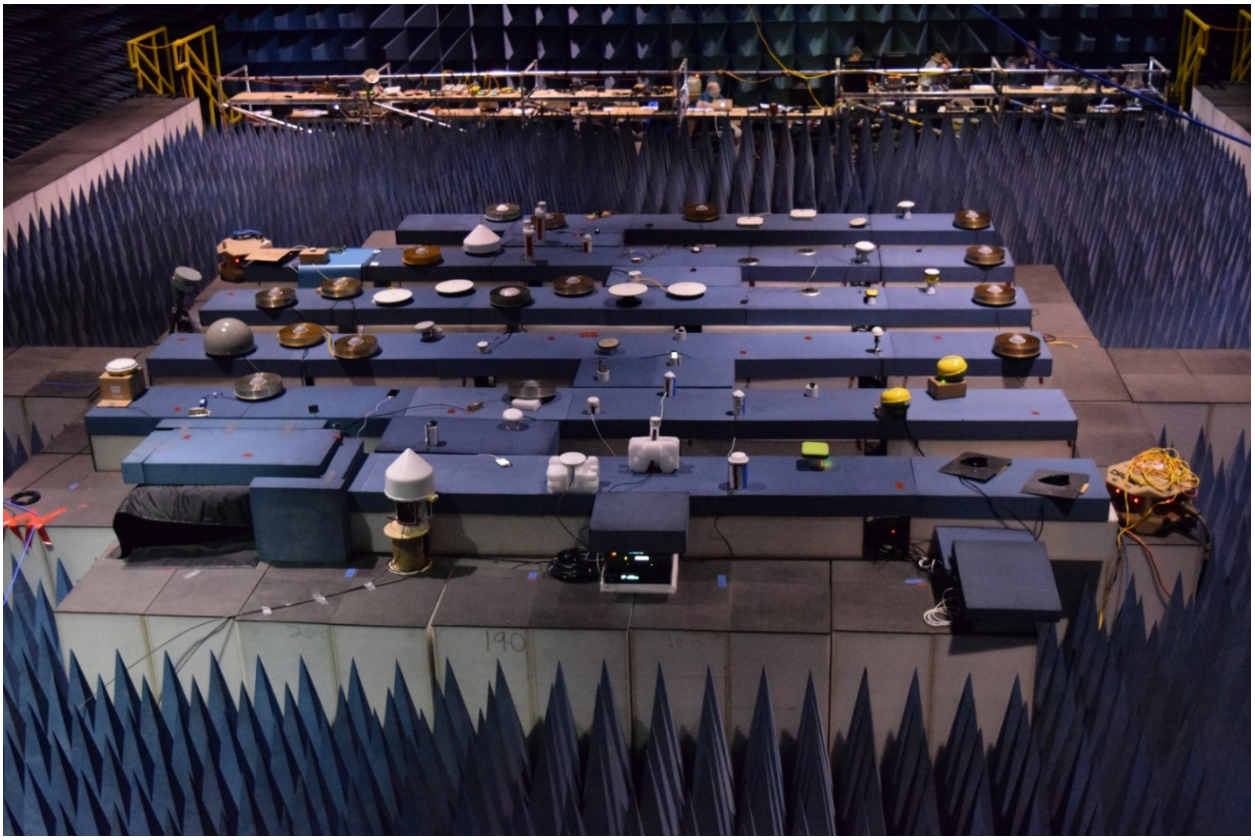

Figure 3-3: Photo of the DUTs on the test grid

3.1.3.1 GNSS Signal Generation

The GNSS signal generation and recording process is shown in Figure 3-4. The recording was conducted at MITRE prior to the test period. Simulated satellite signals were generated using a set of four Spirent GSS8000 GNSS signal simulators. These are commercial research and test devices that produce high-fidelity RF signals as they would appear at the output of a GNSS receive antenna. The GSS8000 simulators allow specification of received signals, received signal power level, satellite orbital parameters, user location, etc. The simulators were programmed to synchronously generated signals for GPS+ Wide Area Augmentation System (WAAS), Beidou, GLONASS, and Galileo. The L1+L2 radio frequency outputs of the simulators generating the GPS+WAAS, Beidou, and Galileo signals were passively combined using a single channel of a Spirent GSS8368 Signal Combiner. The GLONASS L1 signals were passed through the second channel of the GSS8368 signal combiner.

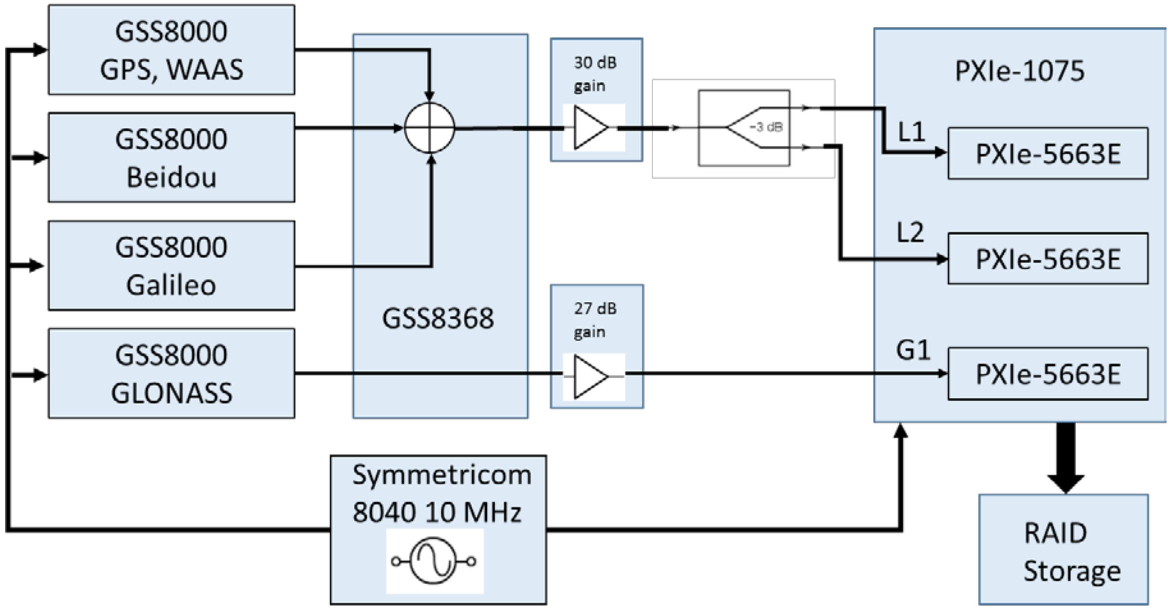

Figure 3-4: GNSS Signal Generation and Recording

The resultant RF data was recorded using a set of three National Instruments (NI) PXIe-5663E Vector Signal Analyzers housed in a National Instruments PXIe-1075 chassis. The three channels were recorded into 26.4 MHz wide bands centered at 1227.6 MHz, 1572.2 MHz, and 1602 MHz at 33 MS/s using 16 bit complex samples. The sampled data was then recorded on an NI HDD-8265 12 Terabyte Redundant Array of Independent Disks (RAID) (see Figure 3-4). The total recording time for the interference test events is approximately seven hours in length.

The GNSS signal playback and transmission process is illustrated in Figure 3-5. During the test period, the recorded GNSS signals were converted back to RF using a set of three National Instruments PXIe-5673E Vector Signal Generators (VSG) using the same sample rate as was used to record the data. The outputs of the three signal generators were combined using a Narda model 4372A-3 passive 3-port combiner. The output of this combiner was passed through a Vaunix Technology LDA-602 variable attenuator.

The attenuation level was established during chamber mapping and calibration (see Section 3.1.4) such that the received signal strength was at or above the power levels specified below. The output of the attenuator was followed by a splitter (that was connected to a spectrum analyzer during the test) and then an RF isolator with approximately 60 dB of isolation to prevent RF power from entering the system through the antenna. The isolator was connected to a custom passive L1/G1/L2 GNSS patch antenna that was suspended from the ceiling of the test chamber (see Figure 3-1). Prior to the WSMR deployment, the GNSS signal playback system was tested in a chamber at MITRE to ensure that the playback accurately reproduced the desired scenarios.

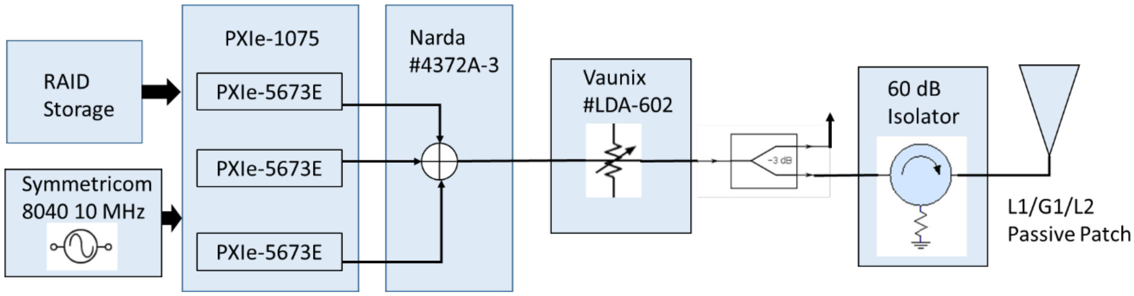

Figure 3-5: GNSS Signal Playback and Transmission

The equipment that was transported to and set up in the chamber is listed in Table 3-2.

Table 3-2: GNSS Signal Generation Equipment

Equipment	Make/Model	Notes
RAID storage	National Instruments HDD-8265	12 TB
3-channel VSG chassis	National Instruments PXIe-1075	Includes computer controller (PXIe-8133) with LabView software.
VSGs (3 each)	National Instruments PXIe-5673E	Each VSG consists of NI PXIe-5450 (400 MS/s I/Q Signal Generator), PXIe-5611 (I/Q Vector Modulator), and PXIe-5652 (RF Signal Generator).
Combiner	Narda 4372A-3	Passive 3-port
Digitally-controlled variable attenuator	Vaunix LDA-602	Provides up to 50 dB attenuation; controlled by VSG chassis computer.
Isolator	Addington Laboratories 222-0170A	Provides approximately 60 dB isolation.
Passive GNSS antenna	MITRE custom	RHCP antenna covers 1559 – 1610 MHz and 1212 – 1242 MHz
Rb Frequency Source	Symmetricom 8040	10 MHz
Amplifiers	MiniCircuits ZRL-2400-LN	23-30 dB gain. Used for chamber calibration (see Section 4.3.4.2).
Cables	Various	As needed and with appropriate connectors.

The GNSS signals that were generated and recorded at MITRE and then broadcast in the chamber at WSMR are indicated in Table 3-3.

Table 3-3: GNSS Signals Generated for Test

Signal
GPS L1 C/A-code
GPS L1 P-code
GPS L1C
GPS L1 M-code
GPS L2 P-code
SBAS L1
GLONASS L1 C
GLONASS L1 P
BeiDou B1I
Galileo E1 B/C

For the interference test events, the transmitted GNSS signal powers were calibrated to yield the minimum signal levels specified in Table 3-4 at the location in the test grid with the lowest received power (see Section 3.1.4). The signal powers were held constant over the duration of the event, except for the linearity test.

Table 3-4: Minimum Received GNSS Signal Power Levels for Interference Test Events

Signal	Minimum Received Power out of 0 dBic antenna (dBW)
GPS C/A-code	-158.5 for 8 SVs, -168.5 for 1 SV, -178.5 for 1 SV
GPS L1 P(Y)-code	-161.5 for 8 SVs, -171.5 for 1 SV, -181.5 dBW for 1 SV
GPS L1C	-157 for 8 SVs, -167 for 1 SV, -177 for 1 SV
GPS L1 M-code	-158 for 8 SVs, -168 dBW for 1 SV, -178 dBW for 1 SV
GPS L2 P(Y)-code	-164.5 for 8 SVs, -174.5 for 1 SV, -184.5 for 1 SV
GPS L2 M-code	-161 dBW for 8 SVs, -171 dBW for 1 SV, -181 dBW for 1 SV
SBAS L1	-158.5 for 2 SVs
GLONASS L1 C	-161 for 10 SVs, -171 for 1 SV, -181 for 1 SV
GLONASS L1 P	-161 for 10 SVs, -171 for 1 SV, -181 for 1 SV
BeiDou B1I	-163 for 10 SVs, -173 for 1 SV, -183 for 1 SV
Galileo E1 B/C	-157 for 10 SVs, -167 for 1 SV, -177 for 1 SV

The user was located at 32N, 106W, 0 m height relative to the WGS-84 ellipsoid and was stationary over the simulated time span. The simulated start time was April 18, 2016 08:00

MDT. Yuma-style almanacs for the GPS, GLONASS, BeiDou, and Galileo constellations are provided in Appendix A.

Errors that the GNSS simulators were capable of emulating were set to zero except for ionospheric delay and tropospheric delay errors, which are described in Appendix A. The objective of the simulator configuration was to minimize pseudorange and carrier phase errors from all sources (e.g., satellite clock errors, satellite ephemeris errors, residual ionosphere, residual troposphere) for the devices under test to enable measurement of the introduced interference source effects without the influence of other errors that are not attributable to the interference source. Since GNSS receivers typically apply tropospheric and ionospheric correction models, these error sources were emulated to minimize residual receiver measurement errors.

3.1.3.2 Interference Signal Generation

The Software Programmable Interference Generator for ABC Testing (SPIGAT) was assembled to generate additive white Gaussian noise (AWGN) and simulated LTE signals as interference at controlled power levels at specified frequencies. This system was automated to execute these tests for a suite of 22 discrete interference frequencies at appropriate signal levels with minimal operator intervention. The frequencies and signals levels tested are shown in Figure 3-6 and the interference system configuration for the radiated test is depicted in Figure 3-7. The VSG generated either 1 MHz AWGN (Type 1) or LTE (Type 2) signals at a fixed level at the appropriate carrier frequency and the adjustable attenuator controlled the signal level input from the VSG to the high power amplifier (HPA).

Using the attenuator in this fashion ensured Adjacent Channel Leakage Ratio (ACLR) from the VSG was maintained through different test levels. The HPA output was provided to an RF switch that directed the interference signal through one of 22 RF cavity filters. Lastly, the amplified and filtered interference signal was directed to a linearly polarized standard gain horn transmit antenna that irradiated the GNSS receivers under test. Directional couplers were included in the signal generation path to provide monitor points and a circulator was added to provide overload protection.

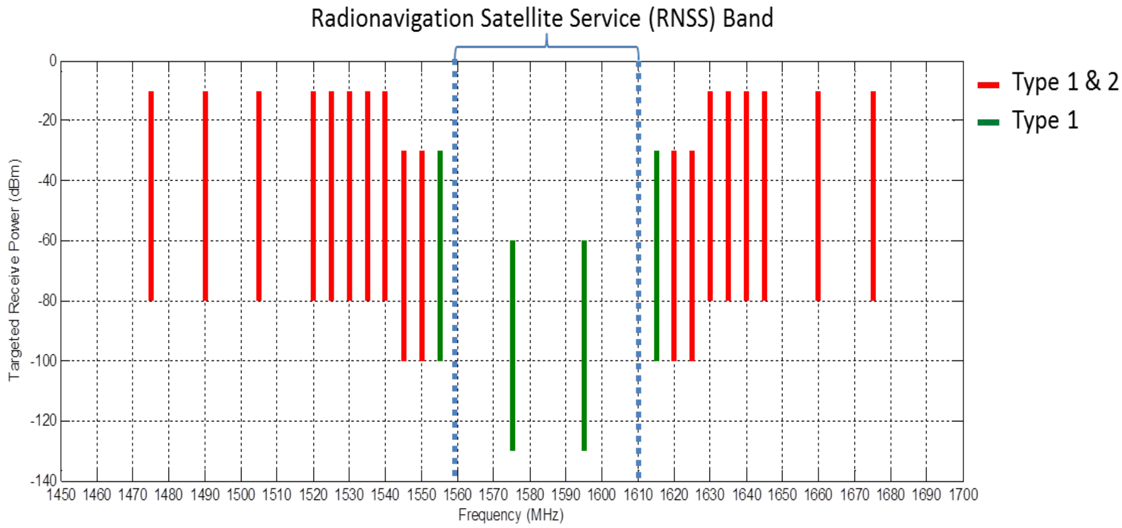

Figure 3-6: Interference Frequencies and Signal Levels Tested

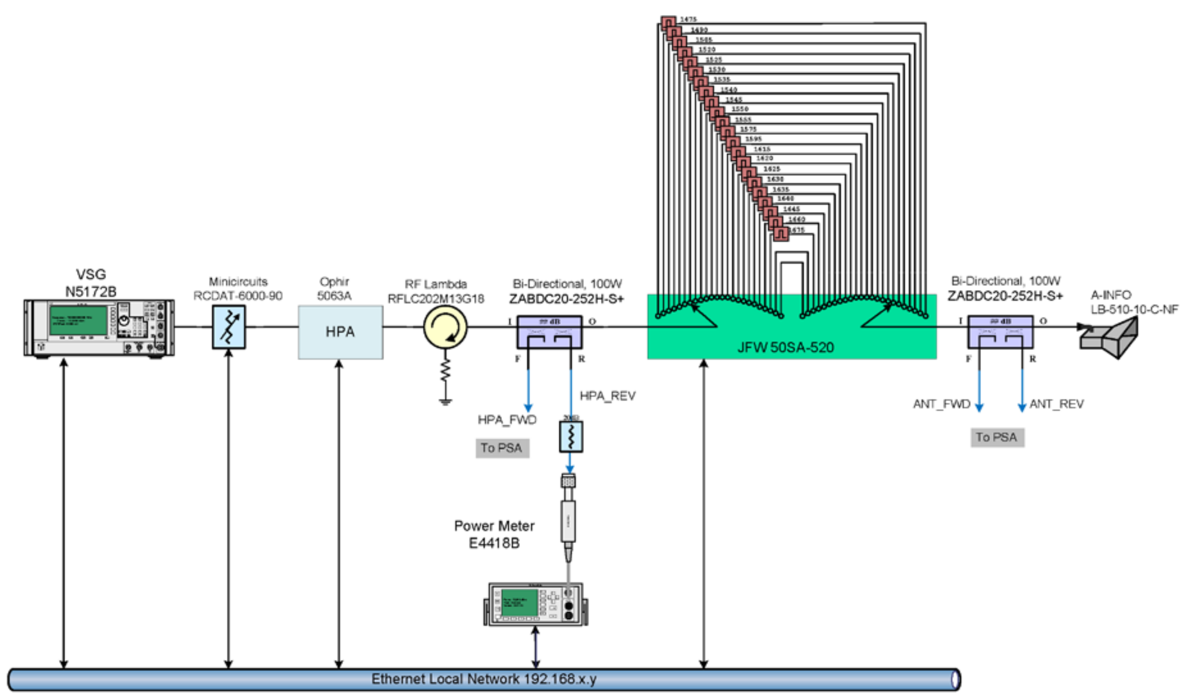

Figure 3-7: Interference System Configuration for Radiated Test

Test execution for each interference test signal was controlled by a pre-defined configuration file. The configuration file contained the frequencies to be tested, power levels, signal type, and test durations. The control computer was "GPS time aware" by obtaining receiver time from a GPS receiver tracking signals directly from the GNSS signal generator. This allowed time alignment with receiver data during processing. The interference control software recorded GPS time and instrument settings once per second into SPIGAT summary files for each test event.

One of the more important considerations for SPIGAT was the RF filters and ensuring they were sufficient to attenuate out-of-band emissions (OOBE) so that degradation measured was due almost entirely to the fundamental signal only. (The impacts of OOBE with the fundamental signal were investigated in the wired testing.) The RF passband cavity filters used to condition the interference were grouped into two categories based on roll-off specification. Filters centered at test frequencies nearer (but outside of) the RNSS band, namely 1540, 1545, 1550, 1555, 1615, 1620, and 1625 MHz were designed to meet tighter roll-off requirements with the primary feature being 65 dB rejection at 9 MHz from center. The remaining filters were designed to meet a more relaxed set of requirements with 65 dB rejection at 20 MHz from center. The measured frequency dependent gain for these two filter types are shown in Figure 3-8. Further details on SPIGAT and WSMR test conditions are provided in Appendix A.

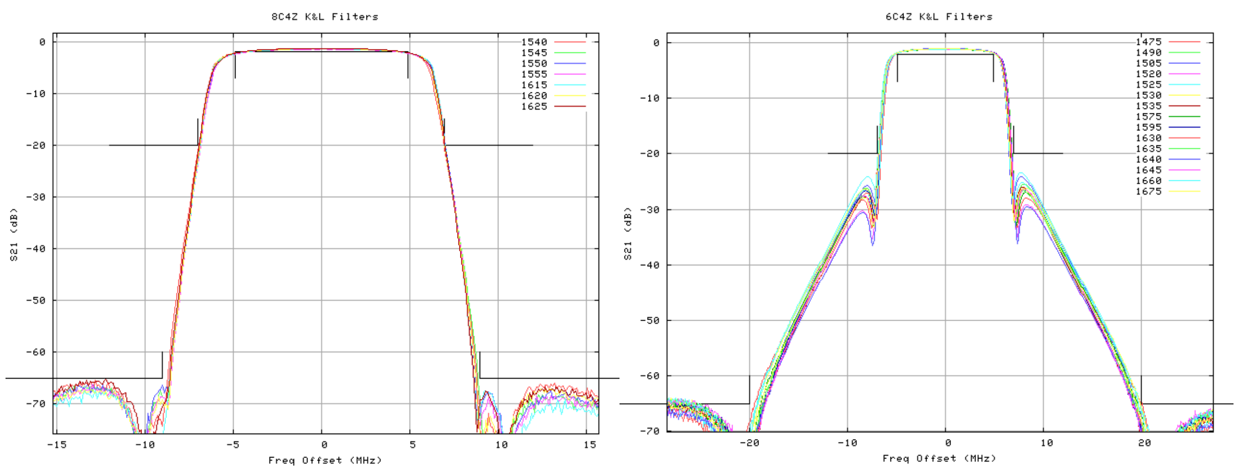

(a) **(b)**

Figure 3-8: Measured gain response for (a) bandpass RF filter with tighter rejection requirements, (b) bandpass RF filter with more relaxed rejection requirements.

3.1.3.2.1 Type 1 Signals

The Type 1 signal was selected for testing at all 22 frequencies to provide a narrowband signal for assessment of a general receiver mask not specifically tied to LTE. The signal tested was bandpass AWGN with bandwidth B=1 MHz. Some early consideration was given to using continuous wave (CW) interference but this 1 MHz signal was adopted based primarily on concerns some receivers might employ techniques specifically designed to mitigate CW signals. The AWGN signal was generated offline and had a duration of approximately 0.021 seconds. This signal file was loaded into the VSG, up-converted to the appropriate frequency, and played out continuously end to end from VSG memory. Figure 3-9 is a spectrum analyzer capture of the Type 1 signal as received in the EMVAF test area during testing.

Figure 3-9: Type 1 Signal Captured during WSMR Testing @ 1530 MHz

3.1.3.2.2 Type 2 Signals

The Type 2 signal emulated LTE characteristics representing both a downlink and an uplink. The downlink was emulated as a fully loaded base-station with Orthogonal Frequency Division Multiplexing (OFDM), and the uplink with Sub-Carrier OFDM (SC-OFDM). The LTE digital waveforms were generated using the MATLAB LTE package. As with the Type 1 signal, these LTE representations were loaded on the VSG, up-converted to the appropriate carrier frequency, and played out end to end from VSG memory. The durations of the downlink and uplink files were two seconds each. The specific settings and commands used in MATLAB are provided with Appendix A. Figure 3-10 is a spectrum analyzer capture of the Type 2 signal as received in the EMVAF test area during testing.

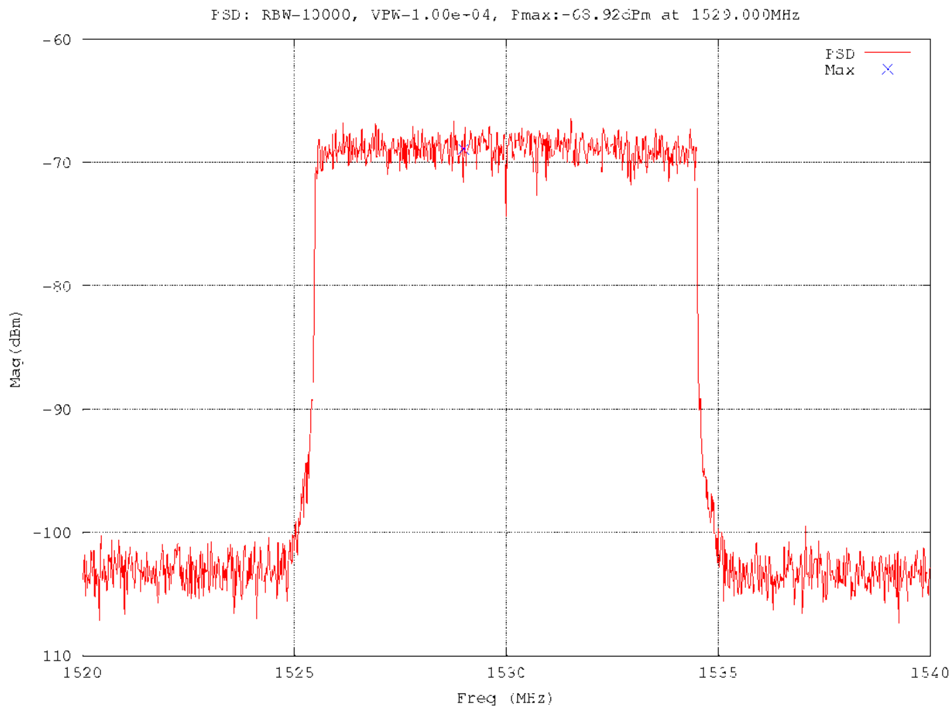

Figure 3-10: Type 2 Signal Captured during WSMR Testing @ 1530 MHz

3.1.3.2.1 Intermodulation

The Type 1 and 2 interference signals provide a measure of the effect of an interfering signal on a particular GPS/GNSS receiver but do not capture impacts of spurious emissions due to two or more signals operating simultaneously at different center frequencies. The intermodulation signal test was included to demonstrate this potential impact by simultaneously transmitting Type 2 downlink signals at center frequencies of 1530 MHz and 1550 MHz. The 3rd order intermodulation product of these center frequencies falls near the center of the L1 band. For this specific test, the 1550 MHz signal was generated so that it was approximately 10 dB lower than the 1530 MHz signal. The downlink LTE representation discussed earlier was up-converted to 1530 and 1550 MHz and played out end to end from VSG memory. The duration of the intermodulation file was 0.5 seconds. Figure 3-11 is a spectrum analyzer capture of the intermodulation signal as received in the EMVAF test area during testing.

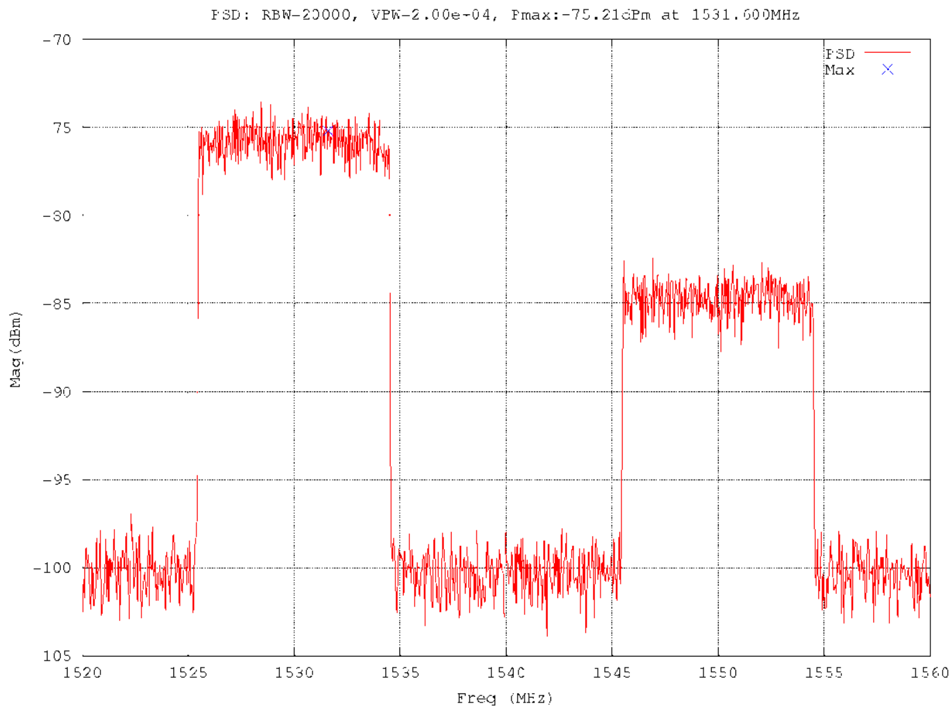

Figure 3-11: Intermodulation Signal Captured during WSMR Testing

3.1.4 System Calibration and Chamber Mapping

System calibration and chamber mapping included several efforts at WSMR; 1) GNSS calibration, 2) SPIGAT calibration, 3) and, chamber mapping. GNSS calibration is described in Section 3.1.4.1 and the remaining topics are discussed in Section 3.1.4.2 and Appendix A.

3.1.4.1 GNSS System

To calibrate the GNSS signal power levels, the playback system was modified slightly from the configuration shown in Figure 3-5. Two LNAs were inserted after the variable attenuator to increase the output power level. This power increase allowed the received GNSS signal levels to be accurately measured by a spectrum analyzer connected to a RHCP cavity-backed spiral antenna that was moved across 45 points in the test grid. The gains of the two LNAs were determined from measurement (see Figure 3-12).

The calibration proceeded in two steps. First, the VSGs in the playback system were utilized to produce tones at two frequencies (1227 MHz and 1561 MHz) to determine the variation in received power across the test grid at these frequencies. These variations, as measured using a RHCP cavity-backed spiral antenna at 45 locations spanning the test grid, are shown in Figure 3-13 and Figure 3-14. The numerical values on each of these plots are in dBm.

Second, to establish the output power of the three VSGs in the playback system, a GNSS signal from a single satellite was emulated (GPS P-code for 1227 MHz, GPS P-code at 1575 MHz, and

GLONASS C for 1602 MHz) and the received power measured at the location at the edge of the test grid where the received power was a minimum. The measured power, adjusted by the known LNA and cavity-backed spiral antennas gains, was compared to the target received power levels in Table 3-4. The resultant differences were used to establish power settings for each of the three VSGs in the playback system for the test events. The VSG output powers were adjustable both relatively and absolutely (through power commands sent digitally by computer interface to each VSG to change relative gains, and through removal of the two LNAs as well as commands to the digital variable attenuator that followed the combined VSG outputs). The objective of this calibration process was to ensure that the power levels specified in Table 3-4 were achieved or exceeded out of a 0 dBic receive antenna at any location in the test grid. As evident from Figure 3-13 and Figure 3-14, when the target minimum received GNSS signal levels were achieved at the worst-case location in the grid (grid corners), they were exceeded by up to 3.7 dB at the center of the grid.

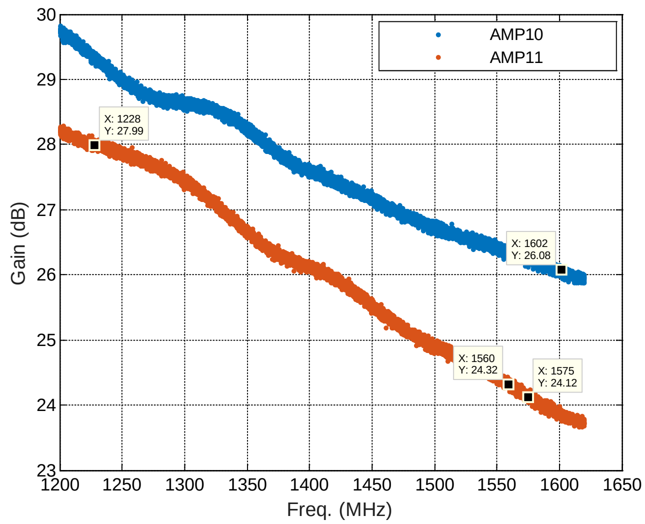

Figure 3-12: Measured Gain of Two MiniCircuits ZRL-2400-LN Amplifiers

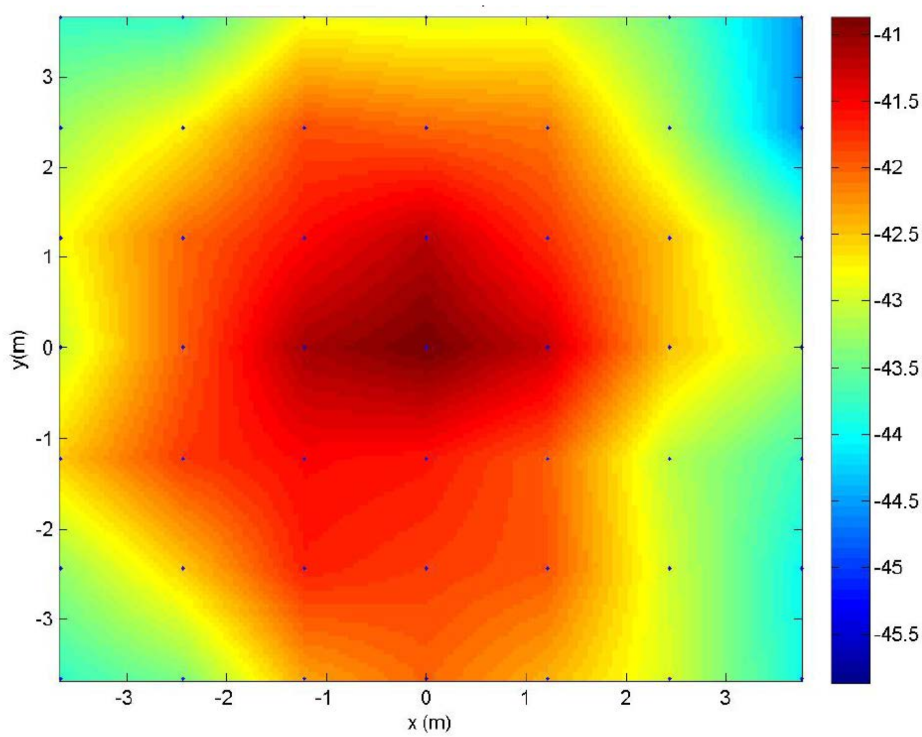

Figure 3-13: GNSS Signal Received Power Variation across the Test Grid (1227 MHz)

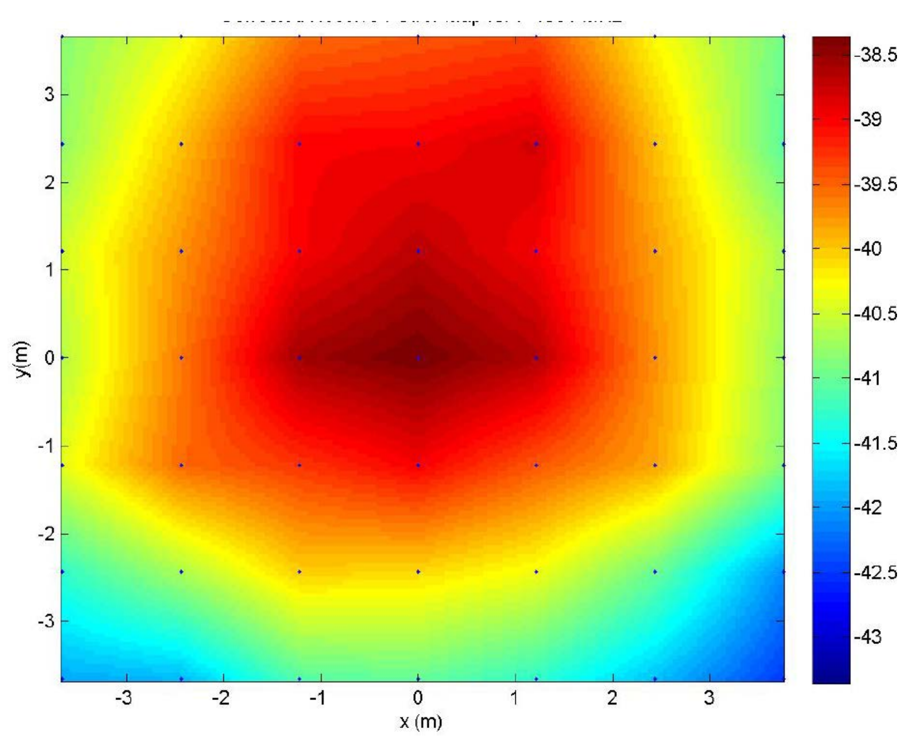

Figure 3-14: GNSS Signal Received Power Variation across the Test Grid (1561 MHz)

3.1.4.2 SPIGAT

The interference system was calibrated to determine the system biases for each interference frequency and to ensure the intended power levels were achieved in the test area. This calibration was accomplished by selecting a reference location at the edge of test area at approximately the 3 dB beamwidth of the interference transmit antenna and measuring CW tones generated by SPIGAT at all 22 discrete frequencies. The CW tones were measured using a cavity backed spiral antenna (AST-1507AA) mounted on a tripod, calibrated RF cable, and a spectrum analyzer (Agilent E4445A). This procedure resulted in a correction table per frequency utilized by SPIGAT. The interference linearity was also measured from this reference location to demonstrate received power over the test range at each frequency matched the intended levels.

3.1.4.3 Chamber Mapping

Chamber mapping was conducted after calibration was complete to determine RF power variation across the test area. Mapping used a grid of 45 measurement points separated by approximately four feet which encompassed the test area. Chamber mapping was completed at the beginning and end of DOT testing with all equipment installed in the test area. These two mappings were very consistent and final mapping values used with receiver processing represented their average. Examples of the final power mapping at 1475, 1575 and 1675 MHz are provided in Figure 3-15. This figure shows the expected performance of the interference antenna beamwidth becoming narrower at higher frequencies. The location of each receiver tested was known relative to the mapping grid and this mapping data was used to modify SPIGAT test event summary files and generate unique interference power profiles per frequency for each receiver location.

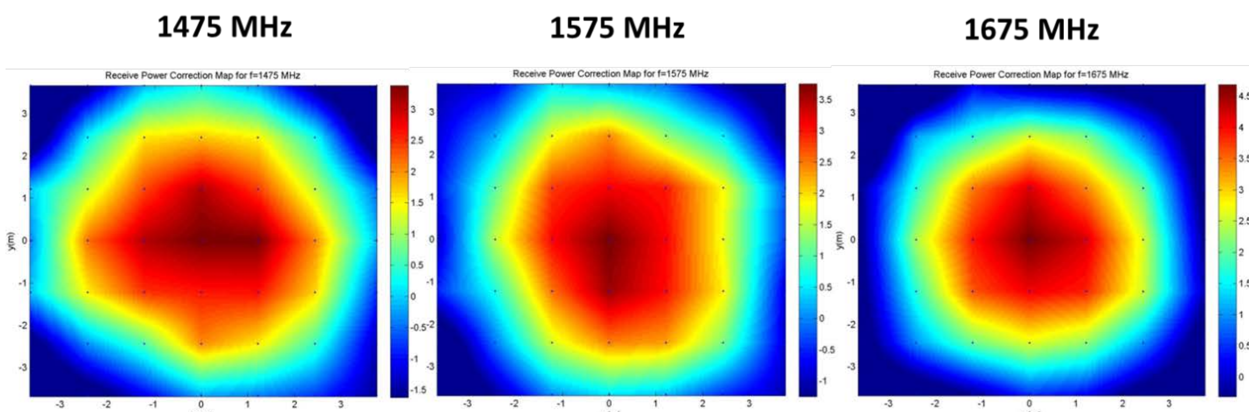

Figure 3-15: Power Correction Representations for Three Frequencies

3.1.5 Test Sequence

The test schedule executed at WSMR is shown in Table 3-5. In addition to Type 1, Type 2, and intermodulation signals described previously there was also a CNR linearity test. Table 3-5 shows the day each test was executed and test number. Type 1 and Type 2 signal tests were given priority so these were tested on separate days to increase the likelihood of obtaining a more robust data set. The in-band test mentioned in this table was the result of removing Type 1 signals directly in the RNSS band from this test sequence and testing separately. A discussion of the rationale for this change is provided later in this section. Lastly, each test event listed in the table was preceded by a stabilization period of at least fifteen minutes with the GNSS system turned ON to allow participants to reset equipment, verify GNSS signal tracking, and ensure data collection was started.

Table 3-5: Test Schedule

Day of Week (24-28 April 2016)	Test and Number
Monday	CNR linearity - Test01
Tuesday	Type 1 signal - Test02 Type 2 signal – Test03
Wednesday	Type 2 Signal – Test04 Type 1 Signal – Test05
Thursday	In-Band – Test56 CNR linearity - Test07 Intermodulation – Test89

3.1.5.1 Linearity Test

The GPS/GNSS receivers' CNR estimators need to operate in their linear region. A linearity test was conducted on the CNR estimators varying GNSS signal power. SPIGAT was not used for this test event. For this test, GNSS signals of each type were generated to match their intended levels during interference testing (i.e. majority of GPS L1 C/A were generated at-158.5 dBW and two SVs were at the lower specified power levels of -10 and -20 dB). After five minutes at these nominal levels, the test sequence had each signal power increased by two dB every 15 seconds until they reached +10 dB relative to the nominal level. Each signal power was then decreased by two dB every 15 seconds until they reached -20 dB relative to the nominal level. Finally, each signal power was increased by two dB every 15 seconds until power was returned to nominal levels. The receivers were allowed to track for a brief period following the last signal power step before concluding this test event.

3.1.5.2 Interference Test

Each of the individual interference tests used the exact same sequence. The interference test sequence for each frequency started with a quiescent period of five minutes with no interference to establish baseline CNR followed by stepping through the full power range at two dB steps with 15 second dwells at each level. This sequence was repeated for all desired frequencies for each interference signal. Table 3-6 shows the specific frequencies, power levels, and LTE signal types used in this testing. The power range for the intermodulation test event was -90 to -20 dBm for the signal generated at 1530 MHz and -100 to -30 dBm for 1550 MHz.

As mentioned above, the Type 1 test event had the two in-band frequencies (1575 MHz and 1595 MHz) extracted from the full set of 22 test frequencies and made into a separate test event. During the set-up period at the chamber, some system verification testing revealed that for these two in-band frequencies noise from the high-power amplifier (VSG power turned OFF) would affect receiver performance. The system reconfiguration required to circumvent this issue was to place a 20-dB attenuator at the output of the interference generation system which effectively lowered the output noise floor. The interference power was increased for the addition of this 20-dB attenuator to meet the desired interference test range. For in-band and intermodulation test events, SPIGAT was commanded to run two interference test cycles back to back (hence, Test56 and Test89 designations).

Table 3-6: Interference Signal Parameters

Center Frequency (MHz)	$[p_{min}, p_{max}]$ **(dBm)**	**LTE Interference Signal**		**Bandpass Noise Interference Signal**
		Signal Bandwidth	**LTE Type**	
1475	[-80,-10]	10 MHz, LTE	Downlink	1 MHz
1490	[-80,-10]	10 MHz, LTE	Downlink	1 MHz
1505	[-80,-10]	10 MHz, LTE	Downlink	1 MHz
1520	[-80,-10]	10 MHz, LTE	Downlink	1 MHz
1525	[-80,-10]	10 MHz, LTE	Downlink	1 MHz
1530	[-80,-10]	10 MHz, LTE	Downlink	1 MHz
1535	[-80,-10]	10 MHz, LTE	Downlink	1 MHz
1540	[-80,-10]	10 MHz, LTE	Downlink	1 MHz
1545	[-100,-30]	10 MHz, LTE	Downlink	1 MHz
1550	[-100,-30]	10 MHz, LTE	Downlink	1 MHz
1555	[-100,-30]	-	-	1 MHz
1575	[-130,-60]	-	-	1 MHz
1595	[-130,-60]	-	-	1 MHz
1615	[-100,-30]	-	-	1 MHz
1620	[-100,-30]	10 MHz, LTE	Uplink	1 MHz
1625	[-100,-30]	10 MHz, LTE	Uplink	1 MHz
1630	[-80,-10]	10 MHz, LTE	Uplink	1 MHz
1635	[-80,-10]	10 MHz, LTE	Uplink	1 MHz
1640	[-80,-10]	10 MHz, LTE	Uplink	1 MHz
1645	[-80,-10]	10 MHz, LTE	Uplink	1 MHz
1660	[-80,-10]	10 MHz, LTE	Uplink	1 MHz
1675	[-80,-10]	10 MHz, LTE	Downlink	1 MHz

3.1.6 Data Processing/ITM formation

During testing, organizations used their own programs/software for data collection. This delegation of data collection responsibility was necessary since many of the 80 receivers had proprietary interfaces. At the end of each test day, data collected from each receiver was transferred to DOT's master data repository. The participants were requested to provide a data acquisition system (e.g. laptop) with DVD/CD recording capability or asked to use USB hard drives to transfer data. All data was archived prior to the receivers and participants leaving the test area.

3.1.6.1 Data Conversion and Format

The master data repository was setup inside the chamber to allow participants to transfer data from each receiver to this repository. The master repository consisted of a desktop with a local storage array which accommodated all the data. Each participant was given a blank external hard drive, which stayed with them throughout the test, was dedicated to transfer data to the repository at the end of each test. Blank DVD/CDs were also made available for those who wanted to copy the data to DVDs, then the data were copied to the repository (through the repository desktop).

Data was provided from each participant in National Maritime Electronics Association (NMEA) 0183, Receiver Independent Exchange (RINEX versions 2.11, 3.00, 3.01 and 3.03), or commonly defined comma separated variable format (CSV). The preference was to have data provided in CSV format when possible. Table 3-7 identifies the desired data from each GNSS receiver tested. It was understood that all data types may not be available and for these instances fields should be denoted not available, “NaN”. The CSV format accommodates twelve fields to indicate GPS time, position estimate and satellites tracked for each GNSS constellation and signal type. This data is followed with satellite specific data needed for the analysis. Each constellation signal type is allocated 32 satellites and SBAS is allocated two satellites with the data grouped by data block as described in Table 3-7.

Each receiver has a separate data file for each test run. The nomenclature of the file name is as follows: ParticipantLC_ParticipantID_Test#_Date.extension, where ParticipantLC is a unique indicator for the antenna location (and receiver if integrated), ParticipantID maps to the receiver/antenna tested and origination, Test# indicates the test run number for that day, Date is the day of the actual test, and an extension is used to indicate the type file (ex. NMEA, RINEX or CSV). The ParticipantLC and ID were provided during test set-up. After the test week all the data files were converted to a commonly defined CSV as well as MAT format, as shown in Table 3-7 using MATLAB. To facilitate post-data processing, MATLAB Datenum and GPS Week columns were added at the beginning of the table, and the file’s naming convention was changed to add device under test number (DUT#), participant’s acronym, receiver’s name, and the category for receiver category.

Table 3-7: CSV Data Format

Field #	Parameter	Units	Comment
1	GPS Seconds of Week	Seconds	
2	Latitude	Degrees	relative to WGS84
3	Longitude	Degrees	relative to WGS84
4	Height	Meters	relative to WGS84 (orthometric)
5	GPS L1 C/A-code Tracked		
6	GPS L1 P-code Tracked		
7	GPS L1C Tracked		
8	GPS L2 P-code Tracked		
9	GLONASS L1 C Tracked		
10	GLONASS L1 P Tracked		
11	BeiDou BI1 Tracked		
12	Galileo E1 B/C Tracked		
13	SBAS L1 C/A-code Tracked		
Next are 32 satellite slots per signal type for GPS, GLONASS, BeiDou and Galileo. Each slot contains four data parameters. Satellite order is 1 through 32. SBAS has two satellite slots with four data parameters each. SBAS pseudo random noise (PRN) codes are 135 and 138.			
14	Carrier Phase$_{(\text{PRN-1,GPS C/A})}$	meters	
15	Loss of Lock Flag$_{(\text{PRN-1,GPS C/A})}$	binary (0 or 1)	Cycle slip or loss of carrier phase lock indicator. 0 indicates no loss of lock, 1 means lost lock.
16	Carrier to Noise Ratio$_{(\text{PRN-1,GPS C/A})}$	dB-Hz	
17	Pseudorange$_{(\text{PRN-1,GPS C/A})}$	meters	
18 – 141	GPS L1 C/A-code measurements for satellite signals 2-32		
142 – 269	GPS L1 P-code measurements for satellite signals 1-32		
270 – 397	GPS L1C measurements for satellite signals 1-32		
398 – 525	GPS L2 P-code measurements for satellite signals 1-32		
526 – 653	GLONASS L1 C satellite signals 1-32		
654 – 781	GLONASS L1 P satellite signals 1-32		
782 – 909	BeiDou BI1 satellite signals 1-32		
910 – 1037	Galileo E1 B/C measurements for satellite signals 1-32		
1038 - 1045	SBAS L1 C/A-code measurements for satellites signals from PRNs 135 and 138		

3.1.6.2 1 dB CNR Degradation

The 1 dB carrier-to-noise ratio (CNR) interference protection criterion (IPC) has been used in responding to FCC rulemaking proceedings that assessed the potential impact to GPS services, [2] and was the subject of much discussion and stakeholder feedback at the OST-R workshops.

A 1 dB C/N_0 degradation (-1 dB C/N_0) due to a new interference source is equivalent to an I_0/N_0 ratio of -6 dB, where C is the level of the observable desired information signal, while N_0 is the competing unwanted noise and I_0 is the interference level. This I_0/N_0 ratio of -6 dB means that a new interference level is actually one fourth the level of the existing noise level and the total unwanted $N_0 + I_0$ level is now 25% higher which is highly significant to system designers.

There are multiple interference mechanisms that can degrade C/N_0 of a GPS receiver. However, it is difficult to isolate the specific interference mechanism for each GPS receiver without sufficient technical information, such as receiver design, radio frequency filter selectivity, low noise amplifier gain, noise figure, 1 dB gain compression point and third-order intercept point from the GPS receiver manufacturers. Participation by GPS/GNSS receiver manufacturers in the DOT GPS Adjacent Band effort was on a voluntary basis and there was no obligation to provide this information.

Given the myriad of GPS/GNSS applications requiring accuracy to support their mission applications ranging from tens of meters to millimeters, there is not a single "accuracy degradation limit" that could be applied and trying to do so would be an intractable effort.

3.1.6.3 ITM Data Processing

The Interference Tolerance Mask (ITM) defines, for a given frequency, the maximum aggregate power allowed to ensure the tested GPS/GNSS receiver did not experience more than a 1 dB reduction in CNR for various categories of GPS/GNSS receivers. For a given DUT, the interference power (IP) data was calibrated using the mapping measurements interpolated to the DUT location. The CNR data corresponding to the GNSS signal being analyzed is time aligned with the calibrated interference data.

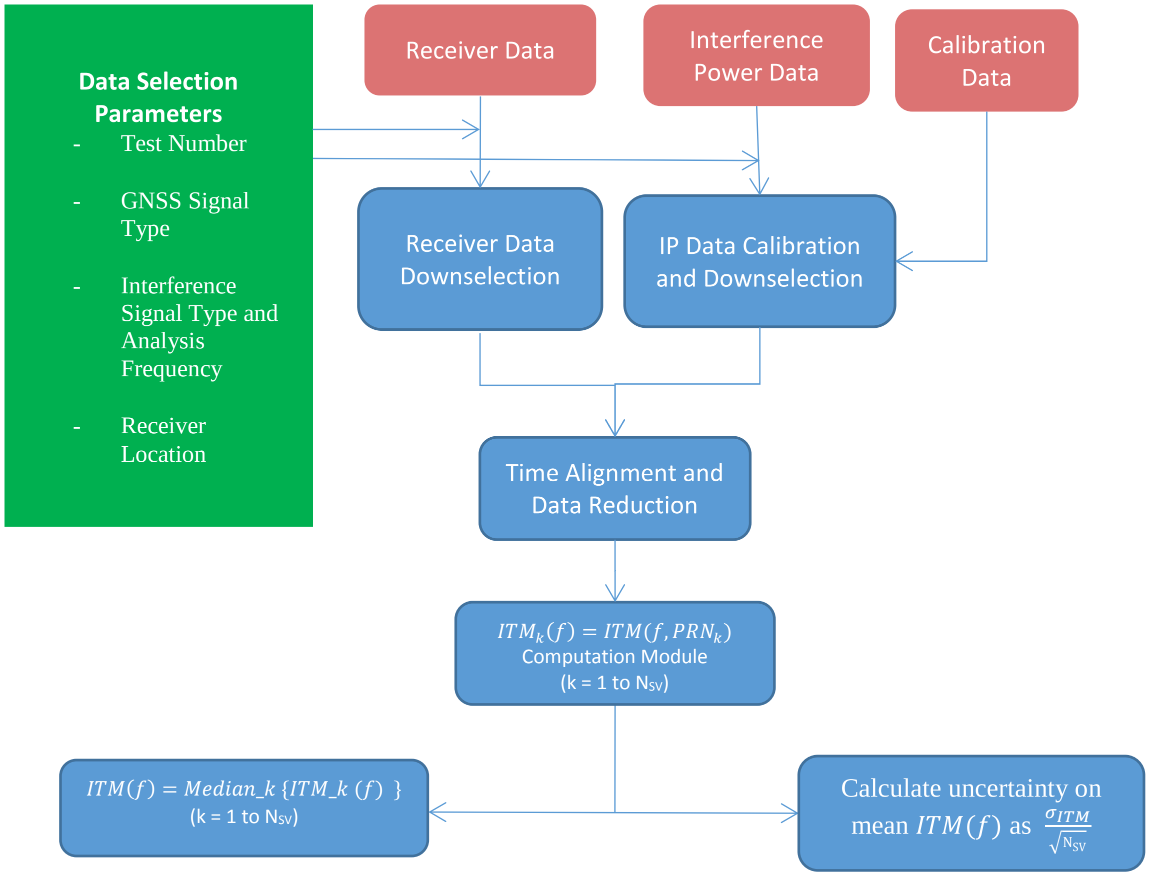

Figure 3-16: ITM Processing Block Diagram

The IP level which causes 1-dB CNR degradation is then determined on a per PRN basis. The median of results across PRNs is the value of the interference tolerance mask $ITM(f)$ at frequency f for that DUT. The use of mean and median produced similar results but the median operation was chosen because it is less sensitive to outliers. Only the PRNs at minimum ICD powers were used in the ITM analysis (not lower power to emulate low elevation satellites). A description of the overall processing is outlined in Figure 3-16.

Figure 3-17 shows the time aligned IP and reduced CNR data. The baseline CNR (CNR_{BL}, magenta dashed line) is calculated by averaging over the last 2.5 minutes of the IP-off interval (black line). During the IP-on interval, data reduction was performed by averaging CNR over the last 12 seconds of each 15 seconds IP step in order to allow for three seconds settling time. The blue trace in this figure is the resulting reduced CNR time series.

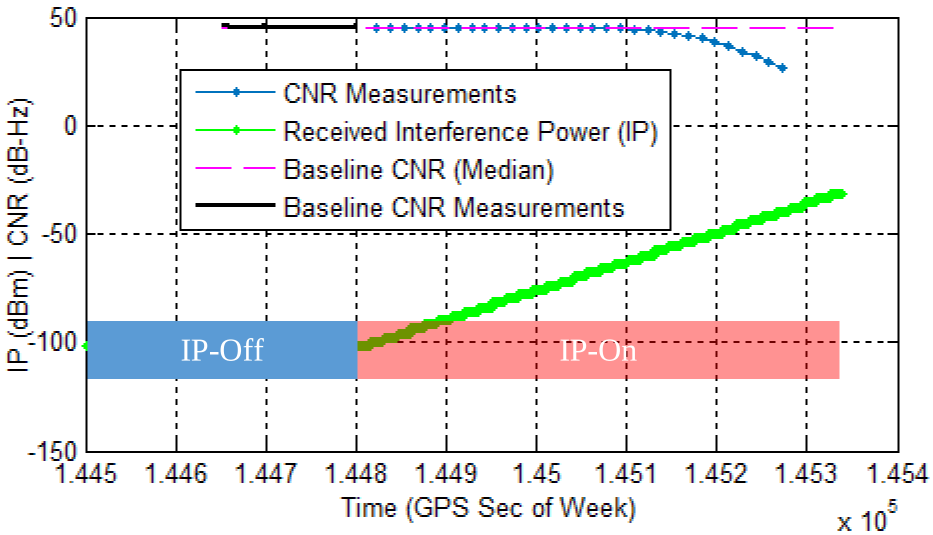

Figure 3-17: Sample plot for calibrated interference power overlaid with time aligned CNR data for a given DUT at a particular interference frequency

The time aligned and reduced CNR data can be plotted directly as a function of IP for each PRN and $ITM(f, PRN_k)$ can be found using linear interpolation as shown in Figure 3-18.

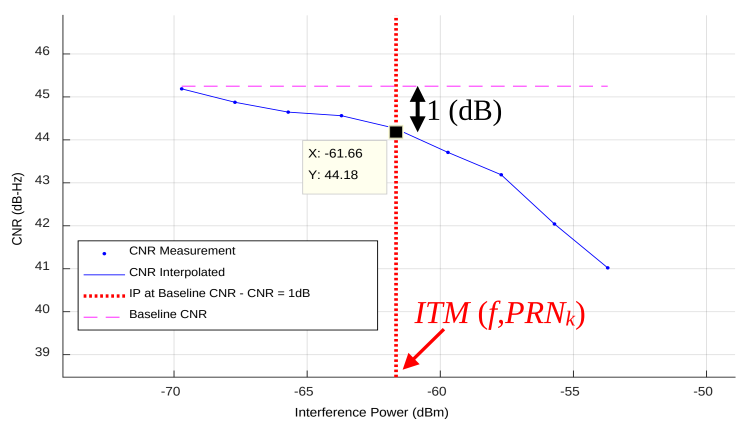

Figure 3-18: Determining the tolerable interference level from the CNR versus interference power for a single satellite after time alignment and calibration of interference power

The test for each interference signal type was performed twice as described in Section 3.1.5. The average of the resulting two interference tolerance values was taken as the final $ITM(f)$ for each interference signal type and GNSS signal supported by a DUT. Figure 3-19 depicts the ITMs for L1 C/A signal for a single DUT and shows repeatability between both LTE tests.

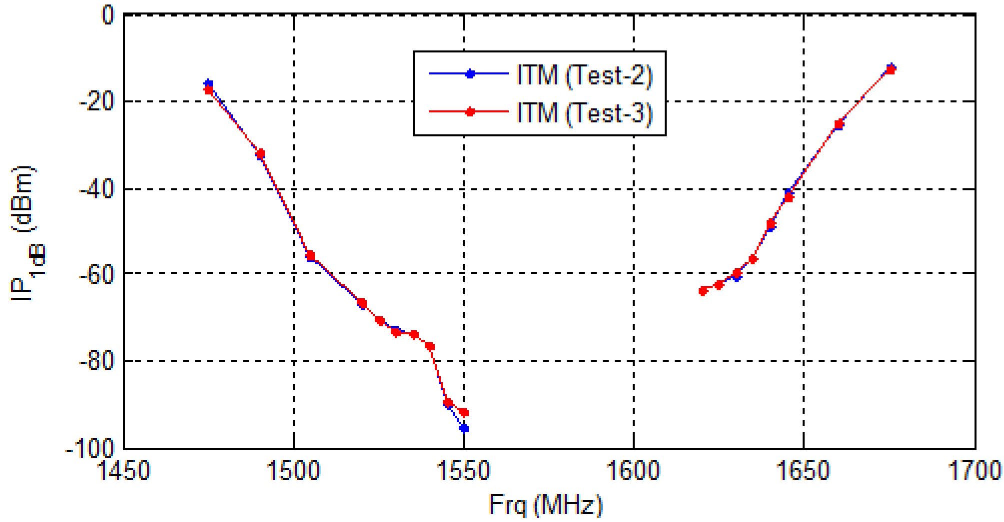

Figure 3-19: Overlaid L1 C/A ITMs from two radiated LTE test events for a single DUT. Test-2 and Test-3 refer to the first and second LTE tests respectively.

It is important to note that the algorithm does not calculate a 1-dB CNR degradation value if the CNR dynamic range defined as the difference between CNR_{BL} and the smallest 12 second average CNR value within each IP progression (CNR_{Min}) is less than 1.5 dB. In addition, the algorithm also checks that this dynamic range is statistically significant. This is done by ensuring that the standard deviation of the difference is small relative to its mean value. This criterion used by the algorithm is shown in the following expression (in dB).

$$\boldsymbol{CNR_{BL} - CNR_{Min} > 3 \times \sqrt{\left(var(CNR_{BL}) + var(CNR_{Min})\right)}} \quad (3\text{-}1)$$

Where $var(.)$ represents the measurement variance divided by the number of measurements for each of the two quantities. Additional quality checks are performed for each IP step. For example, the algorithm requires that at least three measurements be reported within the last 12 seconds interval of each step and that the standard deviation of the mean within each step be less than ½ dB.

The averaging across repeated tests was subject to additional quality control checks. For each DUT, GNSS signal, interference type, and center frequency combination, this average was performed only when the difference between the results produced by the two tests is less than 10 dB. For the cases when the difference exceeded this threshold, the test producing a value closer to the interpolated value between adjacent frequencies is kept, and the result of the other test was disregarded as an outlier.

The differences in results between repeated tests were analyzed as a measure of uncertainty due to environmental and equipment variability and is a real measure of test repeatability. Another uncertainty measure was calculated by considering the variability of $ITM(f, PRN_k)$ across PRNs for each DUT as shown. The empirical cumulative distribution function (CDF) for both error quantities just described are shown in Figure 3-20 for the 10 MHz LTE and Figure 3-21 for the 1 MHz AWGN interference signals. These plots show that 90 percentile of the uncertainty is less than 1.5 dB based on PRN variability analysis and less than 3 dB in terms of test repeatability. This is a near upper bound estimate on the measurement error. The median of both uncertainty measures are less than 0.5 dB.

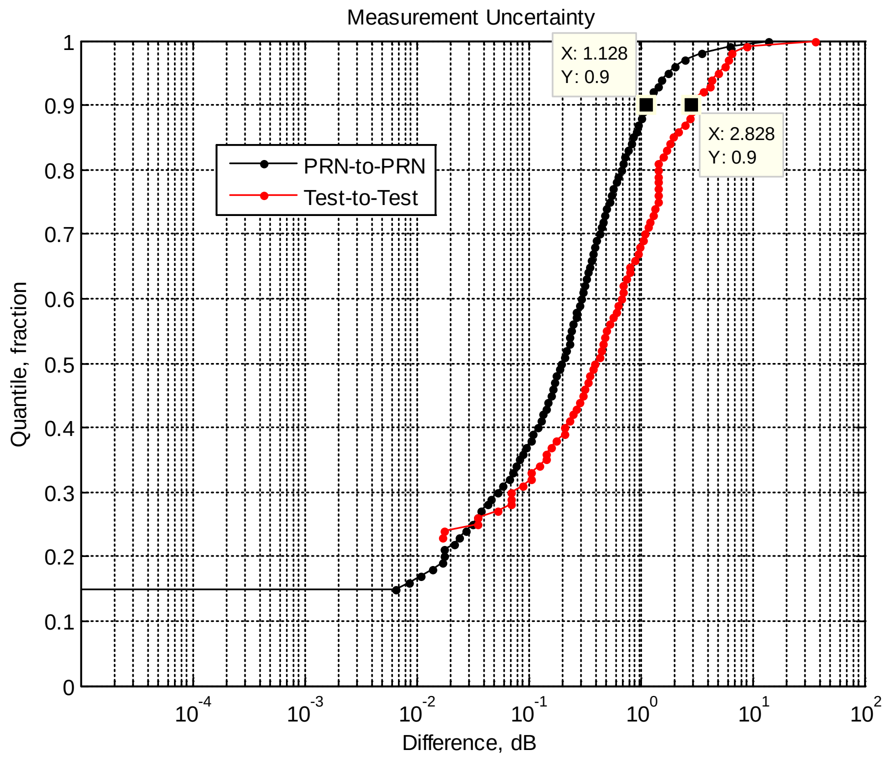

Figure 3-20: CDF of measurement uncertainty calculate from per DUT differences across PRNs (black) and test to test difference (red) for the 10 MHz LTE interference signal

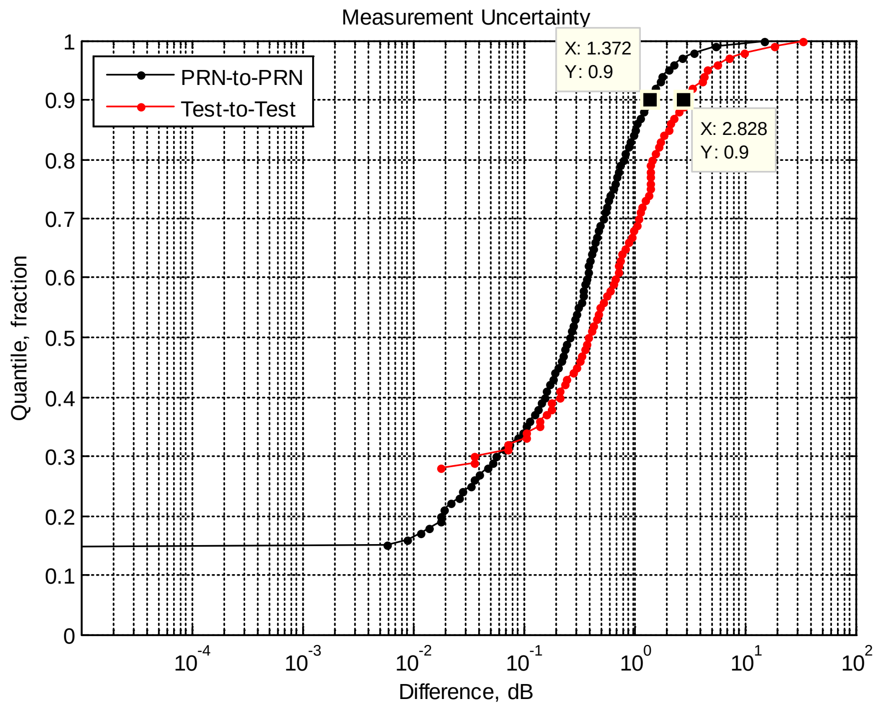

Figure 3-21: CDF of measurement uncertainty calculate from per DUT differences across PRNs (black) and test to test difference (red) for the 1 MHz AWGN interference signal

3.1.7 ITM Aggregation and Test Results

The bounding ITM mask is the one that protects all receivers within a category. The value of the bounding ITM at each frequency is found by taking the minimum of ITM(f) across all receivers in the category (i.e. at a particular frequency, this is the smallest interference power that causes 1-dB degradation for any receiver in the category). Multiple bounding ITMs are generated based by determining one for each interference signal type and GNSS signal combination. The bounding masks for each category corresponding to the 10 MHz LTE interference signal and L1 C/A GPS signal are shown in Figure 3-22. This plot shows the HPR and SPB categories to be the most susceptible in terms of received interference power levels with the cellular category generally being the most tolerant of LTE interference.

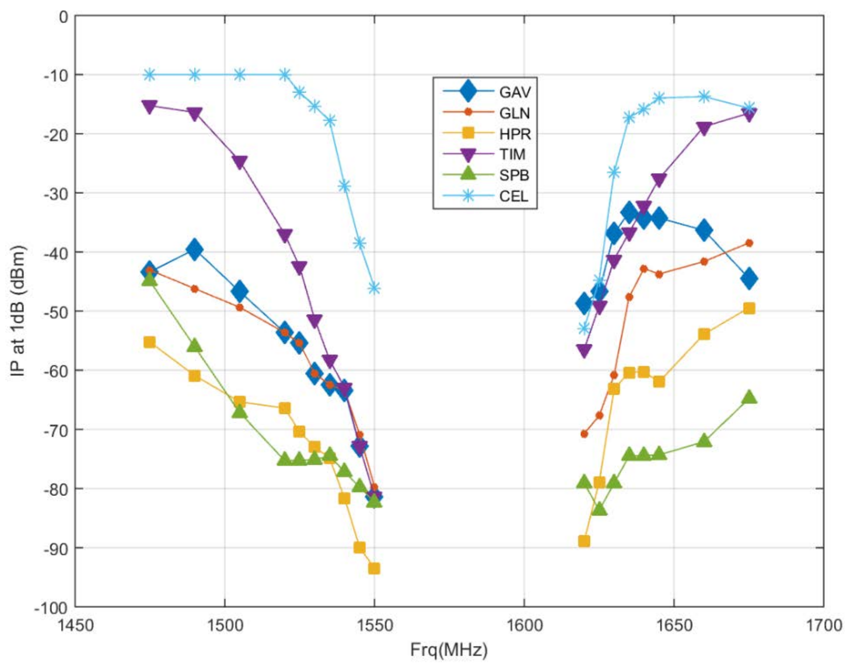

Figure 3-22: GPS L1 C/A bounding ITM for each category of receivers

These ITMs are also calculated for all other emulated GNSS signals. This is shown in Figure 3-23 for the HPR receiver category. Interference power levels from a 10 MHz LTE type signal should not exceed any of the masks depicted in this figure if all GNSS signals are to be protected for the HPR category.

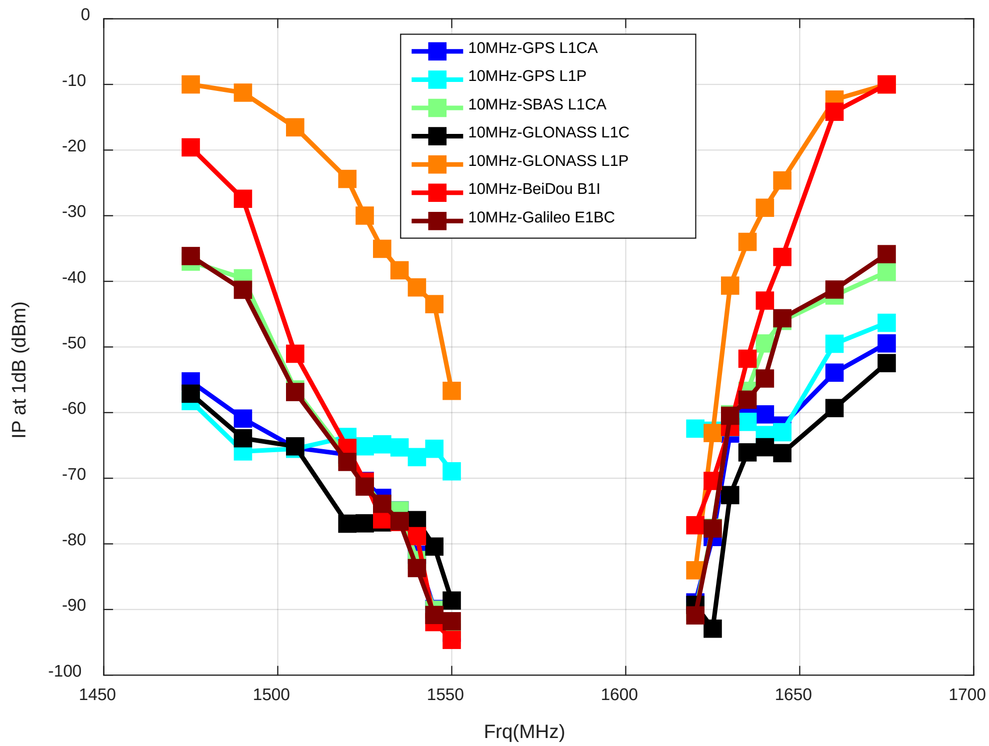

Figure 3-23: HPR bounding ITMs for each of the emulated GNSS signals

Figure 3-24 overlays the HPR bounding ITMs corresponding to both the 10 MHz LTE interference signal (solid lines) and the 1MHz AWGN interference signal (dotted lines). In general, the results show a weak dependence for the bounding ITMs on interference signal type helping to further generalize the results beyond the LTE type signal if needed. An exception to that is the GLONASS L1 P bounding ITM that shows up to 10 dB more sensitivity to the 10 MHz LTE signal. This is likely due to one or more receivers processing GLONASS L1 P signal that did not collect valid data during the 1 MHz interference signal test.

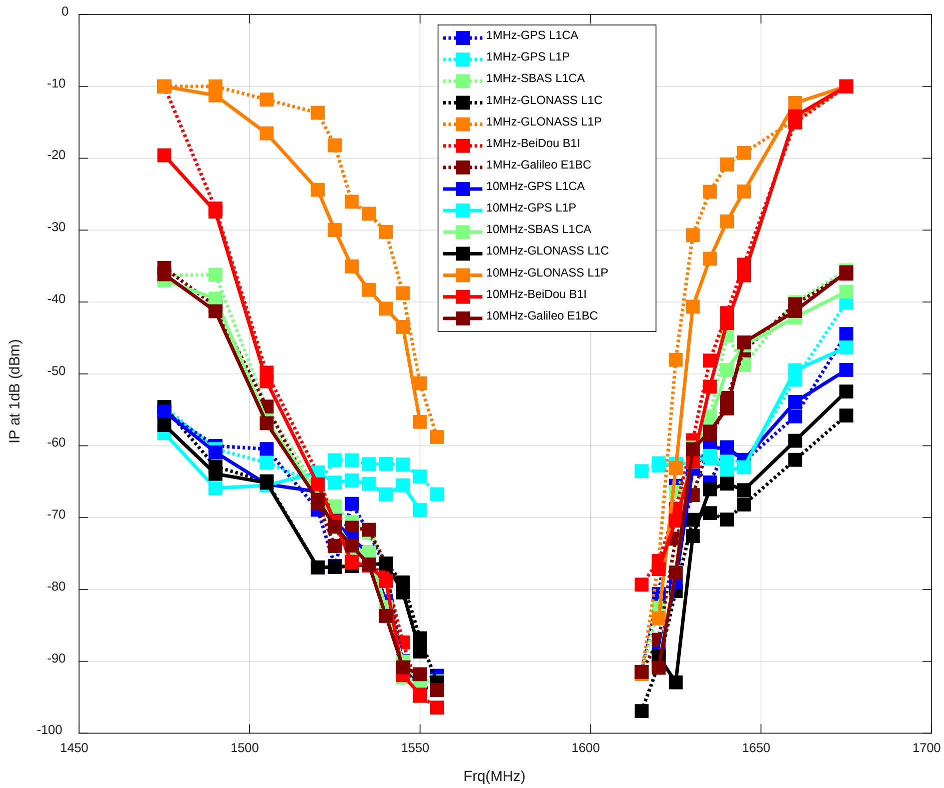

Figure 3-24: HPR Bounding ITMs for each of the emulated GNSS signals. ITM bounding masks for the 1 MHz AWGN and 10 MHz LTE interference signals are shown

Figure 3-25 (a) shows the aggregate result for the HPR category and L1 C/A GPS signal type. The lower and upper bounds, as well as the various percentile levels are presented to give an indication of the data distribution. The lower the percentile level the more protection it offers. For example, the 10th percentile indicates the received interference power level that leaves 10% of the tested receivers unprotected while the 90th percentile is the value that leaves 90% of the receivers unprotected. In order to ensure tolerable level of interference to all tested receivers only the lower bound (or minimum value) is considered. Figure 3-25 (b) shows the same percentile results but for ITMs that protect all emulated GNSS signals processed by the tested HPR receivers. This is done by first calculating the minimum ITM across the supported GNSS signals for each DUT and then calculating the various percentiles across DUTs. These two plots indicate that the interference power levels needed to protect all GNSS signals are generally lower but comparable the L1 C/A ITM levels for the tested receivers.

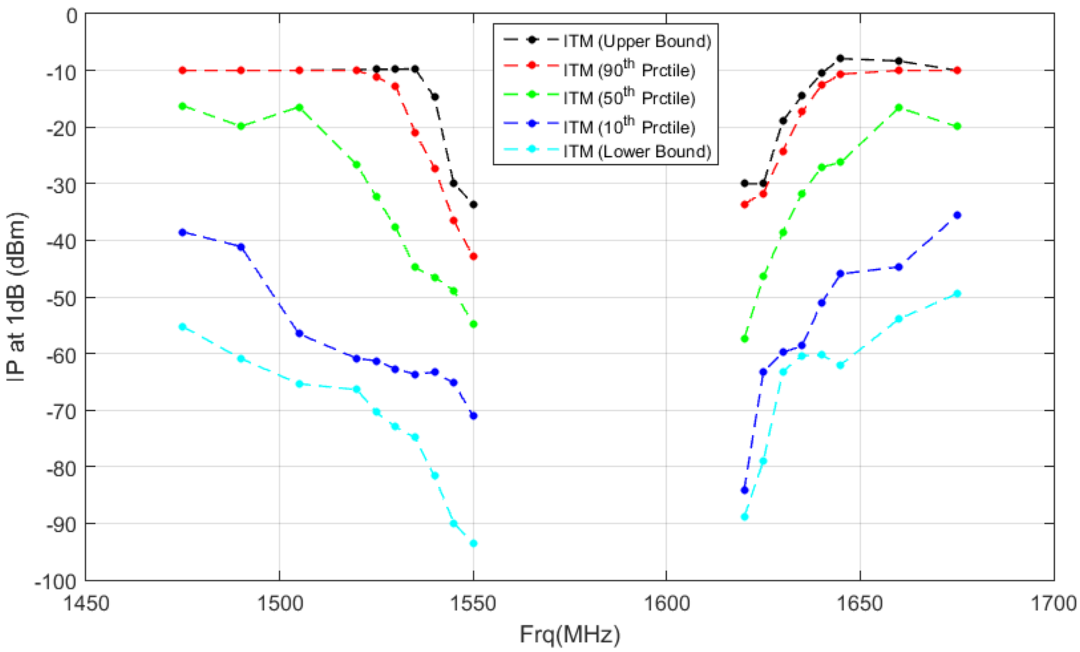

(a)

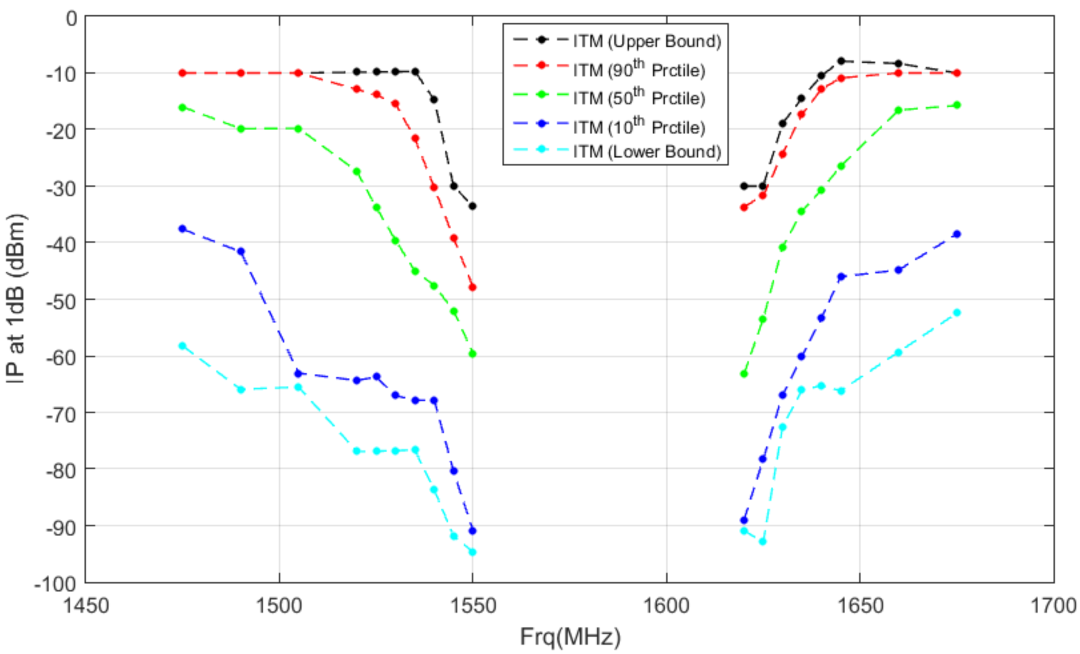

(b)

Figure 3-25: 10 MHz Statistical Mask Results for High Precision receivers for (a) GPS L1 C/A (b) All Emulated GNSS Signals.

A comprehensive set of bounding and statistical ITMs have been produced for all receiver categories and GNSS signal type combinations, and are shown grouped by interference signal type in Appendix B.

These bounding masks can then be used in an inverse modeling analysis to compute the tolerable transmitter EIRP levels corresponding to a given transmit application and use-case parameters. In particular, the bounding masks for the L1 C/A GPS signals are used later in this report to calculate tolerable EIRP levels by receiver application.

3.1.8 Loss of Lock Data Processing

As discussed in Section 3.1.5.2, the ITMs are the interference levels that resulted in a 1 dB degradation in CNR. As illustrated in Figure 3-26, most receivers continued to report CNR measurements after the interference level exceeded the ITM. Within this report, "loss of lock" is defined to be situation in which the interference increased to the point where the receiver ceased reporting CNR for a particular signal and a particular satellite. The "loss of lock" point is interpreted herein to mean that the DUT is no longer able to track that signal type (i.e. L1 C/A).

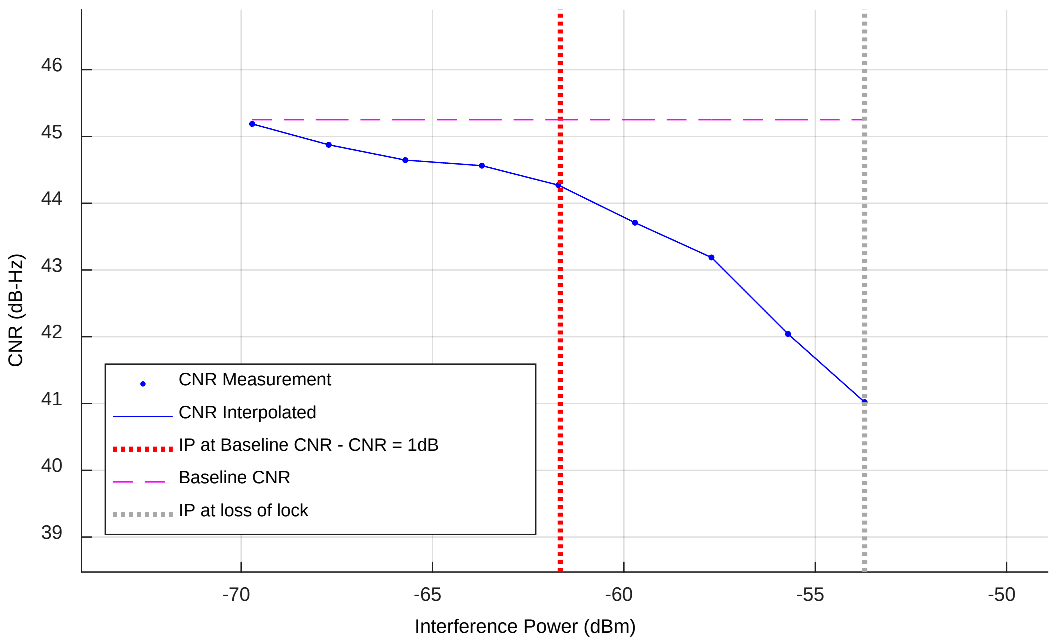

Figure 3-26: Determination of Loss of Lock Interference Level from CNR Data

The processing of CNR to yield interference levels corresponding to loss-of-lock was consistent with the processing used to determine ITMs, with the exception illustrated in Figure 3-26. Namely, that the loss-of-lock interference level was determined based upon the highest level of interference for each signal/satellite for which the DUT reported a CNR value. Although, as discussed in Section 3.1.6.1, collected data for each DUT included a "loss-of-lock indicator" this data was found to be unreliable, not available, or inconsistent amongst DUTs. Therefore, the approach outlined above was adopted to determine the loss-of-lock interference levels.

Two loss-of-lock levels were determined for each DUT, for each interference type, and for each interference frequency:

1. High-elevation satellite – this interference level corresponded to loss-of-lock for the nominally powered GNSS signals (See Table 3-4), i.e., the ones that were not attenuated by 10 dB or 20 dB with respect to the specified minimums in applicable Interface Control Documents or Interface Specifications. This interference level was averaged across all applicable (up to 10) satellites.
2. Low-elevation satellite – this interference level corresponded to loss-of-lock for the GNSS signals that were 10 dB below nominal (see Table 3-4). Only one such signal was broadcast for each GNSS constellation (GPS, GLONASS, Galileo, BeiDou). The "low-elevation" designation is appropriate, since as discussed in Section 3.3 typical DUT antennas provide approximately 10 dB less gain towards low-elevation angle satellites than they do towards zenith. In the chamber testing, the GNSS transmit antenna was at zenith so all GNSS signals arrived from zenith in the testing. This situation is different from the real-world, in which GNSS signals can arrive from all elevation angles in the upper hemisphere.

The loss-of-lock levels computed using the above method should be viewed as the received interference power levels for which there is very high confidence that high- or low-elevation angle satellites are completely unusable by a GPS/GNSS receiver. These estimated loss-of-lock levels may be significant overbounds for several reasons including:

- As noted in Section 3.1.4.1, DUTs in the center of the test grid experienced received GNSS signal levels that were more than 3 dB greater than the minimum specified levels for each GNSS signal type. If they were presented with minimum specified GNSS signal levels, it is likely that these DUTs would lose lock on GNSS signals in the presence of lower levels of interference.
- It is likely that many DUTs continued to track and output C/N_0 for satellites that would no longer be useful for navigation due to poor tracking quality. For instance, many DUTs reported GPS C/A-code C/N_0's below 20 dB-Hz. The GPS C/A-code signal includes 50 bps navigation data that is unencoded (i.e., no forward error correction is utilized). At 20 dB-Hz, the bit-energy to noise density E_b/N_0 is 3 dB and it is not theoretically possible to read the navigation data as necessary for positioning without external assistance. With an E_b/N_0 of 3 dB, it is unlikely that the DUT could track carrier phase to provide a coherent phase reference, but even if it could the probability of correctly decoding a 300-bit GPS navigation data subframe without error is less than 0.0001.

Figure 3-27 and Figure 3-28 show interference powers resulting in loss-of-lock for high-elevation and low-elevation angle satellite GPS C/A-code signals, respectively. The interference powers resulting in loss-of-lock for high elevation angle satellites were typically 15 – 25 dB higher than 1 dB ITMs. The interference powers resulting in loss-of-lock for low elevation angle satellites were typically 5 – 15 dB higher than 1 dB ITMs.

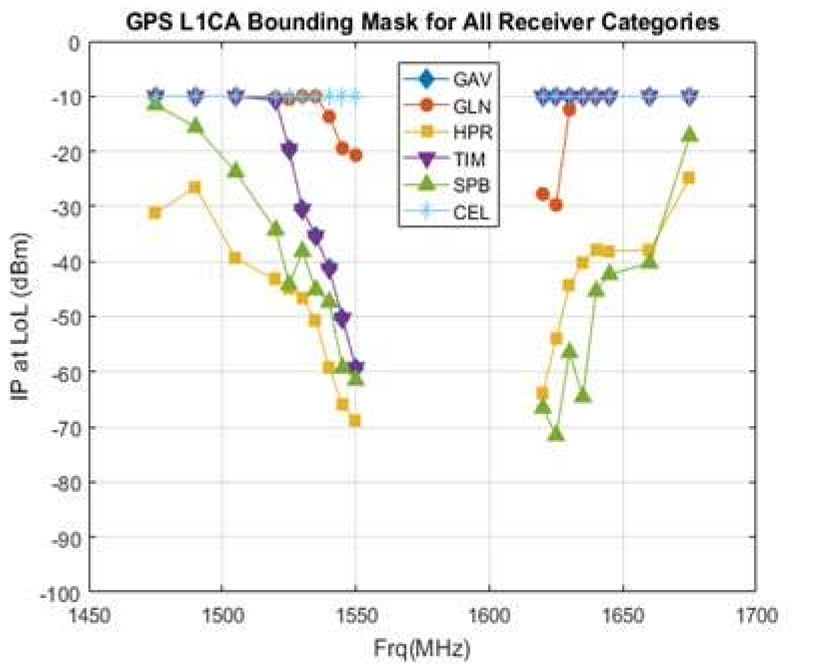

Figure 3-27: Interference Power resulting in Loss of Lock for GPS L1 C/A-code (High Elevation Angle).

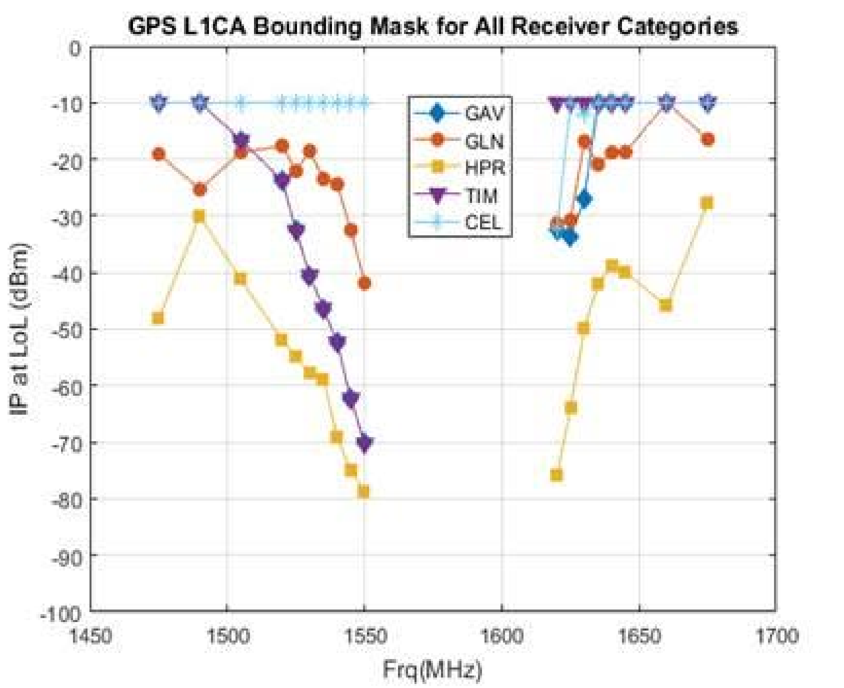

Figure 3-28: Interference Power resulting in Loss of Lock for GPS L1 C/A-code (Low Elevation Angle).

Additional loss of lock results are provided in Appendix C.

3.2 Conducted (Wired) Testing

Wired tests were executed subsequent to WSMR radiated tests for specialized scenarios suited to a laboratory environment. This testing was conducted during July 2016 at Zeta Associates Inc. in Fairfax, VA. The specific objectives for wired testing included: (1) evaluation of the impact of adjacent-band interference on signal acquisition, (2) comparison between wired and radiated receiver susceptibility to adjacent band interference with 1 MHz bandpass noise and 10 MHz LTE (same signals as used in the anechoic chamber), and (3) assessment of the impact of an adjacent band transmitter noise floor (out-of-band to the interference source, in-band to GPS/GNSS) in addition to the fundamental emission.

3.2.1 Devices Test

For this testing, fourteen of the 80 receivers tested at WSMR were selected and provided by USG partners. These receivers covered all GPS/GNSS categories from WSMR except Space Based. The receiver categorization, and specific port location are given in Table 3-8. Notice the majority of receivers tested were from the high precision category.

Table 3-8: Receivers Tested

8-Way Splitter w/Individual Amps. After	8-Way Splitter w/Single Amp. in Front
1. Monitor (spectrum analyzer)	1. TIM
2. HPR	2. GAV
3. HPR	3. HPR
4. CEL	4. HPR
5. GLN	5. HPR
6. HPR	6. HPR
7. HPR	7. HPR
8. Monitor (spiral enclosure)	8. HPR

3.2.2 Signal Generation

Wired testing utilized the same core signal generation equipment as used for radiated testing at WSMR. The conducted circuit is shown in Figure 3-29. In addition to the GNSS playback and SPIGAT systems used at WSMR, a circuit was added for simulating out-of-band emissions (OOBE--lower left in figure where this is added in-band noise to GNSS but out-of-band for fundamental interference signal). The interference, GNSS and OOBE signals are added by a power combiner and conducted to the devices under test via multi-port power splitters with an isolator at each port to prevent port interaction. After the isolator, a broadband LNA provides necessary gain as a substitute for the active antenna in the radiated environment, with test power referenced to the LNA input. To allow static configuration throughout testing, adjustable attenuators were included on the GNSS and OOBE signal paths not only to set proper levels but also to serve as switches (when at high attenuation) for complete removal of these signals as necessary. Other modifications to the interference system included the substitution of a lower power HPA (more than adequate for the reduced attenuation of the conducted path) and a notch filter targeting the RNSS band.

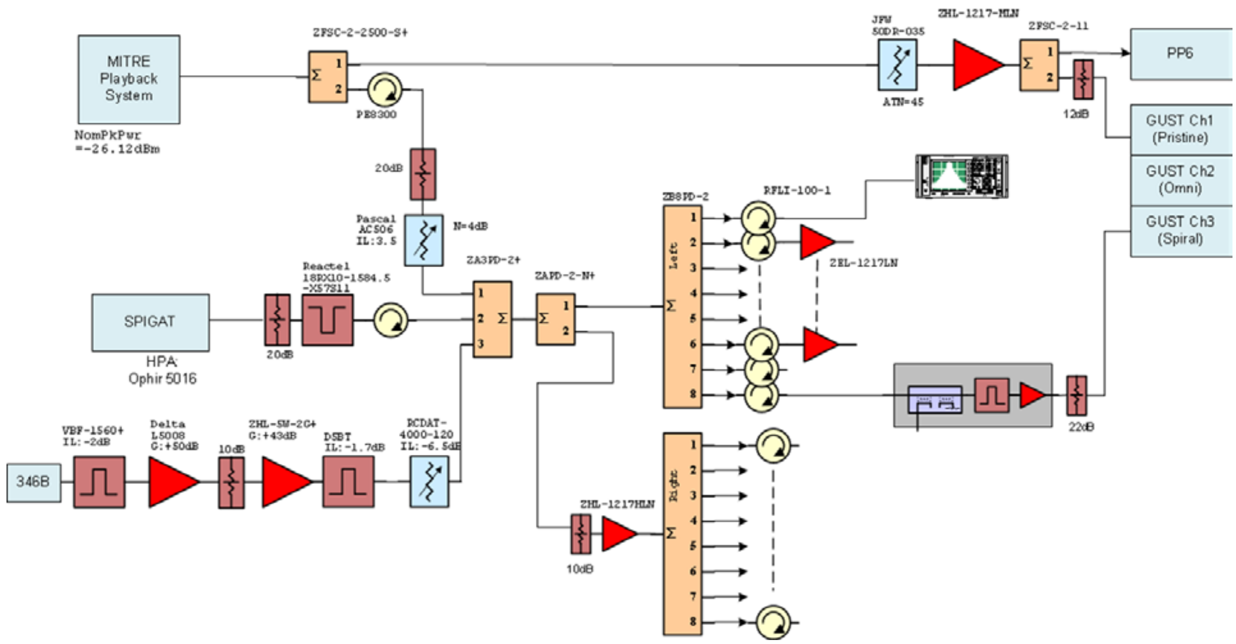

Figure 3-29: Interference System Configuration for Wired Tests

3.2.2.1 Signal Acquisition

Signal acquisition tests were executed at four adjacent-band frequencies using LTE signals at 1525, 1550, 1620 and 1645 MHz. The test sequences removed the GNSS signals for 30 seconds and then allowed at least 90 seconds after they were reintroduced for the receiver to reacquire and track. (The original test plan used 120 seconds to allow GNSS signals to be reacquired, but after analyzing pre-test data it was determined this time could be shortened to 90 seconds to expedite the test.) These tests are therefore more indicative of Warm or Hot Start versus the potentially more challenging acquisition condition of Cold Start. This sequence of removing and reintroducing signals was repeated in sets of five iterations starting with a set where interference was turned OFF. After this quiescent period, the interference was turned ON and after each successive completion of five iterations its power was incremented by 2 dB. Interference power ranged from -60 to -10 dBm for the outer two frequencies (1525 and 1645 MHz) and -80 to -30 dBm for the inner two frequencies (1550 and 1620 MHz). The maximum power tested in each range matched the maximum power used in the baseline LTE tests for these frequencies.

3.2.2.2 Out-of-Band Emissions

Out-Of-Band Emissions (OOBE) refer to the emissions from adjacent frequency band terrestrial deployments into the 1559-1610 MHz band. For OOBE tests, the OOBE circuit generated a flat wideband noise pedestal centered on the RNSS band with spectral density controlled by the programmable attenuator. OOBE density levels used for testing were defined by associating the LTE power levels at the specified maximums of 62 dBm (32 dBW) for base stations and 23 dBm (-7 dBW) for handsets with each wideband OOBE limit as summarized in Table 3-9. The LTE/OOBE ratio is defined at these limits and applied (added) to the target LTE signal power at each point in the test to determine the corresponding OOBE level that should be received. Figure 3-30 depicts the relationship between the OOBE (in dBW/Hz) and LTE power levels (in dBm) at the receiver's RF input port. This relationship is linear with a slope of one since OOBE and LTE signal powers undergo the same path loss (neglecting the slight dependence of path loss on frequency). This figure also shows the approximate OOBE level (horizontal dashed line) for a receiver noise floor of -201.5 dBW/Hz and associated LTE receive power levels (intersection of the dashed horizontal line and LTE receive power vs. received OOBE lines) which would cause a 1 dB CNR degradation for the various handset and base station limits outlined in Table 3-9. Additional details on the conducted testing OOBE levels are provided in Appendix D.

Table 3-9: Ratio of OOBE limit density to LTE power for setting OOBE testing levels

	OOBE density [dBW/MHz]	LTE power [dBW]	ratio OOBE/LTE [dB/MHz]
FCC base station*	-70	32	-102
FCC handset*	-70	-7	-63
Proposed base station**	-100	32	-132
Proposed handset**	-105	-7	-98

* Based upon FCC Mobile Satellite Service Ancillary Terrestrial Component (ATC) rules, contained within Title 47 of the Code of Federal Regulations, Part 25.

** Based upon characteristics of a proposed adjacent-band LTE network.

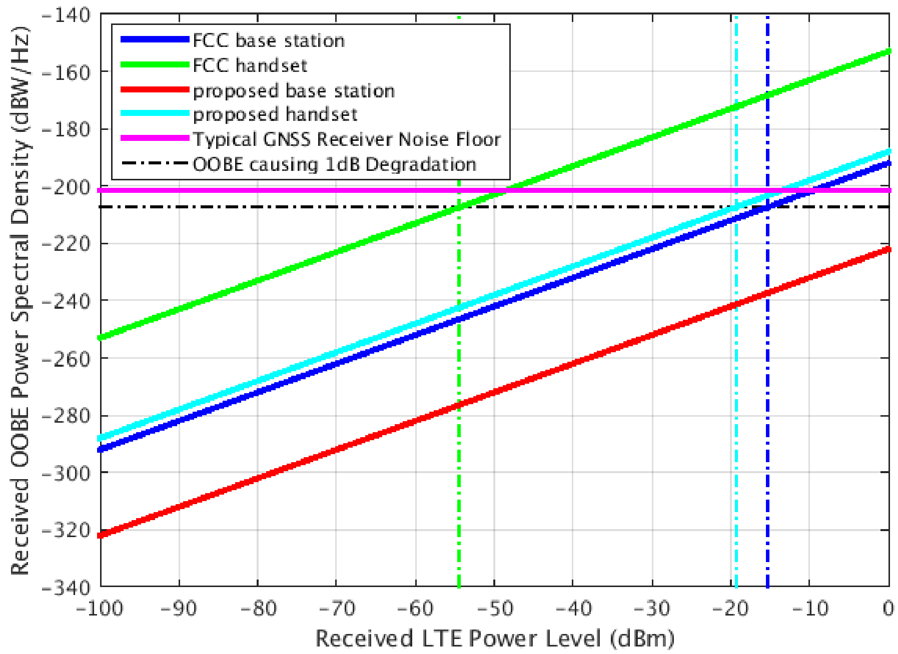

Figure 3-30: OOBE Levels Associated with LTE Signal Power used in Testing

3.2.3 System Calibration

Calibration of SPIGAT was accomplished in the same fashion as described for WSMR with 22 CW tones at each frequency and measuring with a spectrum analyzer to generate a bias table. The spectrum analyzer in this instance was connected to the power splitter versus the cavity backed spiral in the chamber. The GNSS playback signal levels were verified by showing CNR estimates from the GPS receiver used for monitoring at WSMR matched the levels observed in this laboratory setting.

3.2.4 Test Sequence

Wired tests were executed for baseline 1 MHz bandpass noise and 10 MHz LTE signals, FCC and proposed OOBE levels, and signal acquisition. Tests were numbered 10 through 18 with Table 3-10 summarizing the test schedule.

Table 3-10: Wired Test and Data Summary

Day of Week (25-29 July 2016)	Test and Number
Monday	Type 2 – Test10 Type 1 – Test11
Tuesday	Type 2 w/OOBE FCC – Test12 Acq. @ 1525 MHz – Test13 (120 sec. dwell)
Wednesday	Test14 stopped early/network issue Acq. @ 1620 MHz – Test15
Thursday	Acq. @ 1645 MHz – Test16 Acq. @ 1550 MHz – Test17
Friday	Type 2 w/Proposed OOBE – Test18

3.2.5 Data Processing

The following sections detail results from the wired testing for GPS L1 C/A processing only. Processing for wired results followed the approach discussed above for determining 1 dB CNR degradations as a function of interference power. Signal acquisition processing required its own considerations and is discussed in that section.

3.2.5.1 Comparison Tests

The comparison tests were intended to demonstrate equivalence between the radiated and wired test environments. Two example results of interference power causing 1 dB CNR degradation are shown in Figure 3-31 for the LTE interference signal. Example (a) in this figure compares results for a high precision receiver. Here performance matches very well for frequencies closest to the RNSS band while for frequencies further away the radiated performance is superior. This divergence is an expected result since at WSMR the receiver used its native antenna which included some filtering (along with a low noise amplifier) which served to suppress peripheral interference. The difference, therefore, is directly related to not having this filter/LNA module available in the wired testing. Example (b) of that same figure is a case where the antenna was integrated with the enclosure. For wired testing the signal could be inserted directly after the passive element. In this instance, the radiated and wired results match very closely because both include all components influencing mitigation of adjacent interference. In general, comparisons of radiated and wired tests showed expected agreement with differences attributable to bypassing of active antennas in the wired test.

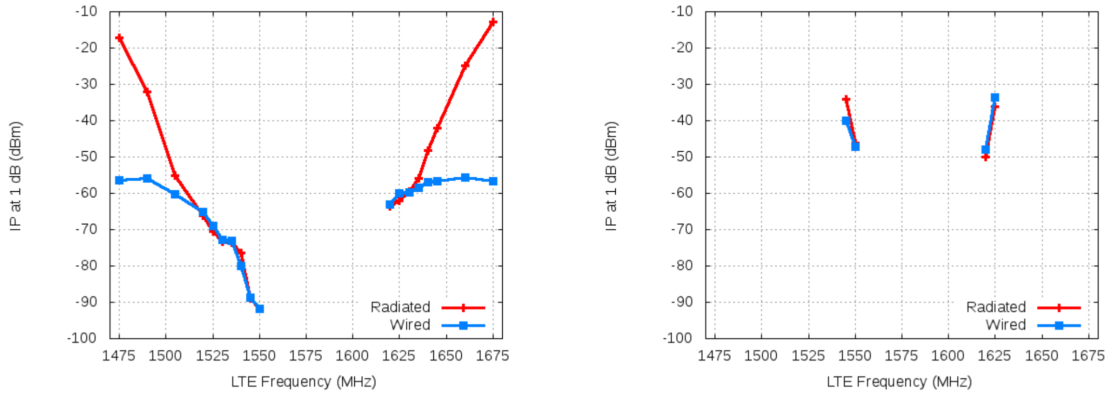

(a) **(b)**

Figure 3-31: Comparison of IP causing 1 dB degradation for the LTE Interference Signal from Radiated and Wired Testing for: (a) High Precision receiver and (b) Cellular device.

3.2.5.2 OOBE Results

Tests conducted with OOBE were executed by adding noise in the RNSS band as shown in the wired test description. Figure 3-32 provides examples of two receivers with significantly different rejection performance for adjacent band interference. These examples show baseline (wired) performance of interference power causing a 1 dB degradation contrasted with OOBE performance for FCC prescribed and proposed levels for one applicant. As Figure 3-30 predicted, receiver performance can be impacted by inclusion of OOBE at FCC base station and FCC handset levels. This result is clearly demonstrated in (b) since this receiver provides good rejection of adjacent interference and therefore inclusion of noise in the RNSS band results in 1 dB CNR degradation not observed with the baseline test. The most distinct difference in performance is evident for handset frequencies, where adding OOBE at the FCC limits result in 1 dB CNR degradation at approximately -50 dBm compared with much more robust performance when OOBE is not included. The proposed base station OOBE limits did not result in 1 dB CNR degradation with the LTE power levels tested and for proposed handset limits the 1 dB CNR degradation level was observed at approximately -15 dBm : In context of distance and presuming complete rejection of adjacent band interference, the proposed OOBE limits for base station and handsets suggest 1 dB CNR degradation could be expected within approximately 4 meters (3.5 m) and 2 meters, respectively. These numbers were obtained for a receiver noise level of -201.5 dBW/Hz and assuming free space path loss and an omnidirectional transmitter antenna gain pattern.

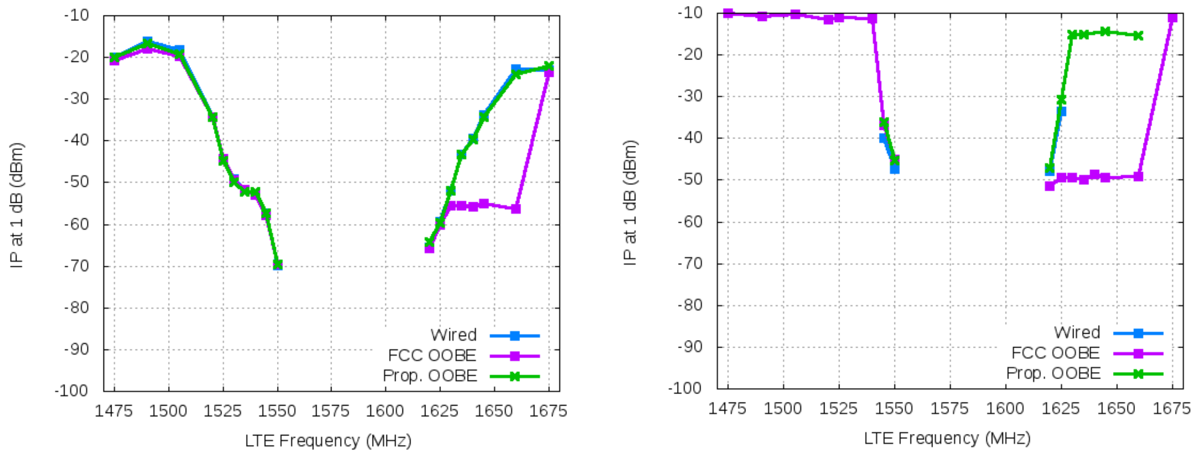

(a) **(b)**

Figure 3-32: Interference power causing 1 dB CNR degradation for baseline and OOBE tests for (a) High Precision receiver and (b) Cellular device.

3.2.5.3 Acquisition Results

Receiver acquisition tests were processed to show both average acquisition time, and the interference power level when receivers could no longer acquire. Acquisition time was computed for L1 C/A signals at the specified minimum power level (-128.5 dBm for L1 C/A) and also for one satellite that was set 10 dB lower to represent low elevation or challenged environments. For the specified minimum signals, the acquisition time was defined as the receiver acquiring and tracking four or more of these satellites. Since more than four satellites are generally in view at the specified minimum levels this is considered a modest criterion for establishing acquisition. For the low elevation satellite, the acquisition time was simply when this satellite was first acquired and tracked. At each interference power level, acquisition time from the five iterations was averaged to provide a single value. Note that at each power step an acquisition time was computed only if the receiver met the acquisition criterion for all five iterations.

The results from all receivers tested were compiled for each test frequency and are shown in Figure 3-33 through Figure 3-36. Figure "(a)" provide the number of receivers satisfying the acquisition criteria for specified minimum ("ICD Min. Power") and low elevation ("Low Elevation") signals. Additionally, the figure shows the number of receivers at each interference power step where the CNR degradation is less than 1 dB ("IP @ 1 dB"). For example in Figure 3-33 (a), there were two receiver where the interference power associated with their 1 dB CNR degradation was less than the starting power level of -60 dBm and therefore this count starts at ten. This figure shows further that this count of "IP at 1 dB" appears closely associated with the number of receivers capable of acquiring the signal emulating low elevation conditions.

For the GPS receivers tested, the 1 dB C/N0 degradation point can be an indicator of negative impact to signal acquisition time in low elevation satellite conditions.. Figure "(b)" show average acquisition time for specified minimum and low elevation signals and generally demonstrate acquisition degradation with increasing interference power.

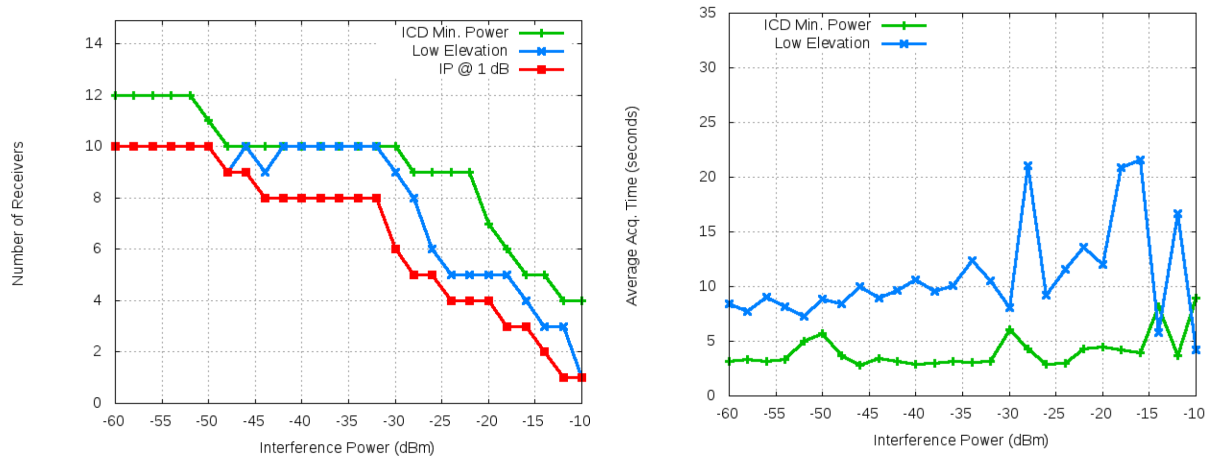

(a) **(b)**

Figure 3-33: Summary acquisition performance for 1525 MHz for ICD minimum and low-elevation satellites. (a) Number of DUTs, and (b) average acquisition time.

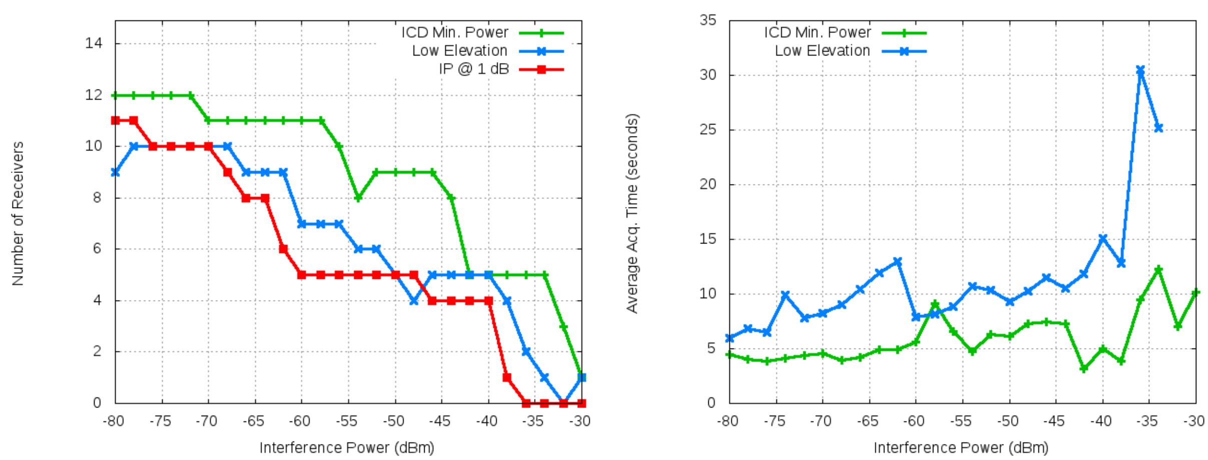

(a) **(b)**

Figure 3-34: Summary acquisition performance for 1550 MHz for ICD minimum and low-elevation satellites. (a) Number of DUTs and (b) average acquisition time.

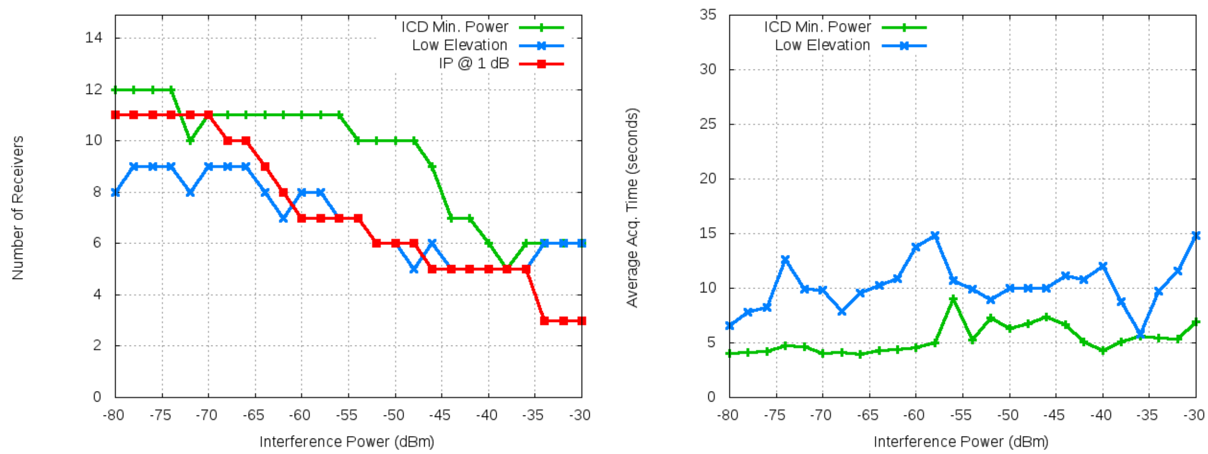

(a) (b)

Figure 3-35: Summary acquisition performance for 1620 MHz for ICD minimum and low-elevation satellites. (a) Number of DUTs, and (b) average acquisition time.

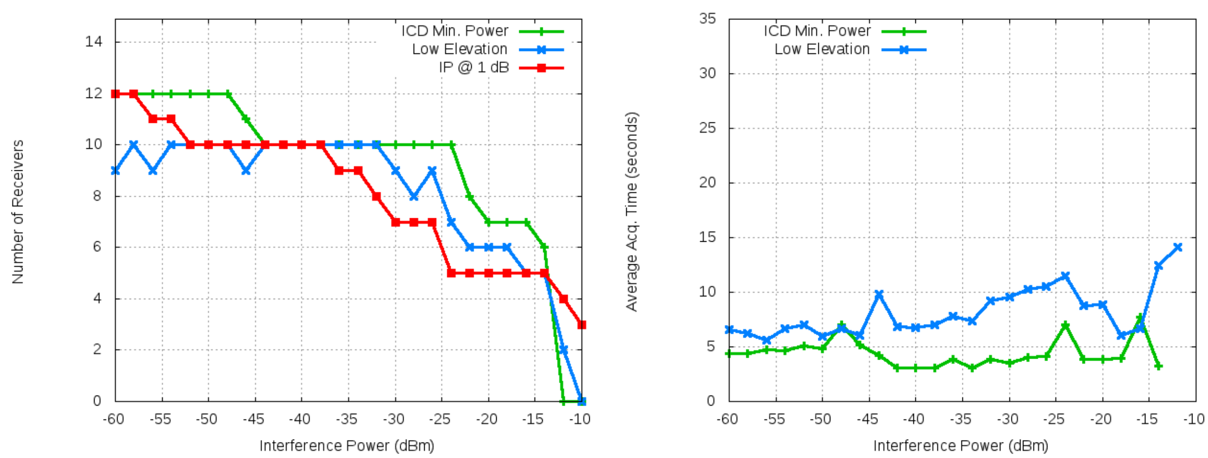

(a) (b)

Figure 3-36: Summary acquisition performance for 1645 MHz for ICD minimum and low-elevation satellites. (a) Number of DUTs, and (b) average acquisition time.

3.3 Antenna Characterization

Twenty GNSS antennas, most of which were involved in the WSMR testing, were characterized with respect to frequency selectivity, elevation pattern, and RF gain/compression characteristics through anechoic chamber/live-sky/RF measurements in order to help interpret the WSMR test results and facilitate the calculation of tolerable transmit power.

A representative set of antennas was characterized though a set of activities including:

1) Anechoic chamber measurements - From June through August 2016, the gain patterns for 14 external antennas were measured in an anechoic chamber at MITRE in Bedford, MA.

2) Live-sky C/N_0 measurements – In August 2016 and February 2017, the relative gain patterns of five antennas that were integrated with GNSS receivers were estimated using live-sky GPS C/A-code C/N_0 measurements.
3) Active sub-assembly measurements - From August through October 2016, the gain and compression characteristics of the active subassemblies of four external antennas were measured at Zeta Associates in Fairfax, VA.

The following subsections describes these antenna characterization activities and the resultant measurements.

3.3.1 Selected Antennas

Table 3-11 lists the antennas that were characterized.

Table 3-11: Characterized GNSS Antennas

Manufacturer	Model	Characterization Approach
AeroAntenna	AT575-142-614-50	Anechoic chamber
AeroAntenna	AT2775-42SYW	Anechoic chamber
Arbiter	AS0087800	Anechoic chamber
Garmin	EDGE 1000	Live-sky C/N_0 measurement
Garmin	eTrex 20x	Live-sky C/N_0 measurement
Garmin	GA-25	Anechoic chamber
Garmin	GA-38	Anechoic chamber
Garmin	GPSMAP 64	Live-sky C/N_0 measurement
Hemisphere	804-3059-0	Anechoic chamber
Javad	Triumph-1	Live-sky C/N_0 measurement
Leica	AX1202GG	Anechoic chamber and active sub-assembly measurements
Navcom	82-001020-3001LF	Anechoic chamber
PCTel	3977D	Anechoic chamber
Samsung	S5	Live-sky C/N_0 measurement
Trimble	Bullet 360 Antenna 101155-10	Anechoic chamber
Trimble	Choke Ring 29659-00	Anechoic chamber and active sub-assembly measurements
Trimble	Zephyr 41249-00	Anechoic chamber
Trimble	Zephyr Geodetic 2 55971-00	Anechoic chamber and active sub-assembly measurements
Trimble	TRM59800 module	Active sub-assembly measurements
u-blox	ANN-MS-0-005	Anechoic chamber

3.3.2 Chamber Measurements

Two-dimensional (elevation and azimuth) gain patterns for incident signals of four polarization types, right hand circularly polarized (RHCP), left hand circularly polarized (LHCP), vertically polarized (V), and horizontally polarized (H) were measured at 22 frequencies: 1475, 1490, 1495, 1505, 1520, 1530, 1535, 1540, 1545, 1550, 1555, 1575, 1595, 1615, 1620, 1625, 1630, 1635, 1640, 1645, 1660, and 1675 MHz. The measurements were made in a 30 ft × 21 ft × 15 ft anechoic chamber at MITRE in Bedford, MA. A calibrated, automated antenna measurement system developed by Nearfield Systems was utilized.

All 14 antennas were active, and the gains measured were thus a combination of passive element gain and amplifier gain. Absolute gain of the passive elements of each active antenna was not directly observable without breaking into the antennas. Antenna directivity, however, was calculated from the patterns using Nearfield Systems' NSI2000 software.

Figure 3-37 and Figure 3-38 provide some example results. Figure 3-37 shows the frequency selectivity of the 14 antennas for incident RHCP signals as seen at antenna boresight. Note the wide variation in selectivity to adjacent-band signals. Figure 3-38 shows the relative RHCP antenna gain vs off-boresight angle at 1575.42 MHz for the 14 antennas. Each curve is normalized to 0 dBic gain at boresight. In this figure, each point in the plotted results represents an average across 180 deg of azimuth. The red vertical lines correspond to 5 deg elevation angle on either side of the antenna. Additional measurements are provided in Appendix E.

The boresight directivities of the 14 measured antennas for RHCP signals at 1575.42 MHz varied from 3.2 dBic to 8.0 dBic with a mean directivity of 5.4 dBic. Assuming 90% efficiency for all of the antennas yields a rough estimate for passive element gains ranging from 2.7 dBic to 7.5 dBic with a mean of 4.7 dBic. In the WSMR radiated chamber testing, all of the tested receivers' antennas were boresighted at the transmitting GNSS signal and interference generator antennas.

The measured relative antenna gain patterns can be utilized to model what gains would be seen towards GNSS satellites and interference sources at other elevation angles in the "real world". For instance, the results in Figure 3-38 justify the interpretation of the GNSS signal levels that were generated at -10 dB power relative to specified minimum levels in the WSMR radiated testing as corresponding to what would be seen in the real world towards low elevation angle satellites for many of the tested antennas (note that the data in Figure 3-38 indicates relative gains ranging from -3 dB to -15 dB for gain towards a satellite at 5 deg elevation above the horizon vs gain towards a satellite at zenith).

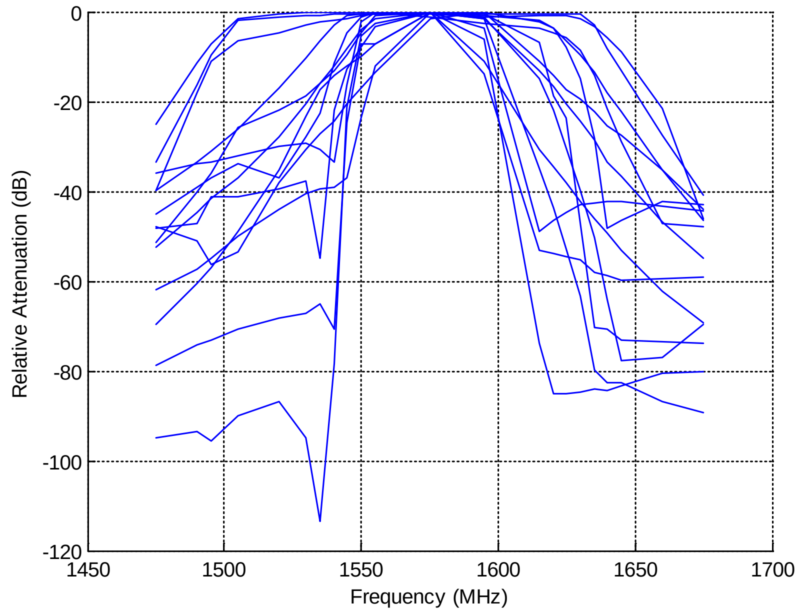

Figure 3-37: Frequency Selectivity of the 14 External Antennas

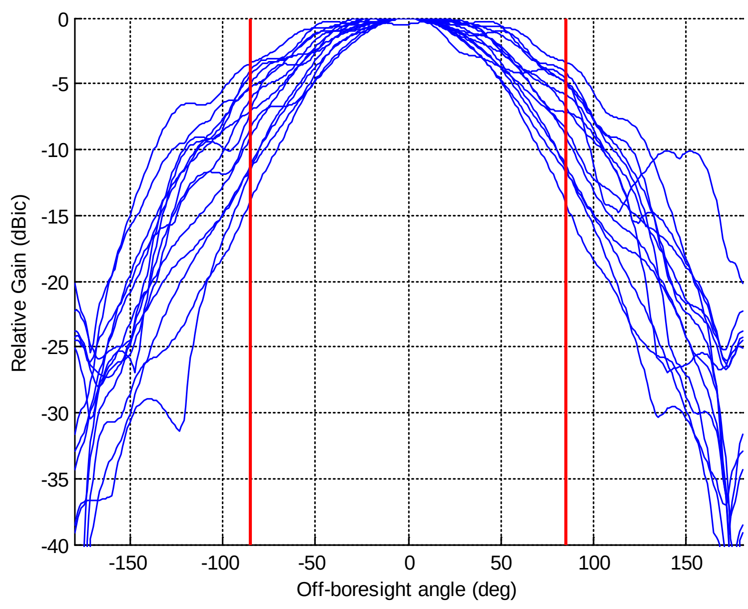

Figure 3-38: Relative RHCP Gain Patterns of the 14 Antennas at 1575 MHz (red vertical lines correspond to 5 deg elevation angle)

3.3.3 Live-Sky Measurements

Some of the GNSS receivers tested at WSMR utilize integrated antennas. Estimates of their relative antenna gain patterns at 1575 MHz were obtained through measurements of GPS C/A-code C/N_0 over short time intervals in an outdoor environment in two locations (rooftop of a building at MITRE's Bedford, MA complex and at Zeta's Fairfax, VA location) with clear sky views. Estimated relative gain pattern results using this method for four integrated GLN antennas are shown in Figure 3-39 and for an integrated HPR antenna in Figure 3-40. Measured GPS C/A C/N_0 from a cellular device is shown in Figure 3-41 as a function of azimuth and elevation. Based on analysis of this data and cellular GPS antenna design, placement and performance, the use case analysis that follows simply assumed 0 dBi for antenna gain in all directions.

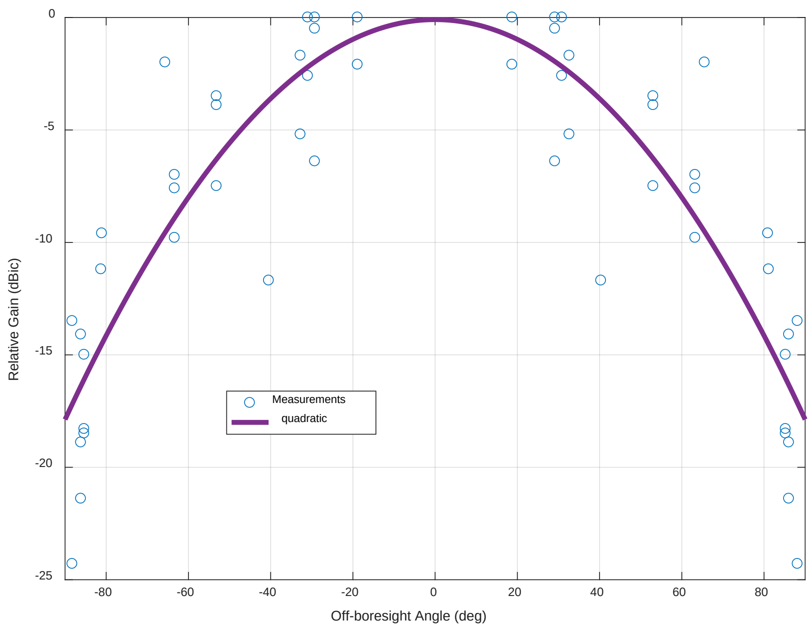

Figure 3-39: Relative L1 RHCP Antenna Gain Estimated from Live-sky C/N0 Measurements for Three GLN Integrated Antennas and Quadratic Fit

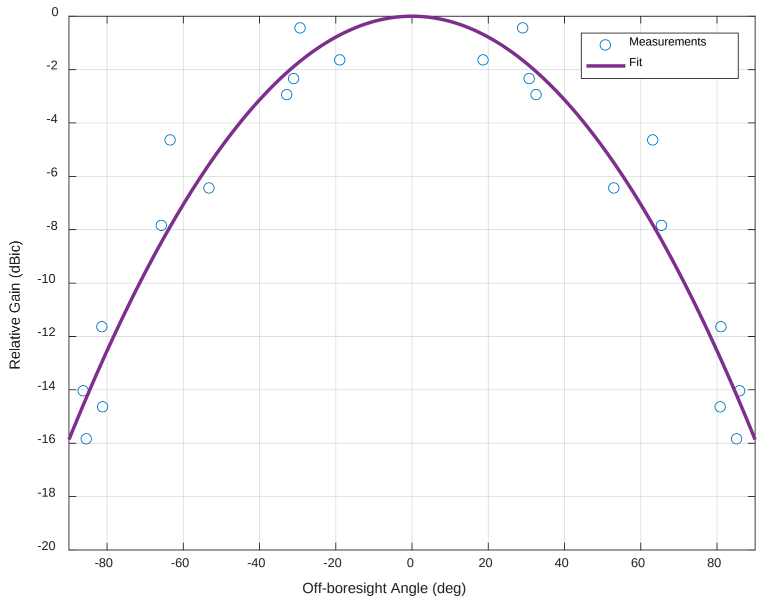

Figure 3-40: Relative L1 RHCP Antenna Gain Estimated from Live-sky *C/N₀* Measurements for an Integrated HPR Antenna and Quadratic Fit

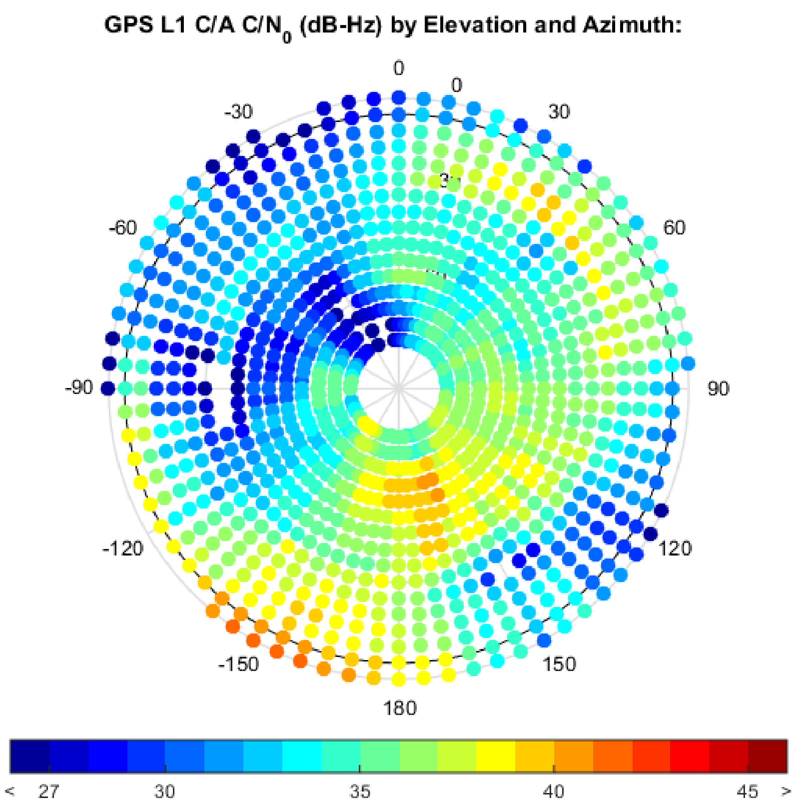

Figure 3-41: Live-sky C/N_0 Measurements for a CEL Device

3.3.4 Bench Test Measurements (Active Sub-assembly Measurements)

Bench test measurements were conducted on a further reduced set of antennas at Zeta to characterize key filter/LNA performance parameters. The antennas were dissembled to access the passive element connection to the filter/LNA assembly and then the response measured with a network analyzer from approximately 1 GHz to 2 GHz. The LNA was powered for this testing by inserting a bias-T on the RF output path and applying the required DC power. Results from three antennas tested are shown in Figure 3-42 where each has been normalized for the measured gain at GPS L1. These three antennas types were utilized at WSMR and as MITRE testing demonstrated have vastly different characteristics presumably to meet their respective functions. One of the filter/LNA devices was relatively narrowband and only passes GPS L1, another was wider and clearly intended to pass both GPS and GLONASS L1, and lastly, the third device was much wider and intended to pass MSS signals, GPS and GLONASS L1.

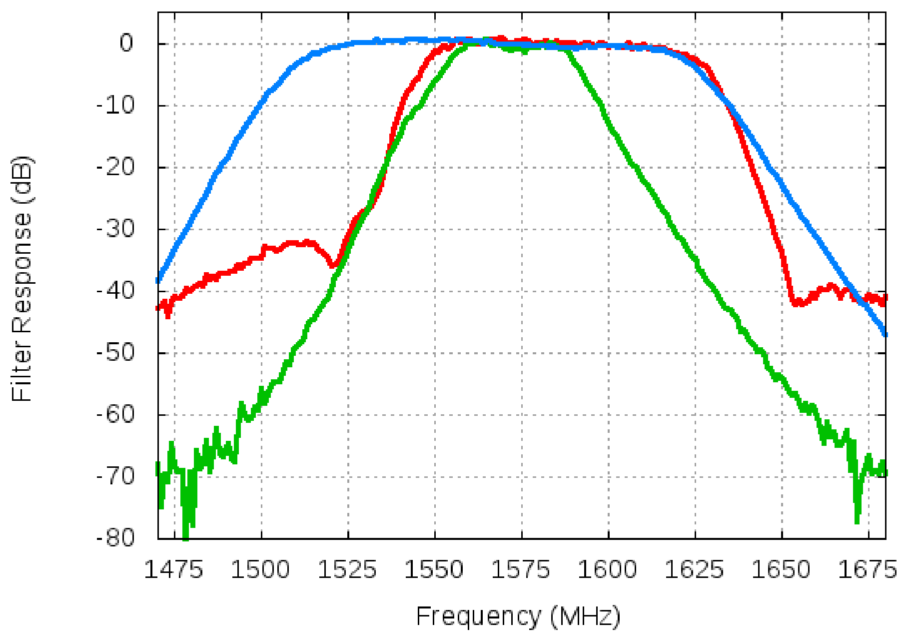

Figure 3-42: Normalized Filter/LNA Responses measured with Bench Testing

In addition to characterizing each assemblies response versus frequency, the devices were also tested with a spectrum analyzer using "Intermod (TOI)" instrument software at the GPS L1 frequency to understand typical LNA characteristics of gain, 1dB compression (P1dB), input and output third-order intercept points (IIP3 and OIP3) (in-band only). These results are shown in Table 3-12 and again demonstrate the significant diversity observed with fielded GNSS antennas.

Table 3-12: LNA Performance Characteristics measured with Bench Testing

Measurement at L1	Assembly #1	Assembly #2	Assembly #3
Gain (dB)	28	40	49
IIP3 (dBm)	-12.7	-39.6	-29.3
OIP3 (dBm)	14.4	-1.4	17.7
Input P1dB (dBm)	-25	-50	-42

The results of the antenna characterization indicate there is a very wide range of up to 80 dB in selectivity farther away from the GPS band (1500/1650 MHz), which can explain the observed 50-dB range in IP for 1 dB CNR degradation. This variation in selectivity is most pronounced for HPR devices, due to the fact that many HPR devices are designed to receive both GNSS signals in the 1559 – 1610 MHz band as well as augmentation data over MSS satellites in the 1525 – 1559 MHz band. HPR devices that are not designed to process MSS signals also tend to utilize wider bandwidths relative to other DUT categories to provide increased measurement precision in the presence of multipath. There is a much narrower range up to 20 dB in selectivity close to the GPS band (1550/1600 MHz) which is lower than the IP for 1 dB CNR degradation observed for these frequencies.

Although changing antennas was not the focus of this effort, cost, viability, etc. should be considered to determine the feasibility of such a solution. Antenna filtering can cause deleterious effects on receiver performance, such as group delay and other distortions. Also, many HPR DUTs are designed to receive augmentation data via MSS and to retain this functionality the receiver passband needs to continue to extend into the applicable portion of the 1525 – 1559 MHz band.

4. TRANSMIT POWER LEVEL ANALYSIS (EXCLUDING CERTIFIED AVIATION)

4.1.1 Approach

This section derives the transmit EIRP levels that can be tolerated by each category of GPS/GNSS receivers except for certified aviation. Two complementary analyses are performed. The first is a forward modeling approach that calculates the receive power map for a given EIRP level and network deployment type. The receive power map is compared with the ITM(f), where f is the frequency of interest, to identify the region where the corresponding category of receivers is not protected from adjacent band interference. The second is an inverse modeling analysis that calculates the tolerable EIRP for any given separation distance between the transmitter and user's receiver over a range of receiver heights.

For the transmit power level analysis, it is necessary to characterize the proposed transmitter network deployment and the GPS/GNSS receiver use case scenarios. To ensure compatibility with all receivers within a category, the bounding ITMs from Section 3 are used. The use of the bounding ITMs ensures that the resultant EIRP values will protect 100% of the receivers tested.

4.1.2 Network Transmitter Parameters

Representative parameters for adjacent-band LTE networks were identified primarily from three sources:

1) International Telecommunication Union Radiocommunication Sector (ITU-R) reports and recommendations.
2) Federal Communication Commission (FCC) Mobile Satellite Service Ancillary Terrestrial Component (ATC) rules, contained within Title 47 of the Code of Federal Regulations, Part 25 (47 CFR 25).
3) Proposals for adjacent-band networks contained within FCC filings.

4.1.2.1 Base Stations

Report ITU-R M.2292 (henceforth "M.2292") provides "Characteristics of terrestrial IMT-Advanced systems for frequency sharing/interference analyses." [3] For the 1-2 GHz band, these include the characteristics listed in Table 4-1 for five deployment types.

Table 4-1: Base Station Characteristics from M.2292

	Macro rural	Macro suburban	Macro urban	Small cell outdoor/Micro urban	Small cell indoor/Indoor urban
Cell radius/ Deployment density	> 3 km (5 km typical)	0.5 – 3 km (1 km typical)	0.25 – 1 km (0.5 km typical)	1 – 3 per urban macro cell, <1 per suburban macro site	Depending on indoor coverage/capacity demand
Antenna height	30 m	30 m	25 m	6 m	3 m
Sectorization	3 sectors	3 sectors	3 sectors	Single sector	Single sector
Downtilt	3 deg	6 deg	10 deg	not applicable	not applicable
Antenna polarization	+/-45 deg	+/-45 deg	+/-45 deg	Linear	Linear
Maximum antenna gain	18 dBi	16 dBi	16 dBi	5 dBi	0 dBi
Maximum EIRP/sector*	61 dBm	59 dBm	59 dBm	40 dBm	24 dBm

*Values shown for this parameter are for 10-MHz LTE signals.

For macrocells, the cell radius and intersite distance are defined in Figure 4-1. Note that for macrocells, the parameters A and B in the figure have the relationship $B = 3A/2$. For small cells, each base station is located at the center of a cell resulting in an intersite distance $B = \sqrt{3}A$.

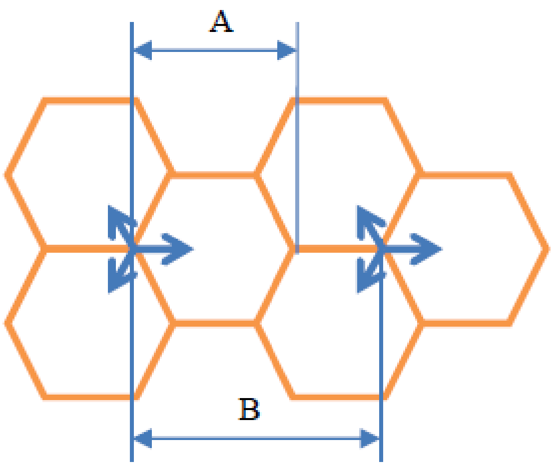

Figure 4-1: Macrocell Radius and Intersite Distance are *A* and *B*, respectively. Each hexagon is referred to as either a sector or cell.

M.2292 references Recommendation ITU-R F.1336 (henceforth “F.1336”) for recommended antenna gain patterns for each deployment type and provides input parameters. The normalized gain patterns for the macro deployments are shown in Figure 4-2 and for the small cell deployments in Figure 4-3.

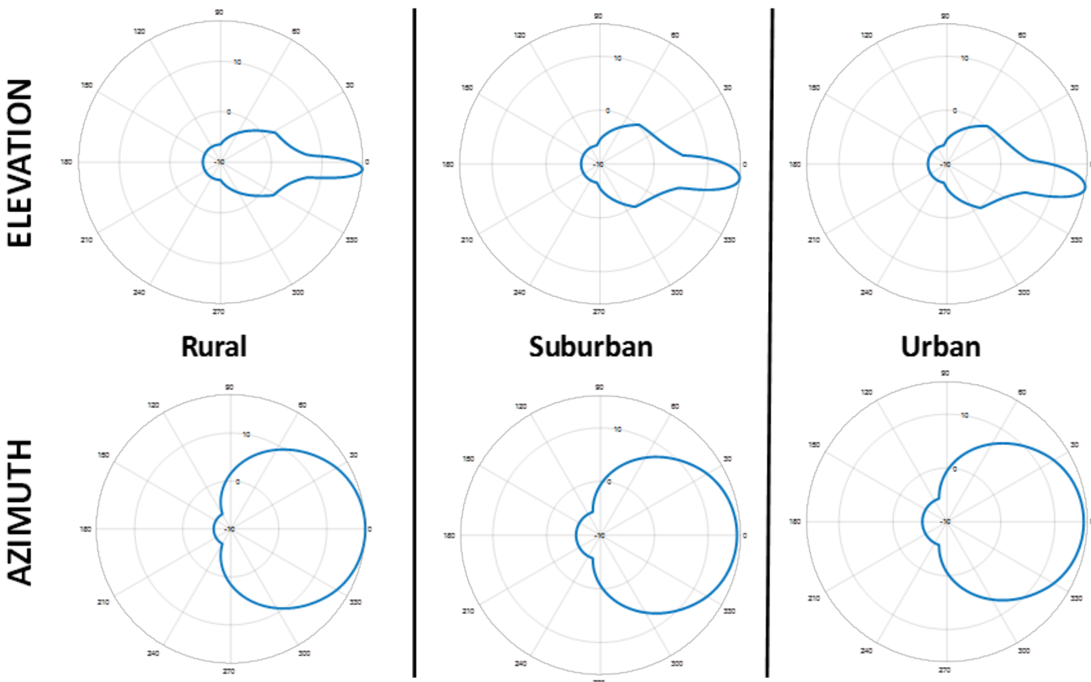

Figure 4-2: Macro Base Station Antenna Gain Patterns (top – elevation; bottom – azimuth)

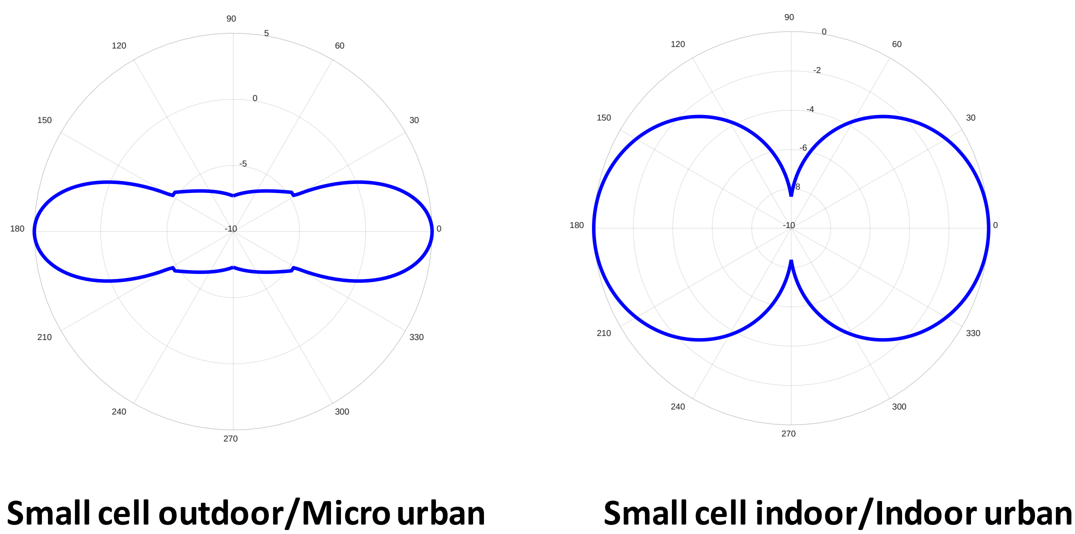

Figure 4-3: Small cell Base Station Antenna Gain Patterns (elevation patterns shown; both patterns are omnidirectional in azimuth)

M.2292 indicates that base stations are only active 50% of the time, resulting in a time-average EIRP that is half of the maximum value shown in Table 4-1. This EIRP reduction was not utilized to be conservative, noting that a base station could be operating with 100% loading for long enough periods to cause disruptions to GNSS receivers. Also for conservatism, the "peak" side-lobe gain patterns from F.1336 were used, as opposed to the "average" side-lobe gain patterns. As suggested in F.1336, the average side-lobe patterns may be more appropriate for studies involving an aggregation of base stations.

For the certified aviation analysis conducted by the FAA, a base station antenna gain pattern based upon a specific LTE network proposal was utilized. See Appendix G.

4.1.2.2 Handsets

For handsets, M.2292 recommends modeling the antenna gain pattern as -3 dBi in all directions with a maximum power supplied to the antenna of 23 dBm. This results in a handset model that uses an isotropic antenna gain pattern with maximum EIRP of 20 dBm. Within this report, two other EIRPs (still paired with an isotropic antenna assumption) are examined: 23 dBm and 30 dBm.

M.2292 indicates that handsets are active 50, 70, or 100% of the time depending on deployment type. As with the base station models in this report, 100% handset activity was assumed for conservatism since this level of activity can occur for short periods for any deployment type. Further, M.2292 notes other factors that can diminish interference effects from handsets including: power control that diminishes typical EIRPs by 21 – 32 dB, building shielding (up to 20 dB), and body shielding (4 dB). These three loss factors are also not considered within this report for conservatism, since there are situations where none of the three losses may apply. For instance, a handset can be outdoors at the edge of cell coverage transmitting maximum EIRP towards a GPS/GNSS receiver without any intervening obstructions.

4.1.3 Use Case Development

Understanding GPS/GNSS receiver use cases scenarios are important so that the geometric parameters, specifically a receiver height and lateral offset from a transmitter can be determined. Also, it is important that use cases representative each receiver category and can provide a worst-case scenario so most, if not all, receivers in that category are protected. In addition, use cases are needed in conjunction with ITMs, propagation models, and transmitter scenarios to determine what power levels can be tolerated adjacent to GPS/GNSS signals.

Use cases were compiled with input from DOT federal partners and agencies. Members of the working group were provided a template that contained questions related to how their organizations use GPS/GNSS receivers to support their mission. In particular, questions included identifying height, speed, terrain, antenna orientation and integration, and urbanization areas.

Also, outreach was conducted with GPS/GNSS receiver manufacturers. Manufacturers were provided the same template as DOT's federal partners. Additionally, manufacturers provided presentations during several of the workshops that summarized use cases by category for the receivers they manufacture.

A summary of the compiled results can be found in Table 4-2. The results generally indicate that each category has a large range of geometric parameters.

Table 4-2: Summary of Compiled Use Case Information

Category	Height (feet AGL)		Speed (mph)	Urbanization	Terrain	Antenna Integration	Antenna Orientation
	Min	Max					
GAV	0	40k	920	Urban/Suburban/Rural	Flat/Sloped/Canyon Open/Impeded Land/Water	Yes/No	Variable
GLN	0	1,000	600	Urban/Suburban/Rural	Flat/Sloped/Canyon Open/Impeded Land/Water	Yes/No	Variable
HPR	0	20,000	180	Urban/Suburban/Rural	Flat/Sloped/Canyon Open/Impeded Land/Water	Yes/No	Variable
TIM	0	1000s	100	Urban/Suburban/rural	Flat Open Land	No	Fixed
CEL	0	100s	100s	Urban/Suburban/rural	Flat/Sloped/Canyon Open/Impeded Land/Water	Yes	Variable
SPB	1,700k	4,300k	16k	n/a	n/a	No	Variable

In an effort to further down-select representative use cases, priorities identified by the space-Based PNT EXCOM and PNT Advisory Board were compiled as a method to prioritize the use case development. These priorities include:

- Existing use cases
- Vital to economic, public safety, scientific, and national security
- Focus on HPR and TIM
- Focus analysis on most sensitive cases
- Apply the 1 dB degradation criteria
- Include Multi-GNSS

When factoring in these priorities, three use case scenarios were identified for further in-depth investigation:

1) Agriculture/Farming
2) Construction/infrastructure
3) Emergency response

A graphic of the emergency response uses case is shown in Figure 4-4. First responders are increasingly using GPS to locate patients both during emergencies and as a normal course of duty. As shown in the figure, there are multiple use of GPS in this scenario applying GLN receivers for navigation of the emergency service response vehicles, as well as asset tracking, including increased awareness of where response personnel and vehicles are located. A GAV receiver on a drone also plays a role in this scenario, supporting the response effort. Drones are becoming of increasing importance in collecting imagery and sensor data in response to natural disasters and other incidents.

This scenario illustrates that use of a GPS/GNSS receiver can be quite close in distance (10’s of meters) to a base station transmitter and potentially very close to a handset as well transmitting in the adjacent band. The GPS/GNSS receiver also potentially could be vertically above the base station height.

Figure 4-4: Emergency Response Use Case

A presentation given at workshop VI can be found in Appendix H, which provides a breakdown of the three use case scenarios. Table 4-3 summarizes the geometric parameters of the three priority scenarios. These applications/use cases happen routinely and bound the impact of base station transmitters.

Table 4-3: Summary of Geometric Parameters

Use Case Scenarios	Use case	Category	Vital Needs	Lateral Distance(s)	Vertical height(s)
Agriculture/ Farming	Precision Farming	HPR	Economic	10 ft and greater from base station	0-20 ft above ground
	Crop Health Monitoring	GLN/GAV	Economic	10 ft and greater from base station	Up to and above base station
Construction/ Infrastructure	Surveying	HPR	Economic	1 city block and greater from the base station	Up to and above base station
Emergency Response	UAS/UAV	GLN/GAV	Public Safety/ National Security	10 ft and greater from base station	Up to and above base station
	Emergency Services	GLN/CEL			
	Emergency Response				

4.1.3.1 Receiver Antenna Patterns

Models for GLN, GAV, TIM, HPR, and CEL receivers relative antenna gain patterns as a function of frequency were developed based upon the antenna characterization activities described in Section 3.3.

The following simple model was found to be representative for relative VPOL and HPOL antenna gain patterns for GLN, GAV, TIM, and HPR receivers:

$$G(\theta) = -\alpha\theta^2$$

where G is the relative antenna gain (dBi), θ is the off-boresight angle (deg), and α is a unitless coefficient.

Based upon curve fits using the 14 external, active antennas that were measured in an anechoic chamber as discussed in Section 3.3, the coefficients in Table 4-4 were determined. The curve fitting approach used was a standard unweighted linear least squares fit of the single parameter equation above.

Table 4-4: Coefficients for GLN, GAV, TIM, and HPR Receivers for Modeling Relative VPOL Antenna Gain at 22 Frequencies*

Frequency (MHz)	α, GLN&GAV	α, TIM	α, HPR
1475	3.6511e-04	6.6446e-04	8.2449e-04
1490	4.0306e-04	7.4609e-04	8.4546e-04
1495	4.5153e-04	7.4928e-04	8.4870e-04
1505	4.6656e-04	7.4815e-04	7.6944e-04
1520	4.9953e-04	7.6698e-04	7.6808e-04
1530	4.9687e-04	7.4564e-04	7.7055e-04
1535	4.4305e-04	7.4764e-04	7.5991e-04
1540	7.0113e-04	7.7206e-04	7.5869e-04
1545	6.5594e-04	7.5573e-04	7.7657e-04
1550	5.0195e-04	6.8500e-04	8.1978e-04
1555	5.4545e-04	6.3767e-04	8.5491e-04
1575	5.7732e-04	5.5176e-04	8.5922e-04
1595	5.3406e-04	6.0901e-04	8.6792e-04
1615	3.9454e-04	5.0824e-04	8.2166e-04
1620	4.2042e-04	5.4509e-04	8.2117e-04
1625	4.5397e-04	5.4762e-04	8.1460e-04
1630	4.7544e-04	6.6388e-04	8.2114e-04
1635	4.2583e-04	6.3971e-04	8.3291e-04
1640	3.5254e-04	5.5736e-04	8.3908e-04
1645	3.4695e-04	5.4974e-04	8.4719e-04
1660	4.4364e-04	5.8069e-04	7.8310e-04
1675	4.7622e-04	5.9775e-04	8.4784e-04

*In the table entries, “e-04” denotes an exponent to the minus 4 power, i.e., “$\times 10^{-4}$”.

As an example of the relative gain patterns, Figure 4-5 shows the modeled relative VPOL antenna gain patterns at 1530 MHz.

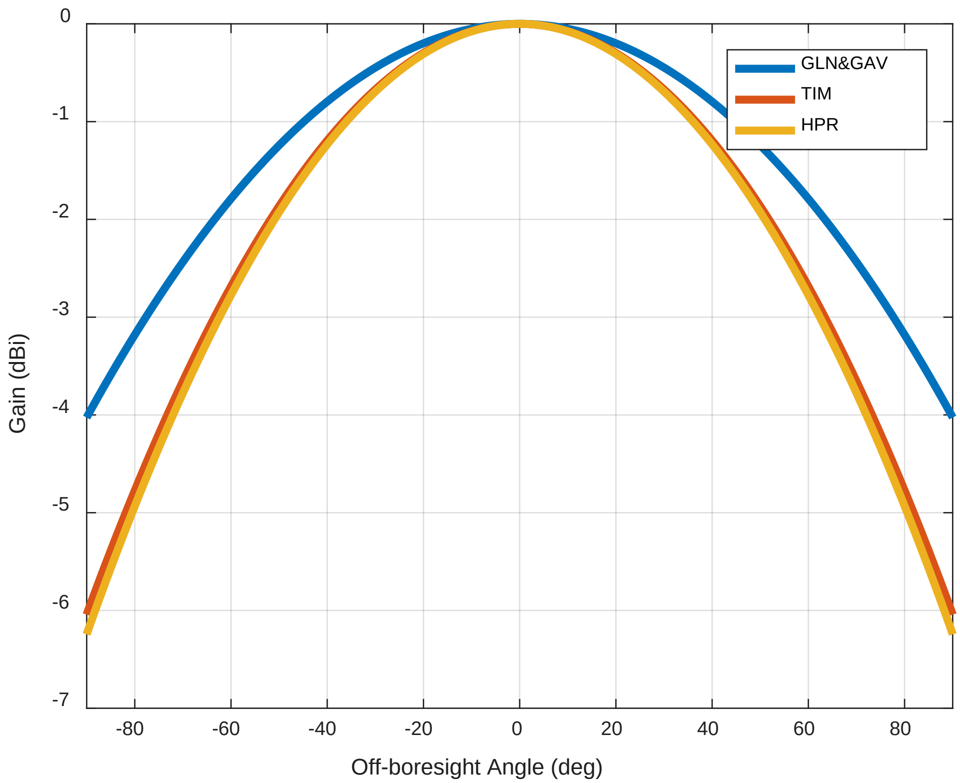

Figure 4-5: Relative VPOL Antenna Gain Patterns for 1530 MHz

The coefficients were generated using the following procedure:

- The 14 measured antennas were grouped by category (GLN/GAV, TIM, or HPR).
- Within each category, and for each frequency, the VPOL antenna patterns were:
    - Adjusted by estimated active subassembly gain at L1 so that they nominally included only passive element gain and filtering.
    - Converted from dBi to linear units, averaged, and then converted back to dBi.
- The mean VPOL antenna pattern for each category and each frequency was then:
    - Forced to be symmetric with off-boresight angle from -180 to 180 deg
    - Fitted with a quadratic polynomial. Since only the relative pattern is of interest, the bias term is not important. The forced symmetry results in the linear term being equal to zero. The quadratic term became the α value within Table 4-4.

This procedure addresses the following considerations:

- Given that only a small set of measured patterns were available for each category, the raw data averaged across units within a category includes variations that would not be expected from a larger sample size.
- When averaging patterns, the pattern for the antenna with the least amount of attenuation at each frequency was deemed to be most important (because an antenna with a tremendous amount of filtering would be associated with a receiver with a high ITM that

is not greatly impacted by adjacent band interference at that frequency). This prompted the averaging of gains in linear units (not dB).

- Asymmetries in gain patterns with positive vs negative off-boresight angle is unimportant since the antenna could be oriented arbitrarily in azimuth relative to an adjacent-band interference source in the real world.

Figure 4-6 provides an example of the data processing. Three GLN VPOL antenna gain patterns at 1530 MHz are shown in the figure. These patterns already have the active subassembly gain at L1 removed from them (15.0 – 19.9 dB for these units). The three patterns are averaged together in linear units, converted back to dBi, and forced to be symmetric with respect to off-boresight angle to form the “Mean” gain shown in the figure. The final curve shown in the figure is the quadratic polynomial fit (obtained with MATLAB polyfit), with the α value shown in Table 4-4 of 4.9687e-04. Using the equation above, this model yields a relative gain value of zero at boresight (by definition) and a relative gain value of $-(4.9687\times10^{-4})(90)^2$ = -4.0 dBi at 90 deg off-boresight angle.

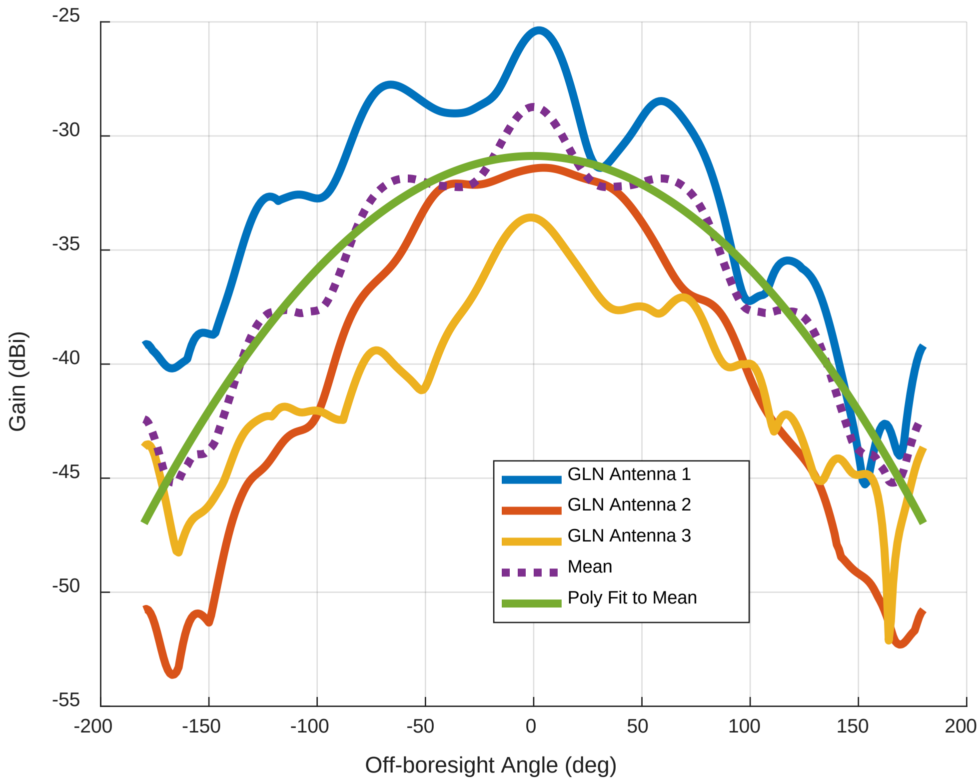

Figure 4-6: Gain Patterns Illustrating Generation of GLN Coefficients for 1530 MHz

The results for HPOL are shown in Table 4-5. For base stations using +/-45 deg cross-polarization, the VPOL and HPOL gain patterns were averaged.

Table 4-5: Coefficients for GLN, GAV, TIM, and HPR Receivers for Modeling Relative HPOL Antenna Gain at 22 Frequencies*

Frequency (MHz)	α, GLN&GAV	α, TIM	α, HPR
1475	4.8398e-04	5.5084e-04	8.4574e-04
1490	4.7233e-04	6.2100e-04	8.3577e-04
1495	4.8102e-04	6.2399e-04	8.3705e-04
1505	5.1078e-04	6.4098e-04	7.6026e-04
1520	5.8403e-04	6.7548e-04	7.4805e-04
1530	6.5353e-04	6.6919e-04	7.4907e-04
1535	7.1505e-04	6.7349e-04	7.3921e-04
1540	6.4548e-04	6.8364e-04	7.4000e-04
1545	5.4709e-04	6.7359e-04	7.6239e-04
1550	5.6432e-04	5.0510e-04	8.1090e-04
1555	5.5046e-04	4.4691e-04	8.4732e-04
1575	4.5639e-04	4.6423e-04	8.5749e-04
1595	5.0855e-04	5.5868e-04	8.5147e-04
1615	6.5552e-04	5.4371e-04	7.9655e-04
1620	6.4930e-04	5.4973e-04	7.9416e-04
1625	6.6186e-04	5.3681e-04	7.8823e-04
1630	6.9139e-04	5.9523e-04	7.9844e-04
1635	7.6854e-04	4.6848e-04	8.0766e-04
1640	7.7504e-04	1.3496e-04	8.0420e-04
1645	7.4623e-04	3.9051e-05	8.0746e-04
1660	7.1712e-04	9.1810e-05	7.5459e-04
1675	5.9731e-04	1.0261e-04	8.5621e-04

*In the table entries, "e-04" denotes an exponent to the minus 4 power, i.e., "$\times 10^{-4}$".

For CEL antennas, a relative gain value of 0 dBi is recommended for all directions for two reasons:

- Cell-phone antennas are typically low-gain, but with erratic patterns depending on the shielding of the cell-phone case, other components, and interaction with the human body holding it (see, e.g., measurements in Section 3.3.3).
- The cell-phone antenna could be oriented in any direction.

4.1.4 Propagation Models

Three propagation models were considered within this report for all receivers except for certified aviation and spaceborne. These models are free-space, two-ray, and the Irregular Terrain Model. The free-space and two-ray models were introduced in Section 4.1.1. The Irregular Terrain Model is an implementation (with improvements) of the Longley-Rice propagation model by the NTIA[1]. Propagation losses yielded by this model (on a median level) differ by less than 2 dB from free-space propagation loss (FSPL) for the relevant distances and frequency range (i.e. distances up to half the interspacing distance between transmitters and frequencies between 1475 and 1675 MHz). However, NTIA additionally recommends using a blended model that is FSPL for small distances and transitions to Irregular Terrain Model starting at a 100 m distance.

[1]See https://www.its.bldrdoc.gov/resources/radio-propagation-software/itm/itm.aspx.

Therefore when the tolerable EIRP levels are considered for distances of 100 m or less, as is the case for civil receivers use cases (excluding use cases for space-based and certified aviation receivers), both the blended and FSPL models yield the same results.

The equations used to perform forward and inverse modeling analysis are first developed for the case of free space path loss propagation. The modified equations for the case of a two-ray path loss are subsequently presented. All of the forward and inverse modeling results presented in this report do not consider OOBE and thus the impact is dictated by the fundamental emissions of the interference source. If an adjacent band system were deployed for which this assumption is invalid, lower EIRP values may be necessary to protect GNSS and would need to be determined for the applicable OOBE limits. See Section 3.2.5.2 for a discussion of OOBE levels.

For receiver power calculations, an LTE signal with dual +/-45° polarization is equivalent to a signal radiating with twice the power and +45° polarization when signals in the two polarizations are uncorrelated. This signal can then be decomposed into vertically and horizontally polarized signals. Considering this along with propagation loss, and receiver and transmitter antenna gains, the corresponding voltage complex amplitude received by an RHCP antenna is shown below

$$\boldsymbol{A_v(\vec{r}_T,\vec{r},f) = \sqrt{2.\frac{P(f)}{2}.\frac{1}{L_P(\vec{r}_T,\vec{r})}.G_{Td}(\vec{r}_T,\vec{r}).G_{Rdv}(\vec{r}_T,\vec{r},f)}.e^{j\frac{2\pi}{\lambda}R_d}} \quad (4\text{-}1)$$

$$\boldsymbol{A_h(\vec{r}_T,\vec{r},f) = j.\sqrt{2.\frac{P(f)}{2}.\frac{1}{L_P(\vec{r}_T,\vec{r})}.G_{Td}(\vec{r}_T,\vec{r}).G_{Rdh}(\vec{r}_T,\vec{r},f)}.e^{j\frac{2\pi}{\lambda}.R_d}} \quad (4\text{-}2)$$

$$\boldsymbol{A(\vec{r}_T,\vec{r},f) = A_v + A_h}$$

$$\boldsymbol{= \sqrt{\frac{P(f)}{L_p(\vec{r}_T,\vec{r})}.G_{Td}(\vec{r}_T,\vec{r})}.e^{j\frac{2\pi}{\lambda}.R_d}.\left(\sqrt{G_{Rdv}(\vec{r}_T,\vec{r},f)} + j.\sqrt{G_{Rdh}(\vec{r}_T,\vec{r},f)}\right)}$$

$$= \left(G_{R,max}\right)^{\frac{1}{2}}.\sqrt{\frac{EIRP(f)}{.L_p(\vec{r}_T,\vec{r})}.g_{Td}(\vec{r}_T,\vec{r})}.e^{j\frac{2\pi}{\lambda}.R_d}.\left(\sqrt{g_{Rdv}(\vec{r}_T,\vec{r})} + j.\sqrt{g_{Rdh}(\vec{r}_T,\vec{r})}\right)$$

(4-3)

where:

$R_d = |\vec{r} - \vec{r}_T|$ is the distance between the transmitter and receiver antennas,

$G_{R,max}$ is the antenna gain at boresight assumed equal for both polarizations,

$g_{Td}(\vec{r}_T,\vec{r})$ is the normalized transmitter gain in the direction of the receiver antenna,

$g_{Rdv}(\vec{r}_T,\vec{r})$ and $g_{Rdh}(\vec{r}_T,\vec{r})$ are the normalized receiver antenna gains in the direction of the transmitter antenna for the case of horizontal and vertical polarizations respectively.

The term $L_p(\vec{r}_T,\vec{r})$ is the free space path loss factor defined in the following equation:

$$L_p(\vec{r}_T, \vec{r}) = \left(\frac{4\pi R_d}{\lambda}\right)^2 \tag{4-4}$$

The power coupled into the receiver from its antenna output is found by taking ½ the amplitude squared as follows

$$P(\vec{r}_T, \vec{r}, f) = \frac{1}{2} G_{R,max} \cdot \frac{EIRP(f)}{L_p(\vec{r}_T, \vec{r})} \cdot g_{Td}(\vec{r}_T, \vec{r}) . \left| \left(\sqrt{g_{Rdv}(\vec{r}_T, \vec{r}, f)} + j . \sqrt{g_{Rdh}(\vec{r}_T, \vec{r}, f)} \right) \right|^2 =$$

$$\frac{1}{2} G_{R,max} \cdot \frac{EIRP(f)}{L_p(\vec{r}_T, \vec{r})} \cdot g_{Td}(\vec{r}_T, \vec{r}) . \left(g_{Rdv}(\vec{r}_T, \vec{r}, f) + g_{Rdh}(\vec{r}_T, \vec{r}, f) \right) \tag{4-5}$$

This power is outside the receiver tolerance when it exceeds the tolerance level $ITM(f) . G_{R,max}$. This inequality is shown in the equation below.

$$\frac{P(\vec{r}_T, \vec{r}, f)}{G_{R,max}} = \frac{1}{2} \cdot \frac{EIRP(f)}{L_p(\vec{r}_T, \vec{r})} \cdot g_{Td}(\vec{r}_T, \vec{r}) . \left(g_{Rdv}(\vec{r}_T, \vec{r}, f) + g_{Rdh}(\vec{r}_T, \vec{r}, f) \right) > ITM(f) \tag{4-6}$$

The forward modeling uses this inequality to determine the impacted region for a predetermined EIRP(f) level.

On the other hand, the inverse modeling solves for the value EIRP $(\vec{r}, f)$ that ensures compatibility for a given transmitter and receiver location. An EIRP map for all receiver locations in a vertical plane relative to a fixed transmitter is created using the following equation

$$EIRP(\vec{r}, f) = \frac{L_p(\vec{r}_T, \vec{r}) . ITM(f)}{\frac{1}{2} g_{Td}(\vec{r}_T, \vec{r}) . \left(g_{Rdv}(\vec{r}_T, \vec{r}, f) + g_{Rdh}(\vec{r}_T, \vec{r}, f) \right)} \tag{4-7}$$

This map is performed in the vertical y-z plane containing the phase center of the transmit antenna and in the direction of maximum gain of a sector antenna and in any direction in the case of an omnidirectional antenna.

For given use cases associated with one category of receivers, the range of GNSS application operational heights and a standoff distance d_s will determine the an EIRP mask $EIRP(d_s, f)$ according to the following equation

$$EIRP(d_s, f) = Min_{\vec{r} \epsilon \boldsymbol{R_{uc}}} \{ EIRP(\vec{r}_T, \vec{r}, f) \} \tag{4-8}$$

Where R_{uc} is the use cases analysis region as shown in Figure 4-7.

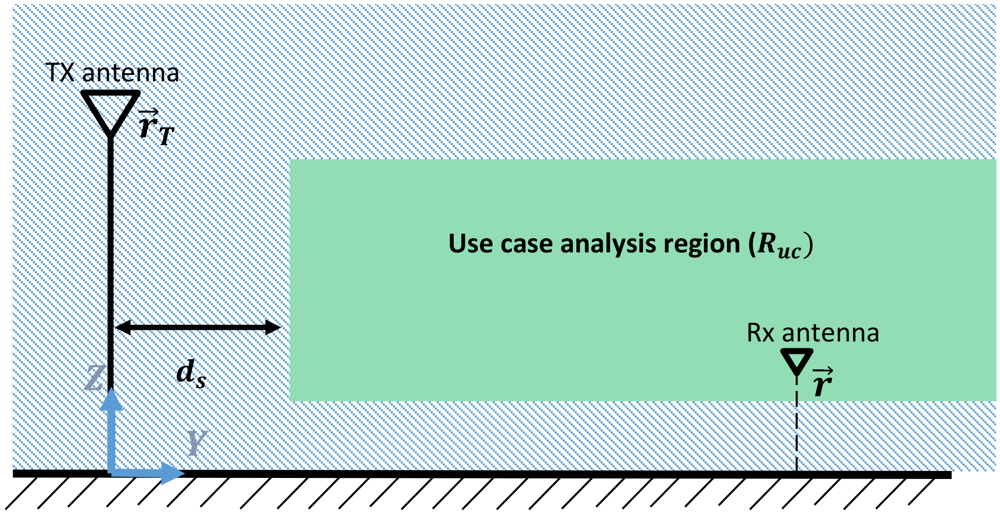

Figure 4-7: Illustration of use case analysis region

In order to ensure compatibility with all receivers within a category the bounding ITMs are used. This will result in EIRP values that protect 100% of the receivers tested. Results for the median ITM within each category are also presented resulting in power levels that would leave 50% of the receivers unprotected.

The inverse modeling modified equation for the case of two ray path loss is shown below.

$$EIRP(\vec{r}, f) = \frac{ITM(f)}{\frac{1}{2} \cdot g_{Td}(\vec{r}_T, \vec{r}). \left(g_{Rdv}(\vec{r}_T, \vec{r}, f) \,.\, PF_{2Ray,v}(\vec{r}, f) + g_{Rdh}(\vec{r}_T, \vec{r}, f). PF_{2Ray,h}(\vec{r}, f)\right)} \qquad (4\text{-}9)$$

Where $PF_{2Ray,v}(r, f)$ and $PF_{2Ray,h}(r, f)$ represent respectively the vertical and horizontal polarization path factors (also sometimes referred to as *path gains* in the literature) derived in Appendix F.

The inverse modeling equation can be easily rearranged to get the inequality expression for the forward modeling

$$\frac{1}{2} EIRP(f). g_{Td}(\vec{r}_T, \vec{r}). \left(g_{Rdv}(\vec{r}_T, \vec{r}, f) \,.\, PF_{2Ray,v}(r, f) + g_{Rdh}(\vec{r}_T, \vec{r}, f). PF_{2Ray,h}(r, f)\right) > ITM(f) \qquad (4\text{-}10)$$

When solving for tolerable EIRP for the case of multiple transmitters, the inverse modeling equations stay the same with a summation in the denominator over all transmitters. For example the FSPL inverse modeling equation takes the following form when aggregate effects are considered.

$$EIRP(\vec{r},f) = \frac{ITM(f)}{\sum_T \alpha_T \cdot \left(\frac{1}{2} \cdot \frac{1}{L_p(\vec{r}_T,\vec{r})} \cdot g_{Td}(\vec{r}_T,\vec{r}) \cdot \left(g_{Rdv}(\vec{r}_T,\vec{r},f) + g_{Rdh}(\vec{r}_T,\vec{r},f) \right) \right)} \tag{4-11}$$

α_T is a power control term for the general case when EIRP is not same for all transmitters. The analysis in this report will use $\alpha_T = 1$ for all transmitters whenever aggregation is considered.

4.1.5 Forward Modeling Results and Sensitivity

Appendix I provides a comprehensive set of forwarding modeling results for two adjacent-band LTE base station deployment types (macro urban and small cell outdoor/micro urban; see Table 4-1) and also for LTE mobile devices. Type 2 (10 MHz LTE) signals were assumed. Base station results were produced for each of the 11 potential adjacent-band LTE downlink frequencies listed in Table 3-6 (1475, 1490, 1505, 1520, 1525, 1530, 1535, 1540, 1545, 1550, 1675 MHz) and handset results for each of the 7 potential adjacent-band LTE uplink frequencies (1620, 1625, 1630, 1635, 1640, 1645, 1660 MHz).

An example of the base station forward modeling results is shown in Figure 4-8. The results shown on the plot assumes a macro urban base station (EIRP = 59 dBm/sector, height = 25 m, other characteristics as described in Section 3.4.2.1) operating at 1530 MHz, free space propagation, and the most sensitive (bounding) GAV GPS/GNSS device category processing GPS C/A-code signals. The three contours in the plot depict the two-dimensional areas where the received interference level from a macro urban base station exceeds three thresholds: (1) the ITM (i.e., where the bounding GAV device category experienced a 1 dB CNR degradation, (2) LOL_L, the loss-of-lock threshold for low-elevation angle satellites, and (3) LOL_H, the loss-of-lock threshold for high-elevation angle satellites.

The base station is situated near the bottom left of the plot with its antennas located at the point (0, 25 m) in *x*, *y* where *x* is the lateral distance from the base station and *y* is the height above ground. The GAV DUT was assumed to have an antenna with the relative gain pattern modeled as discussed in Section 3.4.3.1.

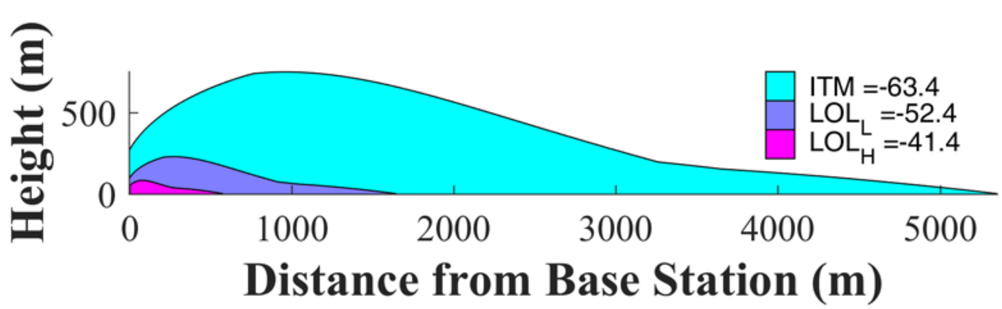

Figure 4-8: Macro Urban Base Station (EIRP = 59 dBm), Bounding GAV, 1540 MHz

Appendix I also includes summary charts such as shown in Figure 4-8. Each summary chart shows, for each applicable frequency, the maximum impacted lateral distance for each DUT type and each LTE transmitter type (e.g. macro urban base station, small cell outdoor base station, handset). For instance, at 1540 MHz Figure 4-9 has three data points that correspond to the maximum horizontal extent of the impacted region contours from Figure 4-8.

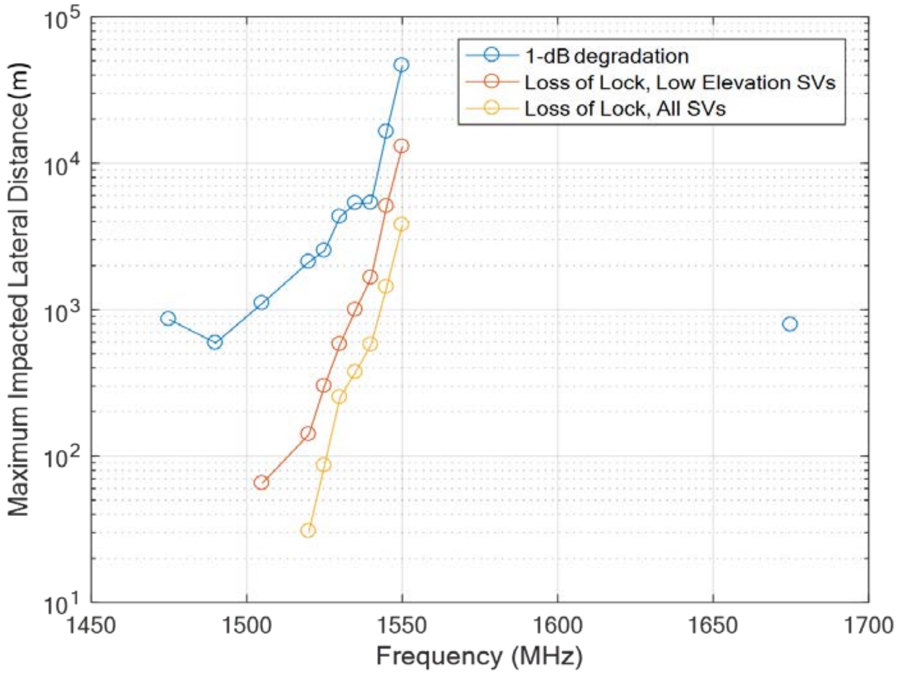

Figure 4-9: Maximum Impacted Lateral Distance for Bounding GAV, Macro Urban Base Station (EIRP = 59 dBm)

Results for the HPR receiver category at 1530 MHz are presented in Figure 4-5. Note the HPR category experienced a 1 dB (or greater) CNR degradation beyond 14 km from the transmitter and loss of lock occurred on low elevation satellites out to 3 km with loss of lock on all satellites out to approximately 1 km.

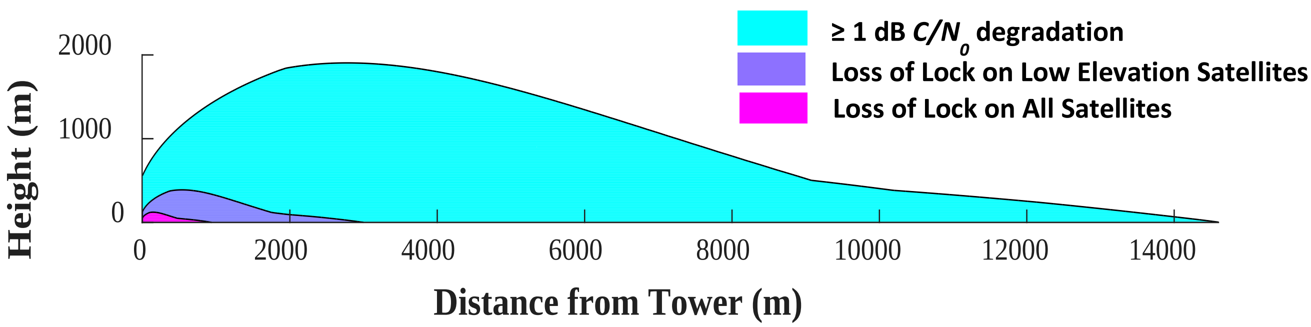

Figure 4-60: Macro Urban Base Station (EIRP = 59 dBm), Bounding HPR, 1530 MHz

Appendix I is organized as follows. For GPS C/A-code and assuming free-space propagation, Section I.1, I.2, and I.3 present forward modeling results for macro base stations, small cell outdoor/micro urban base stations, and handsets, respectively. Section I.4 examines the sensitivity of the results to:

- Less sensitive DUTs – results for the median-performing vs the most-sensitive DUTs.
- GNSS signals – results for other GNSS signal types vs. GPS C/A-code.
- Propagation models – the variability of the results with propagation model.

4.1.6 Inverse Transmit Power Calculation Results and Sensitivity Analysis

4.1.6.1 Inverse Transmit Power Calculation Results

Inverse modeling is used to determine EIRP tolerance masks $EIRP(d_s, f)$ for a category of GNSS receivers and for a given standoff distance ds. The details of this analysis including the relevant equations and parameters are described in section 4.1.4 . This inverse modeling is only applied to the 10 MHz LTE downlink frequencies. The treatment of uplink frequencies is only considered in the forward analysis since at the time of the writing of this report the authors were not aware of any proposals to limit the maximum EIRP for handsets to a value below what is specified in the M.2292 document.

For the HPR category, the EIRP map for the bounding L1 C/A ITM is shown in Figure 4-11 (a) for the single micro urban base station at a center frequency of 1530 Hz. The use case analysis has shown that receiver heights extends to at and above the height of a base station in all categories and therefore the tolerable EIRP as a function of standoff distance can be found by taking the minimum along heights up to and above base station heights as shown in Figure 4-11 (b). The extent of the impact region is >10 km from the transmitter for an EIRP of 29 dBW and 1.8 km for EIRP of 10 dBW.

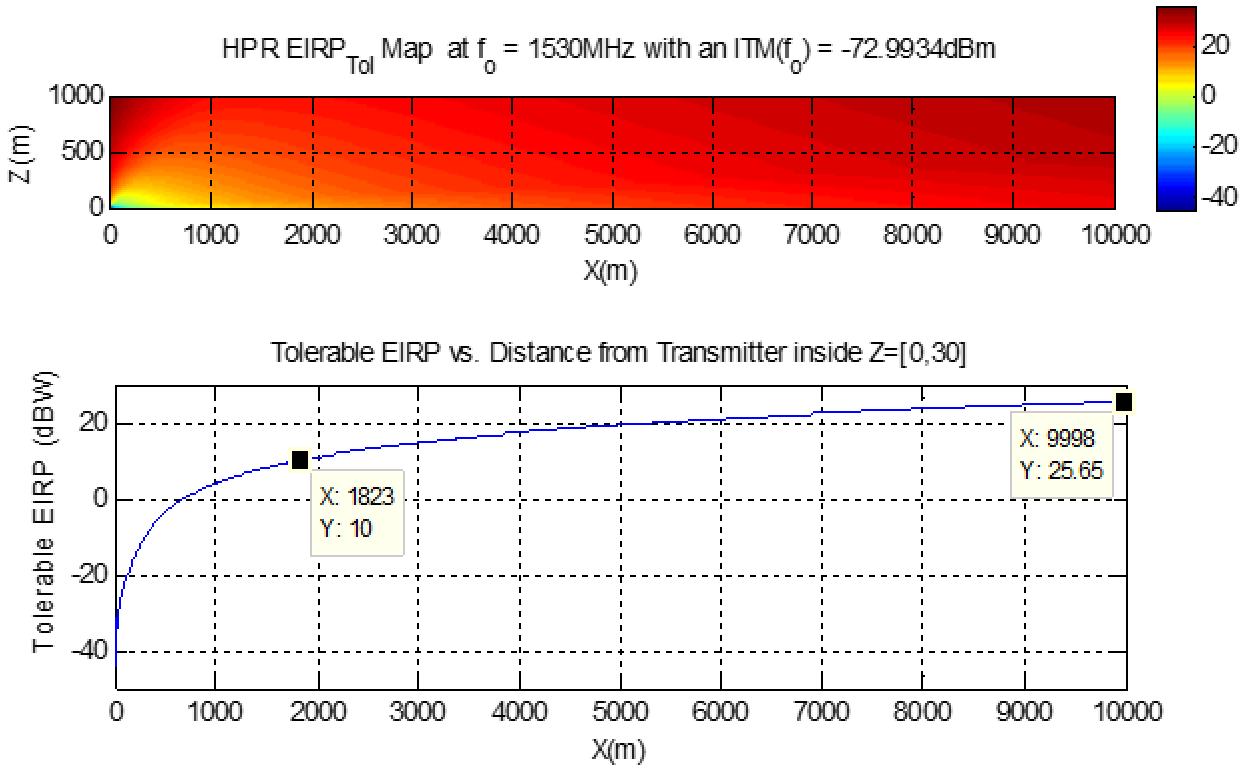

Figure 4-71: Tolerable EIRP results. (top) Tolerable $EIRP(\vec{r}, f)$ map in the vertical computation domain, (bottom) Tolerable $EIRP(X, f)$ as a function of standoff distance X.

However, the computation domain only needs to extend up to half the distance between the nearest two base stations in a uniform network deployment. For the case of micro urban deployment a computation domain up to 500 meters is sufficient. Below is the zoomed in version of the Figure 4-12 to illustrate the EIRP levels that protect HPR receivers processing L1 C/A signals at short distances from the transmitter.

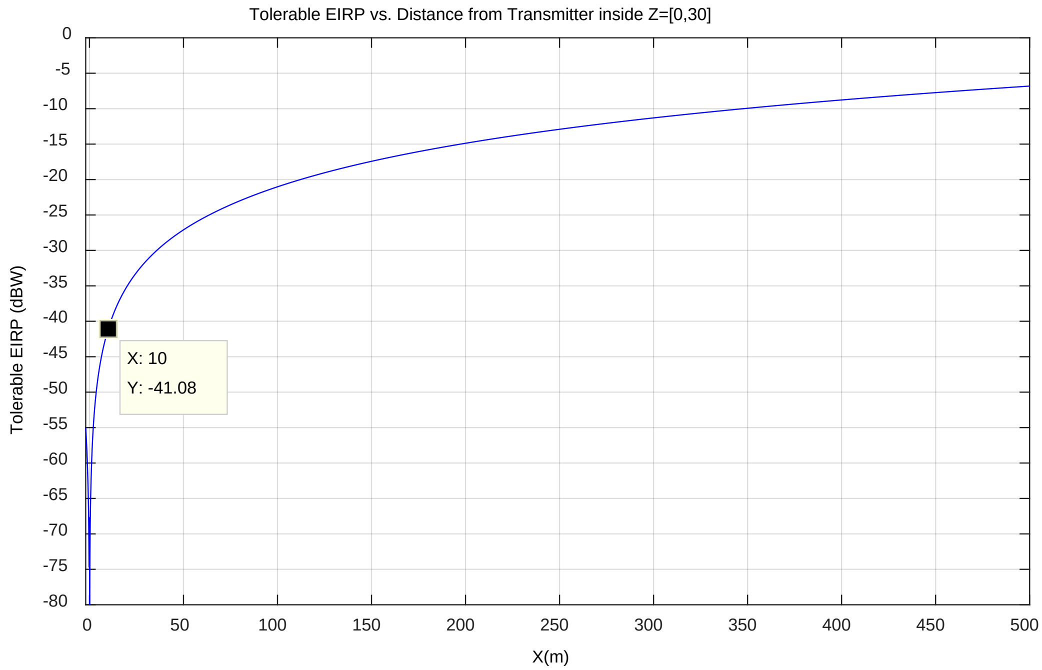

Figure 4-82: Tolerable $EIRP(X, f)$ as a function of standoff distance X up to X=500 m

The marker in this figure indicates the maximum tolerable EIRP, $EIRP(d_s, f)$, with ds=10 m and f=1530 MHz. If this is repeated across all base station frequencies, a maximum tolerable EIRP mask can be generated as shown in Figure 4-13 below.

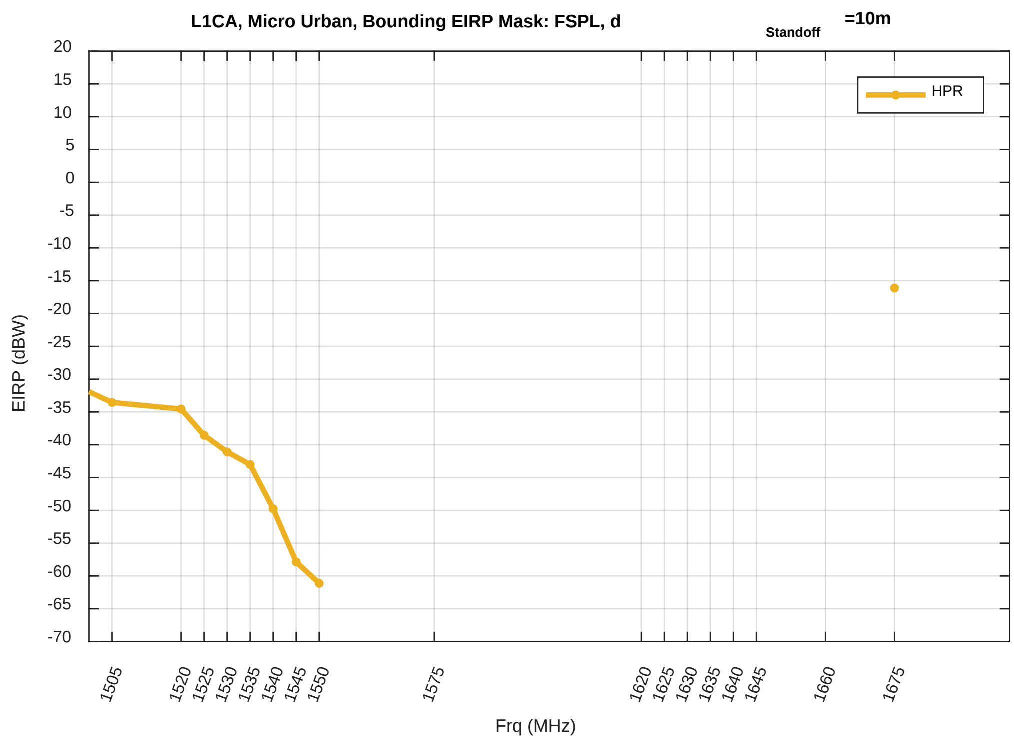

Figure 4-9: EIRP(f,ds=10m) for the HPR category: L1 C/A, micro urban deployment, bounding EIRP Mask, and FSPL propagation

It is worth noting that use cases indicated that receivers can be as close as 10 ft (3.0 m) to the base station. It was not clear that they can approach that distances at heights comparable to that of the base station. If receivers approach the base station height at the 10 ft standoff distance the tolerable EIRP levels will be lower by approximately 5 dB. This analysis can be repeated to generate EIRP masks for all categories of receivers at different standoff distances. Figure 4-14 depicts the L1 C/A EIRP masks for all five categories for the 10 m standoff distance. A more comprehensive set of results for 10, 100 and 500 m standoff distances that protects L1 C/A along with all other emulated GNSS signals are shown in Appendix J.

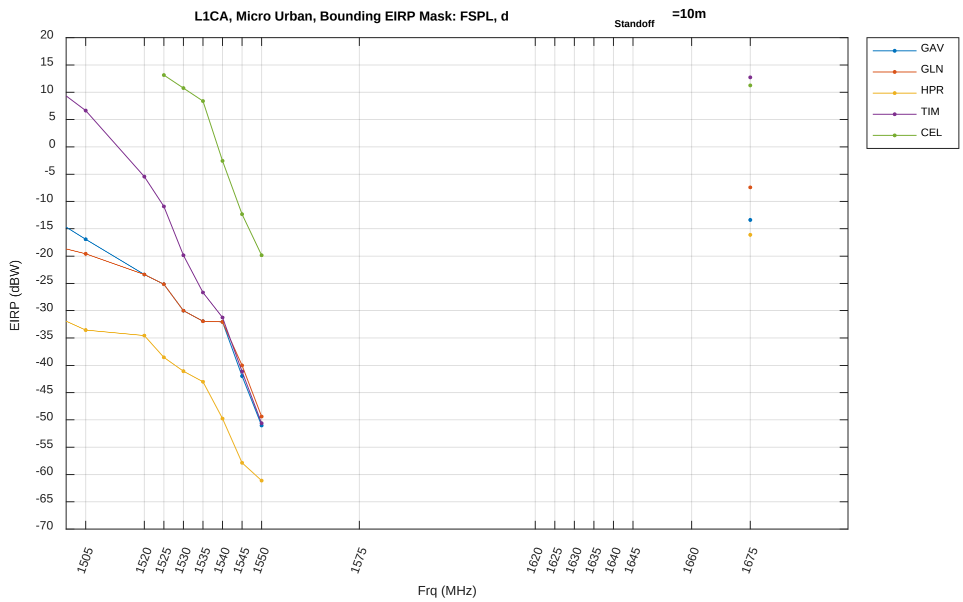

Figure 4-10: EIRP(f,ds=10m) for five receiver categories of receivers: L1 C/A, micro urban deployment, bounding EIRP Mask, and FSPL propagation

The HPR tolerable EIRP levels that protects L1 C/A and all GNSS signals for the same 10 m standoff distance are compared in Figure 4-15.

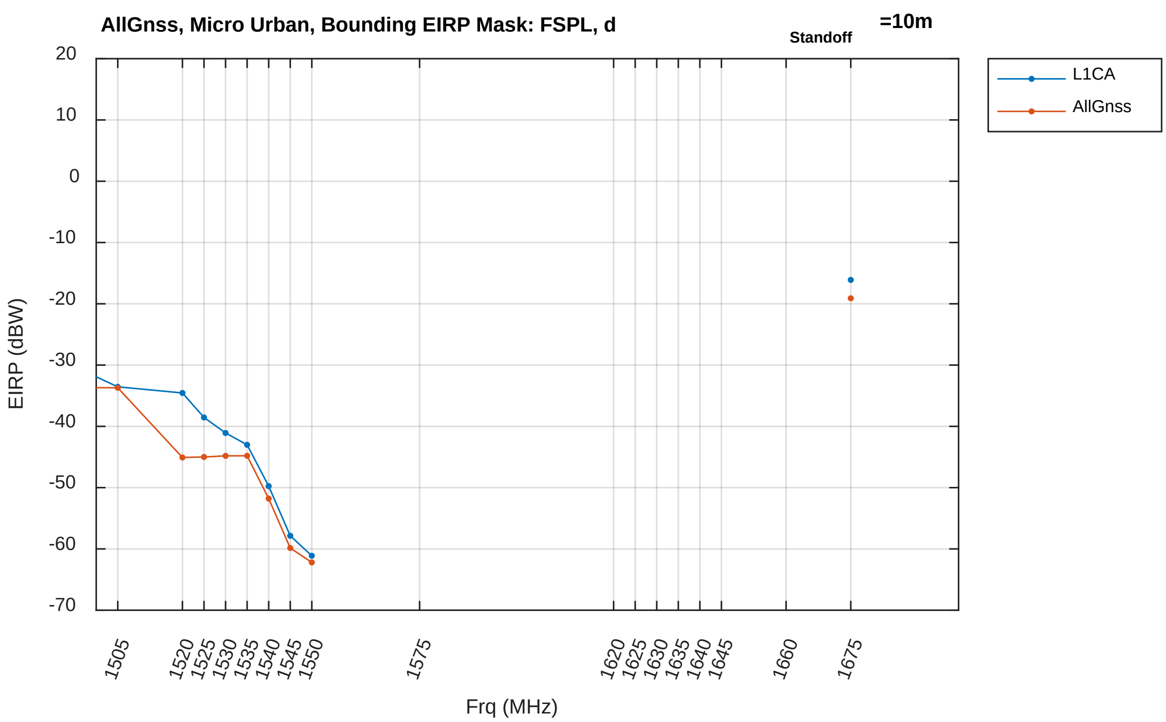

Figure 4-11: Comparison of EIRP(f,ds=10m) L1 C/A and All GNSS masks for the HPR category of receivers: Micro urban deployment, bounding EIRP Mask, and FSPL propagation

As expected, the levels that protect all GNSS signals are lower than the ones that protect L1 C/A signals since they are calculated based on the minimum of all bounds across emulated services. Figure 4-16 presents the resulting all GNSS EIRP masks for five categories of receivers at a standoff distance of 10 m.

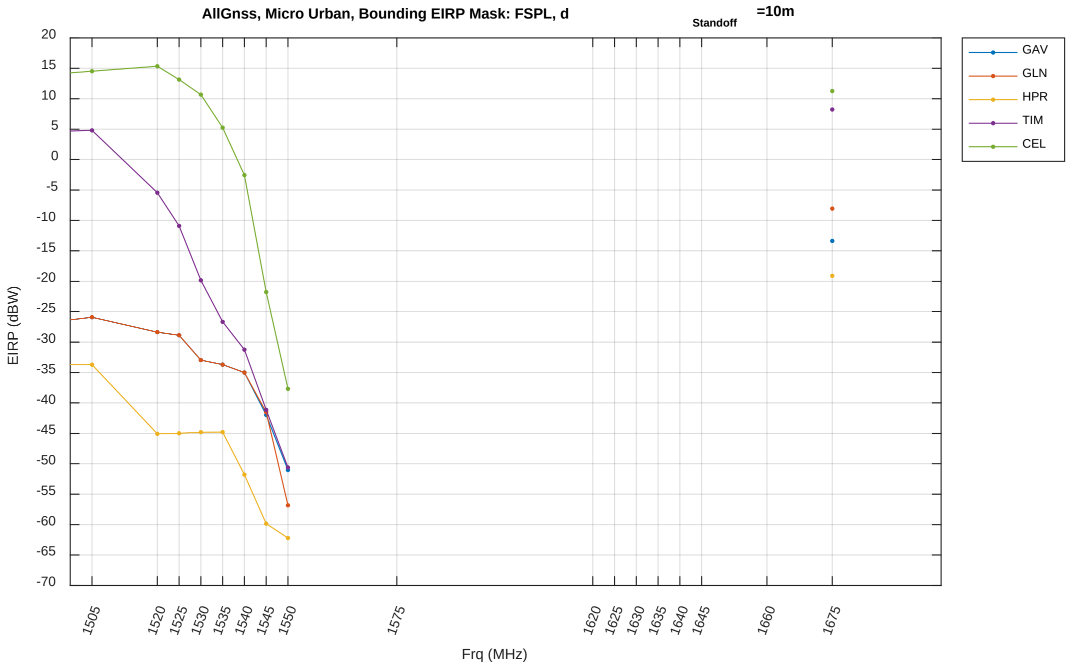

Figure 4-12: EIRP(f,ds=10m) for five categories of receivers: All GNSS, micro urban deployment, bounding EIRP Mask, and FSPL propagation

An exhaustive list of plots that include results for the macro deployments are shown in Appendix J.

4.1.6.2 Sensitivity Analysis

The transmit power level results presented in Section 4.1.6.1 considers only a single transmitter and FSPL propagation model. This subsection examines how these results vary when aggregation effects of multiple transmits are considered. The sensitivity of these results to the propagation model used is also considered. Finally, the transmit power levels corresponding to the median ITMs are also discussed are part of this sensitivity analysis.

4.1.6.2.1 Aggregation Effects

When multiple transmitters are radiating at equal EIRP, the single base station is expected to dominate for small standoff distances. As this distance increases, the aggregate effects become significant and limit the tolerable EIRP levels below that of a single transmitter. The aggregation analysis is here performed using a micro urban deployment of two full rings of adjacent cells around the center cell. In Figure 4-17, the center cell is in white, the inner ring of adjacent cells is in yellow, and the outer ring of adjacent cells is in green. For urban and suburban regions, signals emitted from additional transmitters outside what is simulated here will have diminished effect on aggregate results. Additionally, they are expected to encounter blockage from buildings and terrain that will further diminish their contribution to the final results.

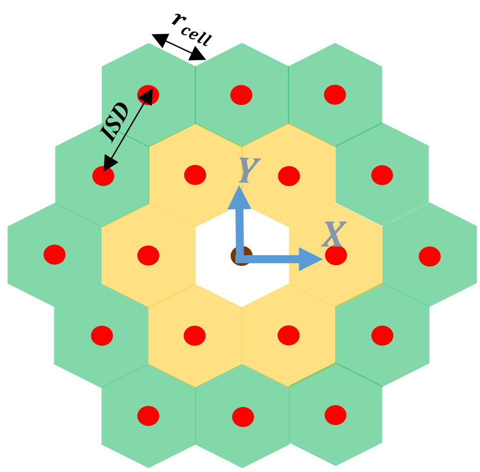

Figure 4-13: micro deployment used for the aggregation sensitivity analysis. A small cell of radius r_{cell}, and transmitters' interspacing distance ISD.

This analysis was performed in the vertical plane for the center transmitter (i.e. y=0 plane) for the HPR L1 C/A Bounding ITM. These results are overlaid with that of a single base station in Figure 4-18.

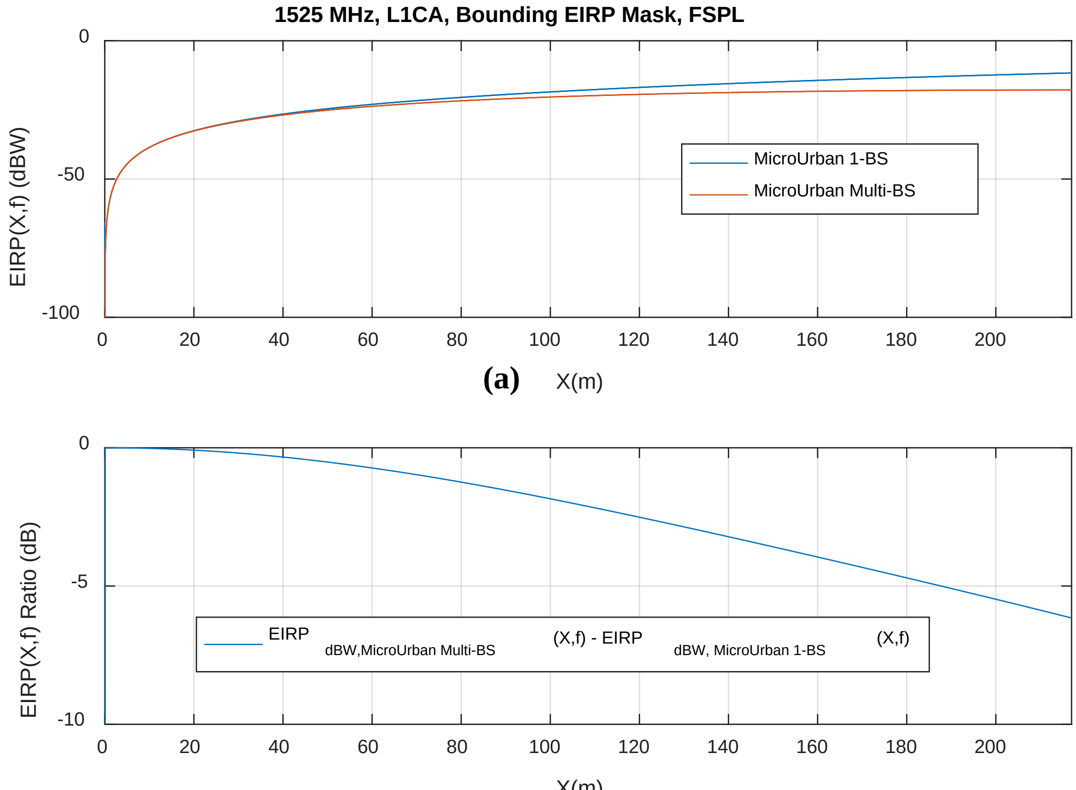

(a)

(b)

Figure 4-18: (a) Overlay of $EIRP(X, f)$ as a function of standoff distance X for the case of single and multiple base stations, (b) $EIRP(X, f)$ ratio in dB for the two cases

As previously discussed, the computation domain was limited to half the distance between transmitters beyond which the tolerable EIRP will start dropping again due to the proximity to the next transmitter. Figure 4-18 (a) shows the aggregation effects to be noticeable for standoff distances greater than 20 m. For example, a standoff distance 100 m the aggregation effect reduces the tolerable EIRP by approximately 1.8 dB relative to the case of a single transmitter. This reduction grows to about 5.5 dB at 200 m standoff distance.

In Figure 4-19 the tolerable EIRP(f,d_s) masks for the single and multiple transmitters cases are compared at a standoff distance of d_s=100 m. It shows similar reduction in EIRP on the order of 2 dB for all frequencies.

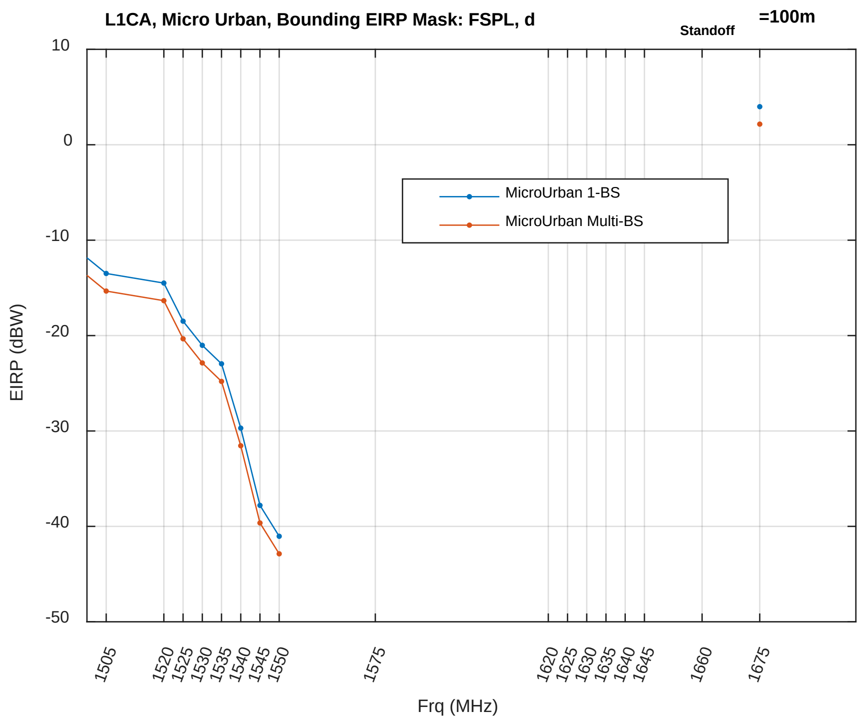

Figure 4-19: Overlay of $EIRP(X, f)$ tolerance masks for the case of a single base station and that of multiple transmitter case

4.1.6.2.2 Effects of Propagation Models

The results shown so far are based on FSPL propagation. The sensitivity of HPR results to the use of two ray path loss as opposed to FSPL model is considered in this section for the case of micro urban single transmitter. The Irregular Terrain Model is the same as the FSPL model for standoff distances up to 100 m and is therefore indirectly accounted for in this analysis. The two ray path loss tolerable EIRP map and the EIRP function of standoff distance are Figure 4-20.

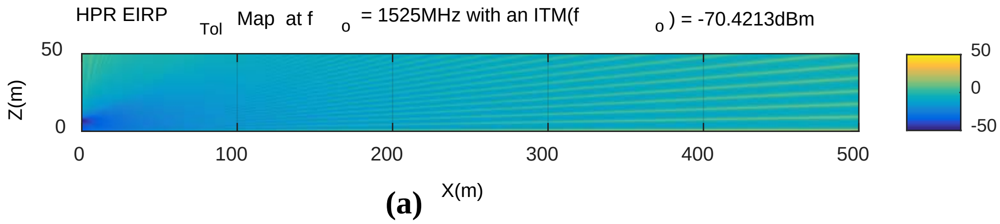

(a)

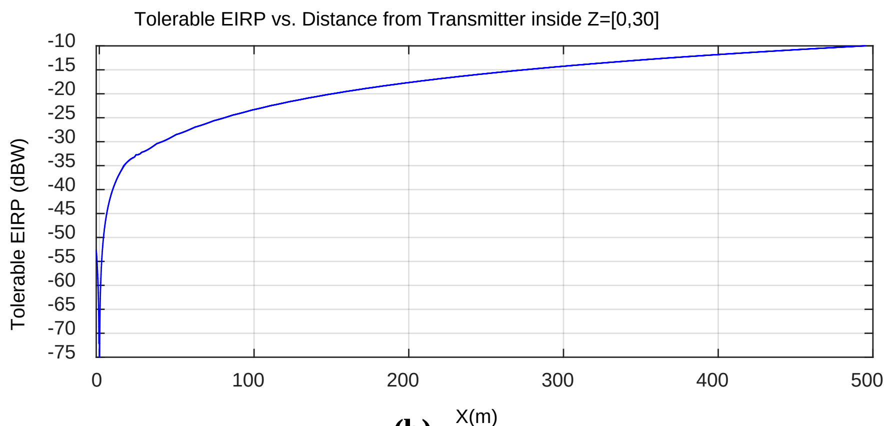

(b)

Figure 4-14: Tolerable EIRP levels for the case of two ray path loss propagation model. (a) Tolerable $EIRP(\vec{r}, f)$ map in the vertical plane, (b) tolerable $EIRP(X, f)$ as a function of standoff distance X.

The two ray $EIRP(X, f)$ is overlaid with the FSPL in Figure 4-21 (a), and their difference is shown in Figure 4-21 (b). These figures show that tolerable EIRP levels are similar for both models up to a distance of about 20 m after which the two ray path loss results in lower tolerable levels. For a standoff distance of 100 m, the two ray path loss results in 4.8dB lower tolerable level than that of FSPL.

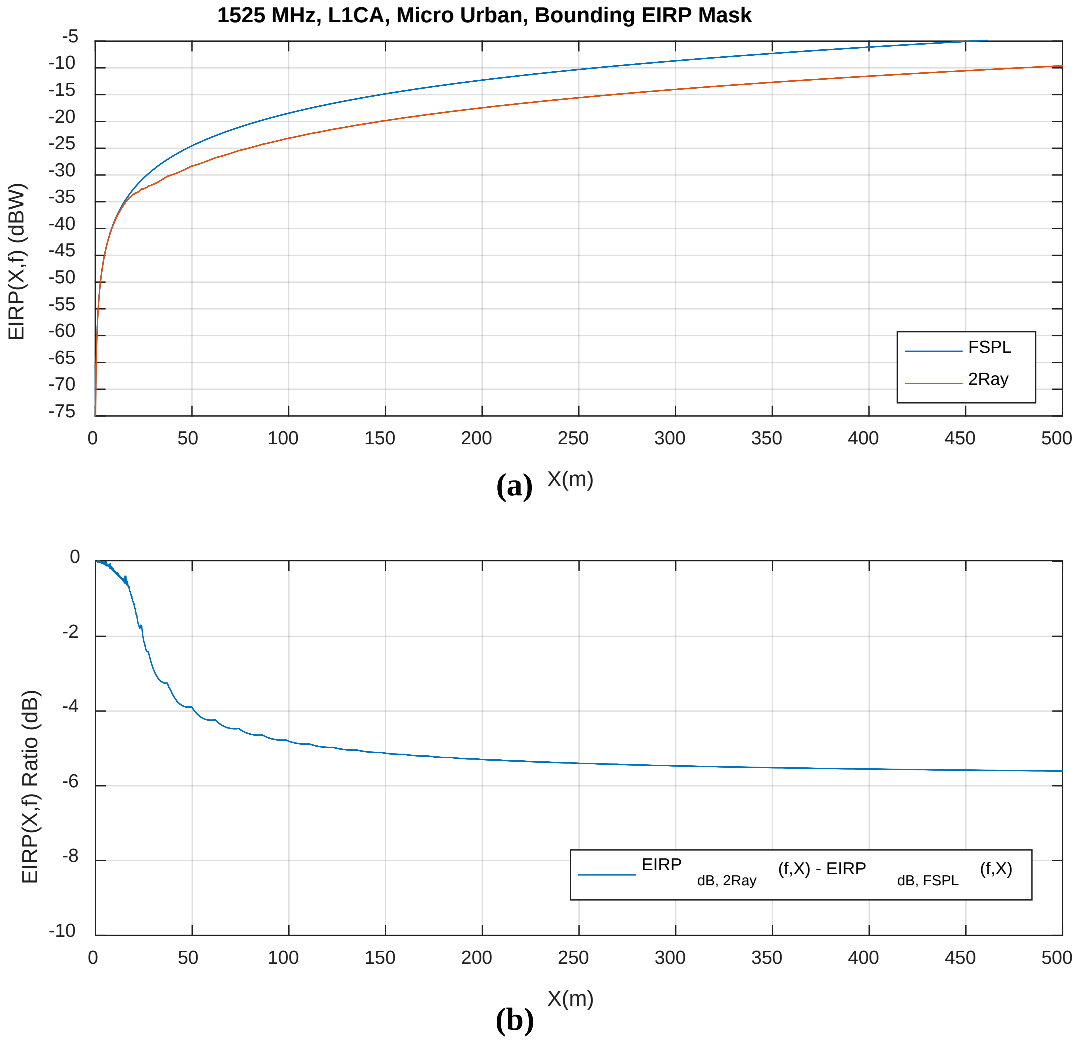

Figure 4-15: (a) Overlay of $EIRP(X, f)$ as a function of standoff distance X for the case of FSPL and two ray path loss propagation, (b) ratio of EIRP(X,f) in the above plot in dB

This analysis is applied to the remaining downlink frequencies and an EIRP tolerance mask for the two ray path loss is produced. This mask is overlaid with that of FSPL in Figure 4-22. A more comprehensive set of results is presented in Appendix J.

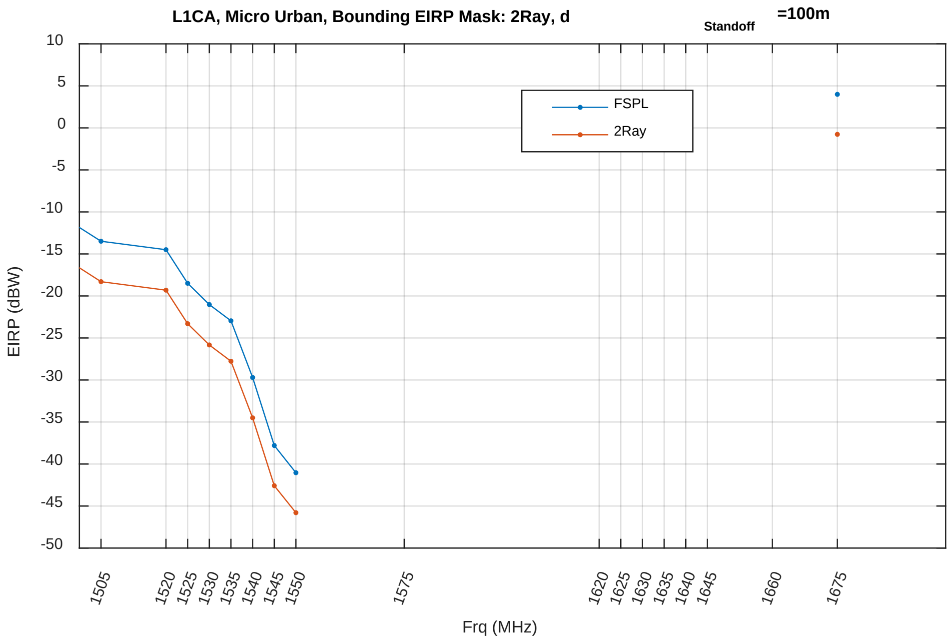

Figure 4-16: Comparison between two ray and FSPL EIRP tolerance masks $EIRP(X, f)$ for X=100m standoff distance

4.1.6.2.3 EIRP masks for Median ITMs

EIRP levels based on median ITMs protect 50% of the tested receivers and leave the rest unprotected. The resulting EIRP levels corresponding to the median masks are shown in Figure 4-23 for a micro urban cell transmitter and L1 C/A signals.

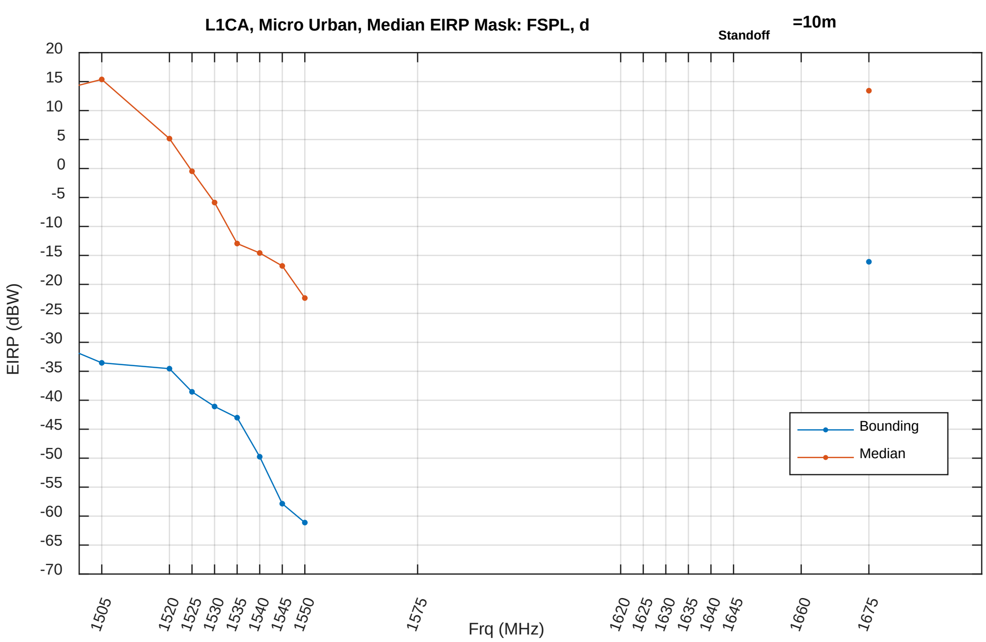

Figure 4-17: EIRP levels corresponding to L1 C/A median ITMs

Because of the linearity of the inverse modeling equation, at a particular frequency, the difference in the tolerable EIRP levels equals the difference between the bounding and the median ITMs for that same frequency in dB.

4.1.7 Summary of Transmit Power Level Calculation

The approach to determine tolerable EIRP levels for a given standoff distance (inverse modeling), as well as the one to determine minimum standoff distance for a given EIRP value (forward modeling) were described in section 4.1.4. Interference source (transmitter) characteristics were primarily obtained from M.2292 (Characteristics of Terrestrial IMT-Advanced Systems for Frequency Sharing/Interference Analyses) and proposals to FCC for adjacent band network applications. Base station characteristics are summarized in Table 4-1 and handset characteristics are summarized in Section 4.1.2.2. Base station antenna patterns are shown in Figure 4-2 and Figure 4-3.

GNSS receiver antenna measurements for each one of the 22 frequencies used in the WSMR tests were done to determine the appropriate antenna pattern to use for each category of receivers. Parabolic fits to these measurements were ultimately used as inputs to the forward and inverse modeling calculations. The results of these fits are shown in Table 3-16 and Table 4-5 for vertical and horizontal polarization respectively. The propagation loss was estimated through the FSPL model and the Two-ray model. Since the Irregular Terrain Model is expected to have the same properties as FSPL for distances up to 100 meters it is indirectly considered as part of the FSPL analysis.

Tolerable EIRP levels for base stations that protect all tested receivers processing the L1 C/A signal are shown in Table 4-6 at standoff distances of 10 and 100 meters for two different deployments. The base station results for receivers that process the other tested GNSS signals are shown in Table 4-7.

Table 4-6: Tolerable Base Station $EIRP(d_s, f)$ for L1 C/A bounding masks for Type-2 Interference signal using FSPL propagation model

			Tolerable EIRP (dBW) by Interference Frequency (MHz)										
Deployment Type	**d_s (m)**	**Cat**	**1475**	**1490**	**1505**	**1520**	**1525**	**1530**	**1535**	**1540**	**1545**	**1550**	**1675**
Micro Urban	**10**	**GAV**	-14.25	-10.21	-16.92	-23.37	-25.15	-29.99	-31.93	-32.06	-41.96	-51.03	-13.38
		GLN	-13.94	-16.9	-19.58	-23.37	-25.15	-29.99	-31.93	-32.06	-40.02	-49.38	-7.41
		HPR	-23.11	-28.65	-33.55	-34.55	-38.55	-41.08	-43.01	-49.75	-57.86	-61.12	-16.1
		TIM	15.22	14.71	6.65	-5.44	-10.9	-19.85	-26.67	-31.24	-41.14	-50.61	12.73
		CEL	n/a*	n/a*	n/a*	n/a*	13.15	10.77	8.39	-2.56	-12.33	-19.85	11.26
	100	**GAV**	5.75	9.78	3.08	-3.37	-5.15	-9.98	-11.92	-12.03	-21.95	-31.02	6.63
		GLN	6.06	3.1	0.42	-3.37	-5.15	-9.98	-11.92	-12.03	-20.01	-29.38	12.59
		HPR	-3.03	-8.56	-13.49	-14.5	-18.49	-21.02	-22.96	-29.7	-37.8	-41.04	3.99
		TIM	35.23	34.74	26.69	14.6	9.14	0.19	-6.63	-11.2	-21.1	-30.6	32.73
		CEL	n/a	n/a	n/a	n/a	33.15	30.77	28.39	17.44	7.67	0.15	31.26
Macro Urban	**10**	**GAV**	-14.77	-10.75	-17.52	-24.02	-25.8	-30.66	-32.59	-32.82	-42.67	-51.67	-14.02
		GLN	-14.46	-17.44	-20.17	-24.02	-25.8	-30.66	-32.59	-32.82	-40.72	-50.02	-8.05
		HPR	-24	-29.54	-34.39	-35.39	-39.38	-41.92	-43.84	-50.58	-58.7	-61.99	-17
		TIM	14.51	13.93	5.87	-6.25	-11.71	-20.65	-27.47	-32.05	-41.94	-51.3	12.42
		CEL	n/a	n/a	n/a	n/a	13.22	10.84	8.46	-2.49	-12.26	-19.78	11.33
	100	**GAV**	5.22	9.24	2.47	-4.03	-5.81	-10.68	-12.6	-12.85	-22.68	-31.68	5.97
		GLN	5.53	2.56	-0.18	-4.03	-5.81	-10.68	-12.6	-12.85	-20.74	-30.03	11.93
		HPR	-4.04	-9.58	-14.42	-15.42	-19.41	-21.95	-23.87	-30.61	-38.73	-42.03	2.96
		TIM	34.5	33.91	25.85	13.73	8.27	-0.67	-7.49	-12.08	-21.96	-31.32	32.41
		CEL	n/a*	n/a*	n/a*	n/a*	33.22	30.84	28.46	17.51	7.74	0.22	31.33

*n/a signifies no CNR degradation of 1-dB was detected within the tested range of interference power

Table 4-7: Tolerable Base Station $EIRP(d_s, f)$ for All GNSS bounding masks for Type-2 Interference signal using FSPL propagation model

			Tolerable EIRP (dBW) by Interference Frequency (MHz)										
Deployment Type	**d_s (m)**	**Cat**	**1475**	**1490**	**1505**	**1520**	**1525**	**1530**	**1535**	**1540**	**1545**	**1550**	**1675**
Micro Urban	10	GAV	-14.25	-27.21	-25.92	-28.37	-28.88	-32.97	-33.7	-35.01	-41.96	-51.03	-13.38
		GLN	-19.94	-27.21	-25.92	-28.37	-28.88	-32.97	-33.7	-35.01	-41.52	-56.83	-8.05
		HPR	-26.11	-33.65	-33.71	-45.08	-45	-44.82	-44.8	-51.79	-59.85	-62.2	-19.1
		TIM	15.22	4.5	4.8	-5.44	-10.9	-19.85	-26.67	-31.24	-41.14	-50.61	8.23
		CEL	10.68	13.7	14.52	15.35	13.15	10.68	5.25	-2.56	-21.78	-37.68	11.26
	100	GAV	5.75	-7.22	-5.92	-8.37	-8.87	-12.96	-13.7	-14.98	-21.95	-31.02	6.63
		GLN	0.06	-7.22	-5.92	-8.37	-8.87	-12.96	-13.7	-14.98	-21.51	-36.83	11.95
		HPR	-6.03	-13.56	-13.65	-25.02	-24.94	-24.76	-24.75	-31.74	-39.79	-42.13	0.99
		TIM	35.23	24.53	24.84	14.6	9.14	0.19	-6.63	-11.2	-21.1	-30.6	28.23
		CEL	30.68	33.7	34.52	35.35	33.15	30.68	25.25	17.44	-1.78	-17.68	31.26
Macro Urban	10	GAV	-14.77	-27.75	-26.51	-29.02	-29.53	-33.64	-34.36	-35.77	-42.67	-51.67	-14.02
		GLN	-20.46	-27.75	-26.51	-29.02	-29.53	-33.64	-34.36	-35.77	-42.22	-57.47	-8.69
		HPR	-27	-34.54	-34.55	-45.91	-45.83	-45.65	-45.63	-52.62	-60.69	-63.08	-20
		TIM	14.51	3.73	4.02	-6.25	-11.71	-20.65	-27.47	-32.05	-41.94	-51.3	7.92
		CEL	10.75	13.77	14.59	15.41	13.22	10.75	5.32	-2.49	-21.71	-37.61	11.33
	100	GAV	5.22	-7.76	-6.53	-9.03	-9.54	-13.65	-14.37	-15.8	-22.68	-31.68	5.97
		GLN	-0.47	-7.76	-6.53	-9.03	-9.54	-13.65	-14.37	-15.8	-22.24	-37.49	11.3
		HPR	-7.04	-14.58	-14.58	-25.94	-25.86	-25.68	-25.66	-32.64	-40.72	-43.11	-0.04
		TIM	34.5	23.71	24	13.73	8.27	-0.67	-7.49	-12.08	-21.96	-31.32	27.91
		CEL	30.75	33.77	34.59	35.41	33.22	30.75	25.32	17.51	-1.71	-17.61	31.33

As expected from the WSMR tests on receiver susceptibility, the smallest base station EIRP is imposed by the HPR receivers. For L1 C/A signals and macro-urban networks, the tolerable EIRP decreases monotonically from about -24 dBW (4 mW) at 1475 MHz, to -42 dBW (< 0.1 mW) at 1530 MHz, to -62 dBW ($< 1\ \mu W$) at 1550 MHz; for micro-urban networks the results increase by a fraction of a dB. For all GNSS signals, the above values decrease by a few dB.

The tabulated results also show that the results are not sensitive to the deployment type when a single base station is considered. The differences between the two deployments are ≤ 1 dB for any frequency, category, and standoff distance combination. The average difference is 0.6 dB. However, the levels that protect all GNSS signals can be as much as 15 dB lower than those needed to protect L1 C/A signals from base station emissions with an average difference of 3.5 dB across all frequencies and five categories considered in Table 4-6 and Table 4-7. It is worthy to note that the difference in results between 10 and 100m standoff distances is a constant of 20 dB with a tolerance of less than 0.1 dB despite accounting for the antenna pattern. This is because for FSPL propagation the tolerable EIRP at a particular standoff distance is found when the phase center of the receiver antenna is approximately aligned with the centerline direction of the transmit antenna's main beam. This will result in a very small difference in angles of incidence and therefore similar receiver gain value at the 10 and 100 meters standoff distances. Therefore, the difference in results between these two standoff distances is primarily controlled by the difference in FSPL which is the ratio of the distances squared in dB.

These values become even smaller if two-ray path loss and aggregation effects are considered. Also, these results did not show significant sensitivity to the transmitter antenna types (omni or sectoral antennas associated with the deployment type).

Tolerable EIRP levels for handsets that protect all tested receivers processing the L1 C/A signal are shown in Table 4-8 at a standoff distance of 10 m. The results in Table 4-8 assume free space propagation and only a single handset. As for the base station results, the EIRP values would become even smaller if two-ray path loss and aggregation effects are considered.

Table 4-8. Tolerable Handset $EIRP(d_s, f)$ for GPS L1 C/A-code bounding masks for Type-2 Interference signal using FSPL propagation model at a standoff distance of 10 m

Tolerable EIRP (dBW) by Interference Frequency (MHz)							
Cat	1620	1625	1630	1635	1640	1645	1660
GAV	-19.2	-17.1	-7.1	-3.7	-5.2	-5.2	-6.6
GLN	-41.3	-38.1	-31.0	-18.1	-13.7	-14.7	-11.9
HPR	-57.0	-47.1	-31.3	-28.3	-28.2	-29.8	-22.1
TIM	-26.3	-19.0	-10.3	-5.9	-1.8	2.7	11.8
CEL	-26.3	-18.1	0.2	9.4	10.9	12.8	13.1

4.2 Spaceborne and Science Applications

This section of the report describes the analysis and evaluation of a proposed LTE base station network operating on adjacent radio frequency bands to space-based receivers. The emphasis of this section is on the assessment to GNSS receivers used as a science application. Additional information can be found in Appendix K.

The following evaluation assesses the impact to one of these GNSS-based science applications, radio occultations (RO), where space-based GNSS receivers are used to perform measurements of the troposphere, stratosphere, and up through the layers of the atmosphere until reaching the ionosphere. This is not to say that the other GNSS-based science applications are not affected by a proposed LTE base station network, but RO science is an application that is particularly susceptible and, thus, the focus of this assessment. RO measurements of the atmosphere, coupled with traditional methodologies for Earth observation, have significantly improved accuracy and predictability of weather forecasts. RO measurements of the ionosphere have also improved our ability to monitor 'space weather' (the distribution of charged particles in the uppermost part of the atmosphere), which is essential to ensure the successful operation of satellites.

Specifically, NASA's assessment focuses on the RO receiver, called the TriG (formerly also known as TriGNSS), which was developed by the NASA/Jet Propulsion Laboratory (JPL). The TriG is the newest RO receiver of the BlackJack class of GNSS receivers and can perform substantially more (up to three (3) times more) measurements than previous versions. The increase in performance is partially due to the TriG's ability to receive signals from all GNSS constellations including the GPS, GLONASS, Galileo, BeiDou, regional space-based navigation constellations such as QZSS and NavIC, and SBAS, such as Wide Area Augmentation System (WAAS) and European Geostationary Navigation Overlay Service (EGNOS).

Radio Frequency Interference (RFI) is a particular problem when GNSS signals are being used for science applications. During RO measurements, the GNSS signal is defocused by tens of dB at low ray heights, where the signal-to-noise ratio (SNR) is already in a marginal zone. In fact, in this already marginal zone, tracking loops cannot be closed and the captured data is running open loop. Additional noise from RFI contaminates these marginal-SNR data over specific areas. The spatially correlated noise can bias the captured data and greatly affect the recent climate record, while providing incorrect weather predictions over the affected areas.

4.2.1 Radio Occultation (GNSS-RO)

RO/GNSS-RO is the disruption/interruption of GNSS signals from a spacecraft by the intervention of a celestial body. RO is a relatively new method for the indirect measurement of temperature, pressure and water vapor in the stratosphere and the troposphere. These measurements are made from specifically designed GNSS receivers on-board a Low-Earth-Orbit (LEO) satellite. The techniques utilize the unique radio signals continuously transmitted by the GNSS satellites (GPS, GLONASS, Galileo, etc.) orbiting the Earth at an approximate altitude of 20,000 km above the surface. The GNSS radio signals are influenced both by the electron density in the ionosphere and by the variations of temperature, pressure and water vapor in the atmosphere which are used in meteorology. RO measurements are also used to derive various ionospheric parameters (Total Electron Content (TEC), Electron Density Profiles (EDP), L-band scintillation, etc.) for understanding earth and space weather dynamics.

From the point of view of a LEO satellite (at an altitude of 700-800 km), the GNSS satellites continually rise above, or set behind, the horizon of the Earth. During these so-called "radio occultation", where the GNSS and the LEO satellite are just able to "see" each other through the atmosphere, the GNSS signals will be slightly delayed and their ray path slightly bent (refracted) on the way through the layers of the atmosphere (see Figure 4-24). The excess range increases as the ray propagates through denser media at lower altitudes (and highly-refractive water vapor in the atmosphere). This delay is a function of density (n/V), which is related to temperature by the ideal gas law: P*V = n*R*T.

A typical occultation sounding will last one (1) to two (2) minutes, and during this time the LEO satellite will receive signals where the ray paths have different minimum distances to the surface of the Earth, from zero up to approximately 100 km. The GNSS satellites transmit on multiple frequencies, and with a receiver rate of 50 Hz this will yield around 6000 rays, making up two profiles of phase residuals up/down through the lowest 100 km of the atmosphere and the ionosphere up to, or down from, the ~700 km height of the LEO satellite.

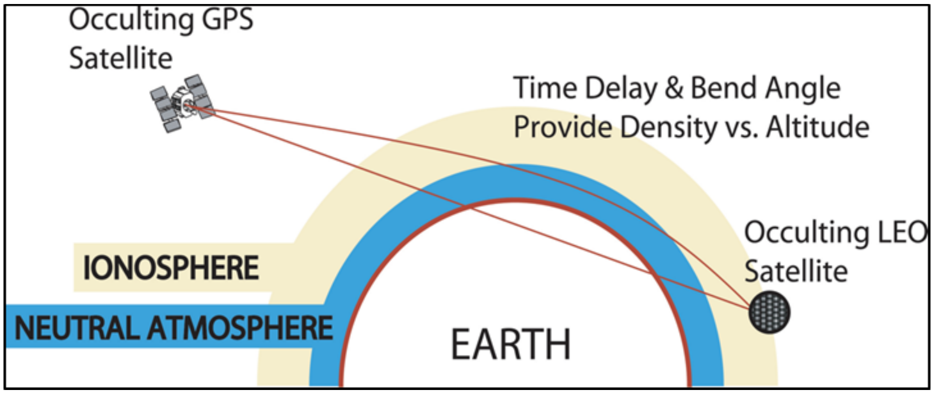

Figure 4-24: Straight Line versus Actual Path of GNSS Signal

The residual positioning error and determination of time delays, derived from the measurements taken during a RO event, are key parameters in the obtaining the temperature, pressure, and water vapor characteristics of the atmosphere at different heights. Given sub-mm measurement precision, RO can determine atmospheric temperature profiles to 0.1 – 0.5 Kelvin (K) accuracy from 8 - 25 km height levels.

NASA has several radio occultation receivers in its portfolio, including the Integrated GPS Occultation Receiver (IGOR), the IGOR+, and the more recently developed receiver called the TriG receiver.

4.2.2 NASA/JPL TriG Receiver Overview

The NASA/JPL developed TriG receiver functions as a multi-function GNSS receiver. This single receiver has multiple antenna inputs and can be configured to operate in a navigation capacity, as well as, simultaneously, in a scientific measurement role. In its traditional function, coupled with a choke ring antenna, the TriG serves as a device for space vehicle navigation and precise orbit determination (POD). The receiver provides accurate information to space vehicle operators on position, velocity, and time.

Configured in a scientific measurement mode, the TriG, coupled with a series of specially designed antenna arrays, performs RO measurements of GNSS signals. TriG receivers are able to receive all GNSS signals: GPS, Galileo, GLONASS, Compass, as well as other navigation signals (QZSS, DORIS, etc.). This capability increases the number of RO measurements that can be made during any given orbit.

4.2.3 Spaceborne Receiver Assessment for Science-Based Applications

NASA has performed an assessment of the potential impacts caused by a proposed terrestrial LTE network operating in the adjacent band to GPS L1. Two (2) future science missions, COSMIC-2 and Sentinel-6 (formerly, Jason Continuity of Service (Jason-CS)), were used as the basis for these assessments. NASA's assessment is to the TriG receiver performing a science application using the RO technique.

To determine the impact to the TriG receiver, the aggregate interference power at the output of the TriG receiver antenna was calculated using MATLAB to model the interference scenario, as well as the TriG receiver system, and simulate the interference effects to the satellites in orbit. Satellites operating in LEO gain a much broader view of the earth (dependent upon antenna characterizations and operating parameters), which must be accounted for in performing the analysis.

Figure 4-18: Example Satellite View of the U.S. Cities

Unlike the assessments performed in Section 3, in-orbit satellites will see a greater number of potential interference sources (e.g. – increased number of terrestrial Base stations (ES)) and the aggregate of those interference sources will be the major contributing factor in the assessment, see Figure 4-25.

4.2.3.1 Summary of TriG Receiver System Characteristics Used for Analysis

Table 4-9 summarizes the satellite TriG receiver system characteristics for the analyses performed on COSMIC-2 and Sentinel-6. The interference threshold in this table is the RFI power at the output of the flight RO antenna which causes a -1 dB C/No degradation in the TriG receiver as used in the COSMIC2-A mission. It was derived from the power density observed by the 0 dBiL standard gain horn used in during the DOT ABC test at a RFI power level causing a 1 dB C/No degradation. Since the TriG choke ring antenna was located at a different spot, it actually received about 3.2 dB more RFI power per meter squared (m^2). In addition, the choke ring antenna had about +3.7 dBi linear gain toward the RFI source, adding 3.7 dB to the threshold power. After these corrections, the LTE power at 1530 MHz that causes a 1 dB C/No degradation is -78.2 dBm + 3.2 dB + 3.7 dB = -71.3 dBm, defined at the output of the receive antenna.

Another adjustment that was made to estimate the effect on the flight receiver is the difference in noise floors due to the extra antenna temperature from black body radiation coming from the ceiling and walls of the WSMR anechoic chamber. During the test, the noise floor is estimated to be 349 Kelvin (K). This is based on preamplifier (Preamp) noise of 51 K, antenna temp of 300 K, and filter loss of 0.8 dB. The noise floor in flight is estimated to be 224 K based on Preamp noise of 51 K, antenna temp of 150 K, and filter loss of 0.8 dB. This difference shows an adjustment to lower the 1 dB threshold by 1.9 dB. Therefore, the normalized in-flight RFI power of is calculated to be approximately -73 dBm (-71.3 dBm – 1.9 dB = -73.2 dBm) from the antenna corresponding to a -1 dB degradation of C/No.

Table 4-9: Summary Table of Satellite TriG Receiver Characteristics Used for Modeling and Simulation

Receiver Characteristic	COSMIC-2	Sentinel-6
Satellite Orbit Altitude	800 km	1330 km
Satellite Orbit Inclination Angle	72°	66°
TriG Forward Receive Antenna Type	12-Element Array	6-Element Array
TriG Forward Receive Antenna Downtilt (relative to satellite velocity vector)	26.2°	34.2°
TriG Forward Receiver Antenna Main-Beam Gain @ 1530 MHz (single subarray)	+ 13.4 dBic	+ 10.5 dBic
TriG Aft Receive Antenna Type	Not modeled	12-Element Array
TriG Aft Receive Antenna Downtilt (relative to satellite velocity vector)	Not modeled	34.0°
TriG Aft Receiver Antenna Main-Beam Gain @ 1530 MHz (single array)	Not modeled	+ 12.5 dBic
Interference Threshold (-1 dB C/N_o)	- 73 dBm	- 73 dBm

4.2.3.2 Terrestrial LTE Deployment Scenarios

The aggregate interference is dependent upon several factors. A few factors are satellite related, including orbital parameters and receiver system characteristics. The other determining factor comes from the interference sources. The most important factor is the transmitter characteristics and the total number of sources (e.g., LTE base stations (BS)). Since TriG receiver systems (performing the RO technique) operate in LEO, they have a direct line-of-sight to a broad area of the U.S., and the aggregate interference is dependent upon the long-term deployment scenario of the LTE operator.

NASA used three parameters, the City Zone model, the City Population and the BS Cell radius to determine the total number of BS that could be deployed in the LTE network. The assumptions used for each of the parameters are described below.

The City Zone model was used to determine the physical area around a city center location that the simulated LTE network would be deployed over. The baseline City Zone model was chosen to conform to the only available accepted model given in ITU Report ITU-R SA.2325-0 [4] (International Mobile Telecommunication (IMT) sharing at 2GHz) for an BS deployment based on three (3) zones (e.g. – urban, suburban, and rural) with given radial distances from a city center latitude/longitude location. An example City Zone model with the typical macro cellular will have a hexagonal grid layout deployed about a city center. Because the LTE services to be provided by the proposed and analyzed network may not be as widespread in terms of city area as the conventional LTE deployment described in SA.2325-0 a second City Zone model with a smaller Suburban and Rural zone size was analyzed. Parameters for both the City Zone models are listed in Table 4-10.

Table 4-10: Zone Model - ES Zone-specific Radial Distance from City Center

Zone Model	Urban Zone (km)	Suburban Zone (km)	Rural Zone (km)
1	0 – 3	3 – 20	20 – 50
2	0 – 3	3 – 10	10 – 30

In addition to a City Zone model it was necessary to define the BS cell radius (CR) parameter in order to determine the BS grid layout within each City Zone. The typical M.2292 zone values listed in Table 4-11 were used as the baseline cell radius (CR) in the simulation.

In consideration to the where the proposed LTE network is to be deployed, the size of the city population was an additional parameter that was included in the simulations. If a U.S. city had a population of greater than 125,000, but less than 250,000, it was included in the analyses for half of the simulations. Cities with populations of over 250,000 were included in all simulations.

Accordingly, the number of assumed cities included in each simulation was chosen from:

- City Population > 125K: 225 cities or
- City Population > 250K: 82 cities

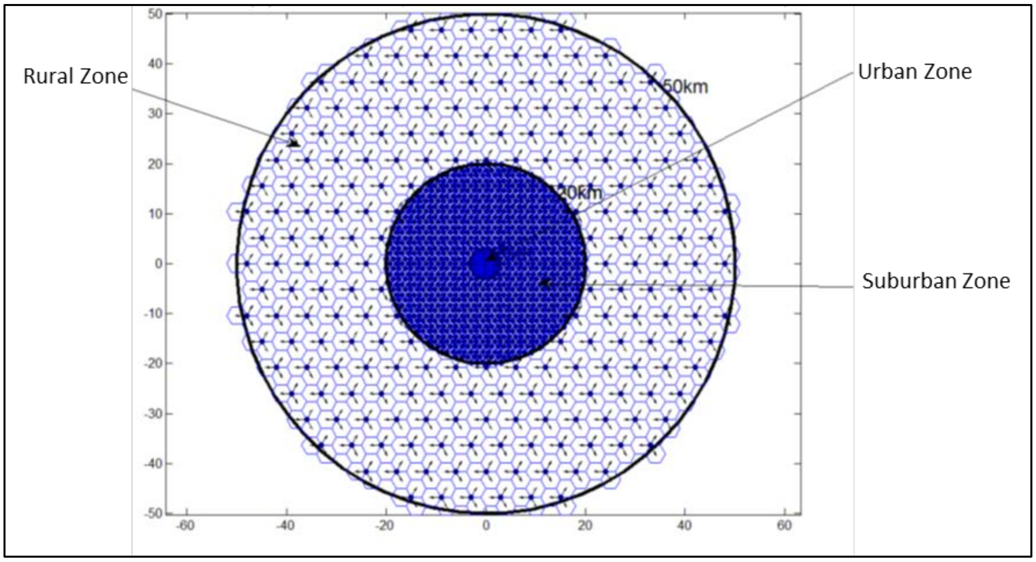

Figure 4-196: Base station Deployment Zone Model (Report ITU-R SA. 2325-0)

Table 4-11: Typical Cell Radius (CR) - M.2292

Zone Type	City Population	CR (km)
Urban	All	0.5
Suburban	All	1.0
Rural	All	5.0

In addition to the above 'typical' model for the cell radius, half of the 16 simulation groups use a variation of the cell model, referred to as 'scaled' model. In the 'scaled' model, the cell radius increases up to double its typical value, as the city population decreases. This decreases the effective number of cell stations, as well as the resulting interference.

Using the set of Zone Model, City Population and Cell Radius parameters, NASA calculated the total number of BS required for deployment for each simulation run. Table 4-12 depicts the number of Base stations for the set of three parameters for a LTE network deployment consisting of only macrocells.

Table 4-12: Total # of BS (Macrocell Deployment Only)

Zone Model	City Population (in 1000s)	Cell Radius	Number of BS			
			Urban	Suburban	Rural	Total
1	> 125	Table 4-10	11,700	143,100	29,700	184,500
1	> 250	Table 4-10	4,264	52,152	10,824	67,240
2	> 125	Table 4-10	11,700	33,750	12,150	57,600
2	> 250	Table 4-10	4,264	12,300	4,428	20,992

4.2.3.3 Summary of BS Transmitter System Characteristics Used for Analysis

In addition to the parameters described above, the following simulation parameters were considered and chosen by NASA for the analysis performed.

- BS antenna side-lobe pattern:
  - F.1336-4 Recommends 3.1. (Macro)
  - F.1336-4 Recommends 3.2. (Micro)

Elevation Mask: Two (2) BS mask angles are utilized for the analysis:

- A 0° elevation mask on the BS so that all BS that see the satellite above 0° elevation angle are included in the aggregate interference calculation, and
- A 5° mask angle so that only BS that see the satellite above 5° elevation angle contribute to the aggregate interference.

BS Activity Factor (AF):

An AF of 3 dB, corresponding to 50% of the Base stations transmitting simultaneously, is used throughout the analysis.

Note: If 100% of the Base stations are transmitting simultaneously, the peak interference levels in the results will be 3 dB higher. In this case the other resulting interference statistics would be increased in time duration or frequency of occurrence as well.

BS Transmitter Power (EIRP):

Table 4-13 depicts the nominal transmit power used for some of the simulations (as per M.2292). Considerations were also given to the maximum transmit powers of 10 dBW and 32 dBW EIRP per channel per sector.

Table 4-13: Assumed Transmitter Levels per Sector (Typical per M.2292)

BS Type	Typical Max. Transmit Power/Channel/Sector (EIRP)
Macrocell - Urban	26 dBW
Macrocell - Suburban	26 dBW
Macrocell - Rural	28 dBW
Microcell (any zone)	7 dBW

4.2.3.4 TriG Receiver Analysis

Two (2) NASA missions (COSMIC-2 and Sentinel-6) that include the TriG receiver, as a science-based function (e.g. - RO technique) were utilized for analysis. A MATLAB simulation program was developed to model the receiver on-board a satellite, using mission-specific parameters, and interference statistics were calculated for an LTE network deployment of BS distributed in U.S. cities.

For the spaceborne receiver analysis the aggregate interference power at the output of the GPS receiver antenna is calculated at ten (10) second time steps in the satellite orbit from BS distributed among U.S. cities. The MATLAB program was set up to model a 10-day orbit of the satellite.

The analysis calculates the interference value and is not dependent upon the carrier signal. The aggregate interference to the receiver antenna output is calculated using a summation of the interference from each source. A simple link budget formula is used to calculate the interference received from a single source, LTE BS. The total aggregate interference is determined through the summation of interference from the individual sources:

$$\mathbf{Rx\ Int\ Pwr_{agg}} = \sum\nolimits_{(\mathbf{Int\ sources})} \mathbf{Tx\ Pwr\ (EIRP)_{off\text{-}boresight}} - \mathbf{FSPL} - \mathbf{Pol\ Loss} + \mathbf{Rx\ Ant\ Gain_{off\text{-}boresight}}$$

where,

Rx Int Pwr$_{\mathbf{agg}}$ = Aggregate interference power level (dBm)

Tx Pwr (EIRP) $_{\mathbf{off\text{-}boresight}}$ = Tx power output including antenna off-boresight calculations (dBm) (See below)

FSPL = Free Space Loss (dB)

Pol Loss = Loss of dissimilar polarizations (Linear to RCHP Polarization = - 3 dB)

Rx Ant Gain $_{\mathbf{off\text{-}boresight}}$ = Rx antenna gain including off-boresight calculations (dBic)

The macro and micro cell sector antenna gain value towards the satellite for each time step was calculated by determining the off-boresight azimuth (AZ) and elevation (EL) look angle gain value from the appropriate F.1336 model gain pattern equations[2].

A total of 96 simulation runs were performed for COSMIC-2, while a lesser, but still representative, number of runs (16 runs) were performed for Sentinel-6. Each of the simulation runs varied one or more LTE BS deployment parameters.
While it is unknown how the LTE operator will be performing their network deployment, the variations in simulation runs should be demonstrative. Further, the variations in runs may be representative of an LTE network through its various phases of deployment (initial deployment through full deployment).

Table 4-14 shows how the various parameters of the terrestrial network and the space receiver are modeled in the different runs of simulation-1 group.

[2] As defined in M.2292 and F.1336-4.

Table 4-14: Summary of Simulation Runs

Run	Sim No.	Run Designator	COSMIC-2	Sentinel-6	BS Tx EIRP	Zone Model	City Population	Cell Radius	Elevation Mask	Macrocell Only	Total # of Earth Stations
1	1	a	X		M.2292 levels	1	> 125K	Typical	0°	X	184,500
2	1	b	X	X	M.2292 levels	1	> 125K	Typical	5°	X	184,500
3	1	c	X		32 dBW	1	> 125K	Typical	0°	X	184,500
4	1	d	X		32 dBW	1	> 125K	Typical	5°	X	184,500
5	1	e	X		10 dBW	1	> 125K	Typical	0°	X	184,500
6	1	f	X	X	10 dBW	1	> 125K	Typical	5°	X	184,500

4.2.3.5 Results

The aggregate interference results for the TriG receiver, functioning as a science measurement instrument, are presented in the following.

The received aggregate interference levels calculated during the simulations range from -90 dBm to -40 dBm.

The following tables use an aggregate interference threshold of -73 dBm (1526 – 1536 MHz) which corresponds to a -1 dB degradation of receiver C/No.

It should be noted that the loss-of-lock threshold for the TriG receiver occurs between -59 to -35 dBm aggregate interference power in the 1526-1536 MHz band. Loss-of-Lock at -59 dBm was seen in Test 04 with RFI at 1525 MHz and LOL at -35 dBm was seen in Test 04 at 1530 MHz.

The entries in the results tables are interpreted as follows:

- Column 3: **Max Int. Level (dBm)**
  Indicates the maximum aggregate interference level calculated at the receiver antenna output.

- Column 4: **% Time > Threshold**
  Indicates the percent time, over the 10-day simulation period, where the aggregate interference at the TriG receiver antenna output exceeds the threshold level (-73 dBm). As an example, if the value is about 10% of the time, the TriG receiver will have C/No degraded by at least 1 dB for a cumulative of 24 hours.

- Column 5: **# of Int Events**
  Indicates that over the 10-day period, the total number of interference events which exceed the -73 dBm threshold.

- Column 6: **Avg Dur Int Event (min)**
  Indicates the mean average duration (in minutes) of an interference event for the entire 10-day period. As discussed before, the duration of an atmospheric occultation (as the signal path moves from skimming the Earth‘s surface to an altitude of about 100 km) is only one to two minutes.

- Column 7: **Max Int Event (min)**
  Indicates the maximum duration (in minutes) that was recorded for a single interference event over the 10-day period.

- Column 8: **Max Allow EIRP Level (dBW/10 MHz)**
  Indicates a reverse-engineered maximum BS transmitter power level (in dBW) distributed across a 10 MHz bandwidth per channel per sector. The reverse-engineered value calculated in this column would bring the interference level to the -73 dBm threshold value for 1 dB C/N_o degradation. The calculated level is based on the maximum interference level received during the 10-day period.

Table 4-15 shows the COSMIC-2 results for the simple scenario of macro cell BS at 32 dBW EIRP.As the number of stations decreases from simulation 1 to 2 for the zone-1 model, and from simulation 5 to 6 for the zone-2 model, there is about 5 dB less interference in zone-2 compared to zone-1, which is expected because the zone-2 model uses about 3 times less stations. There is about 4 dB less interference in models using transmitter elevation mask of 5^o (run d) compared to the 0^o mask (run c), indicating that less than half of the available stations affect the satellite in the 5^o mask case. For the most challenging model (1c), using 184,500 macro cell stations, the tolerable EIRP is 11 dBW.

Table 4-15: COSMIC-2 Interference Results (Macro BS Only, All BS Tx Power 32 dBW)

Sim No.	Run Designator	Max Int. Level (dBm)	% Time > Thresh	# of Int Events	Avg Dur Int. Event (min)	Max Int Event (min)	Max Allow EIRP Level (dBW/10 MHz)
1	c	-52	6.9	141	6.9	14.5	11
1	d	-56	4.7	101	6.5	11.8	15
2	c	-57	5.0	132	5.3	12.0	16
2	d	-61	3.4	96	4.9	10.2	20
5	c	-57	4.5	109	5.7	12.8	16
5	d	-61	3.0	74	5.8	10.2	20
6	c	-62	2.9	99	4.1	10.3	21
6	d	-66	1.9	55	4.8	8.2	25

Table 4-16 shows the Sentinel-6 results for the simple scenario of macro cell ES at 32 dBW EIRP, and as the number of stations decreases from simulation 3 to 4 for the zone-1 model. There is about 2 dB less interference in models using transmitter elevation mask of 5^{o} (run d) compared to the 0^{o} mask (run c), indicating that more than half of the available stations affect the satellite in the 5^{o} mask case. For the most challenging model (3c), using 74,612 macro cell stations, the tolerable EIRP is 23 dBW.

Please note that simulations 3 and 4 use the above mentioned variation of the cell model, referred to as ‘scaled’ model, in which the cell radius increases up to double its typical value, as the city population decreases; this results in fewer stations, and less interference, compared to the simulations 1 and 2.

Table 4-16: Sentinel-6 Interference Results (Macro BS Only, All BS Tx Power +32 dBW/10 MHz)

Sim No.	Run Designator	Max Int. Level (dBm)	% Time > Thresh	Max Allow EIRP Level (dBW/10 MHz)
3	c	-64	7.3	23
3	d	-66	5.2	25
4	c	-68	4.9	27
4	d	-70	3.4	29

5. CERTIFIED AVIATION RECEIVER

5.1 Determination of Tolerable Interference Levels

Certified GPS, GPS/SBAS and GPS/ground-based augmentation system (GBAS) airborne equipment will meet their performance requirements when operating within the radio frequency (RF) interference (RFI) environment defined in appropriate Federal Aviation Administration (FAA) Technical Standard Orders (TSOs). These technical standard orders invoke industry Minimum Operational Performance Standards (MOPS) developed through RTCA (RTCA/DO-229, RTCA/DO-253 and RTCA/DO-316). Sections 3.7.2 and 3.7.3 of the International Civil Aviation Organization (ICAO) GNSS Standards and Recommended Practices (SARPs) [5] also contain Continuous Wave (CW) and band limited noise interference levels, respectively, for which these receivers satisfy their performance specifications and operational objectives.

This analysis addresses all receivers compliant with the requirements[3] of:

- Technical Standard Order (TSO)-C145()[4], *Airborne Navigation Sensors Using The Global Positioning System Augmented By The Satellite Based Augmentation System*. This standard invokes RTCA/DO-229, *Minimum Operational Performance Standards for GPS/Wide Area Augmentation System Airborne Equipment*.
- TSO-C146(), *Stand-Alone Airborne Navigation Equipment Using The Global Positioning System Augmented By The Satellite Based Augmentation System.* This standard invokes RTCA/DO-229, *Minimum Operational Performance Standards for GPS/Wide Area Augmentation System Airborne Equipment*.
- TSO-C161(), *Ground Based Augmentation System Positioning and Navigation Equipment.* This standard invokes RTCA/DO-253, *Minimum Operational Performance Standards for GPS/Local Area Augmentation System Airborne Equipment*.
- TSO-C196(), *Airborne Supplemental Navigation Sensor for Global Positioning System Equipment Using Aircraft-Based Augmentation*. This standard invokes RTCA/DO-316, *Minimum Operational Performance Standards for GPS/Aircraft-Based Augmentation System Airborne Equipment*.
- TSO-C204(), *Circuit Card Assembly Functional Sensors using Satellite-Based Augmentation System (SBAS) for Navigation and Non-Navigation Position/Velocity/Time Output.* This standard invokes RTCA/DO-229, *Minimum Operational Performance Standards for GPS/Wide Area Augmentation System Airborne Equipment*.
- TSO-C205(),*Circuit Card Assembly Functional Class Delta Equipment Using The Satellite-Based Augmentation System For Navigation Applications.* This standard invokes RTCA/DO-229, *Minimum Operational Performance Standards for GPS/Wide Area Augmentation System Airborne Equipment*.
- TSO-C206(), *Circuit Card Assembly Functional Sensors using Aircraft-Based Augmentation for Navigation and Non-Navigation Position/Velocity/Time Output.* This

---

[3] Where specifications are referenced, the latest version is assumed.

[4] "()" encompasses all versions.

standard invokes RTCA/DO-316, *Minimum Operational Performance Standards for Global Positioning System/Aircraft Based Augmentation System Airborne Equipment.*

Note that many receivers were designed to comply with the RFI environments defined within these standards even though they were certified to an earlier standard (TSO-C129a[5]). This analysis does not specifically address receivers that comply only with TSO-C129a. However, that category of receivers[6] was designed to be lower-performance and narrowband. If the receivers assessed under this analysis are shown to be compatible with signals from a network, the FAA then accepts any residual risk that some early-generation GPS receivers not tested to RTCA/DO-229, RTCA/DO-253, and RTCA/DO-316 may experience harmful interference.

5.1.1 Area of Aviation Operation

As the National Airspace System (NAS) continues the transition to Performance Based Navigation (PBN), GNSS and its aircraft-, satellite-, and ground-based augmentation systems (ABAS, SBAS and GBAS) will serve as the key enablers of satellite-based navigation and of surveillance through Automatic Dependent Surveillance-Broadcast (ADS-B).

The Wide Area Augmentation System (WAAS), FAA's SBAS, providing service in North America, was commissioned for initial operational capability in 2003. Users equipped with certified WAAS equipment now have access to precision vertical approach at thousands of airports given the development of Localizer Performance with Vertical Guidance (LPV) procedures across the NAS. WAAS also provides these users with the ability to fly area navigation (RNAV) procedures in the en route and terminal areas. Further, the FAA has approved the use of WAAS for en route and terminal operation in the NAS without requiring any other equipment onboard general aviation aircraft. WAAS is also an essential positioning source for most ADS-B compliant aircraft.

GPS, with aircraft-based augmentations such as Receiver Autonomous Integrity Monitoring (RAIM), serves a large number of users in the NAS. Air carriers and high end business users integrate GPS/RAIM with their Flight Management System (FMS) to conduct RNAV procedures within en route and terminal areas.

Currently, there are two public-use GBAS ground systems in the NAS providing Category (CAT) I procedures serving airports at Newark and Houston. The FAA anticipates increased adoption of GBAS in the near-future as aircraft OEMs continue to equip aircraft with GBAS and a number of airports install GBAS following the successful implementation in Houston and Newark. CAT II and III procedures are also anticipated with new or updated ground systems.

---

[5] TSO-C129, Airborne Supplemental Navigation Equipment Using the Global Positioning System (GPS).

[6] These receivers should not be confused with the "non-certified aviation receivers" addressed elsewhere in this Report.

The analysis in this Report is based on the concept of an “assessment zone” (Figure 5-1) inside of which GPS performance may be compromised or unavailable and GPS-based safety systems will be impacted accordingly due to the elevated levels of RFI.

The derivation of the assessment zone concept was based on engineering and operational assumptions where helicopter operations are the limiting factor. As expected, this concept generated a number of comments and questions from the community. It is worth noting that one rotorcraft operator stated that its pilots use visual reference within the assessment zone and the assessment zone would have no negative impact on their operation. However, from [6], there were unresolved concerns expressed by several, though not all, operators about the assessment zone and its impacts to aviation operations and safety.

These concerns include: technical and human factors issues associated with re-initialization of GPS after loss of the signal or when the signal reception is intermittent; workload and human factors impacts on pilots to monitor and track assessment zone locations; the possibility that pilot workload, confusion, or error could lead to aircraft inadvertently entering an assessment zone and losing needed GPS functionality; and impacts to onboard and ground systems that are dependent upon GPS, such as ADS B/C, or fixed-wing and helicopter terrain awareness warning system (TAWS/HTAWS) including obstacle alerting [6].

The FAA has not completed an exhaustive evaluation of the operational scenarios in developing this assessment zone. Further, the current analyses do not include an operational assessment of the impact of the assessment zone in densely populated areas. For example, the risk posed to people and property for operations such as unmanned aircraft systems (UAS) using certified avionics may be significant as such aircraft may be required to operate within the assessment zone.

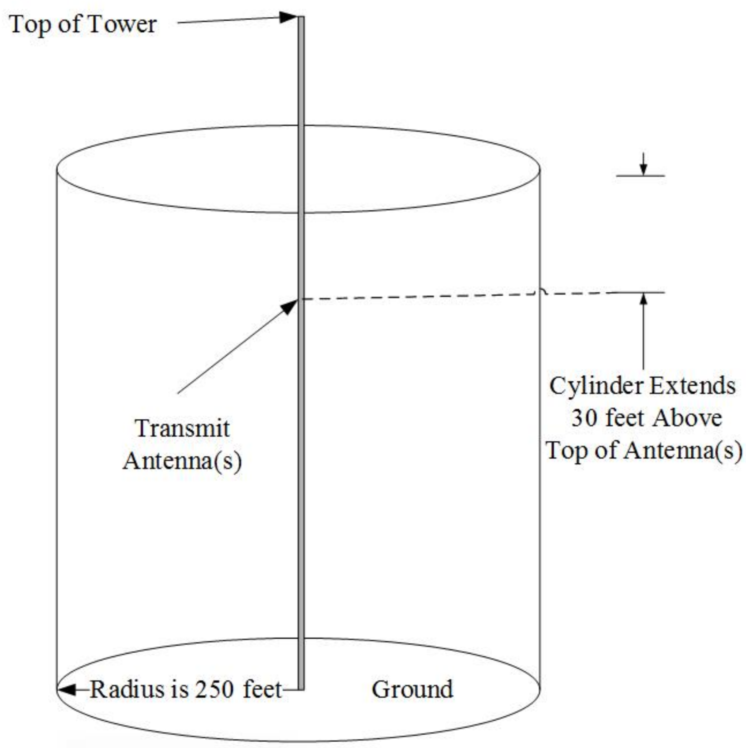

Figure 5-1: Candidate Assessment Zone (Not to Scale)

5.1.2 Tracking and Acquisition Thresholds

The tracking and acquisition performance requirements for GPS airborne receivers are defined in FAA TSO-C145, TSO-C146, TSO-C161, TSO-C196, TSO-C204, TSO-C205 and TSO-C206. The RFI aspects of these standards are identical. The relevant characteristics were first published in 1996 and invoked by the FAA in May of 1998. The same requirements have been harmonized internationally [[5], paragraph 3.7.4] since 2001. The passband for this equipment is from 1565.42 MHz to 1585.42 MHz.

5.1.2.1 Receiver Tracking Limit Criteria for Adjacent-Band RFI

MOPS adjacent- and in-band RFI rejection requirements are specified for continuous wave (CW, narrowband) radio frequency interference for the GPS band. All TSO (and European TSO [ETSO]) approved equipment is designed and tested to ensure that these requirements are satisfied. For convenience, the CW susceptibility limit curve for receiver tracking mode is shown in Figure 5-2. The adjacent-band susceptibility limits will be applied in the RFI impact analysis of the broadband wireless handset and base station emissions. Adjacent band base station broadband emission RFI effects are modelled as if the entire fundamental emission power is concentrated at the emission center frequency.[7]

[7] This assumption was validated during previous activities performed in 2011.

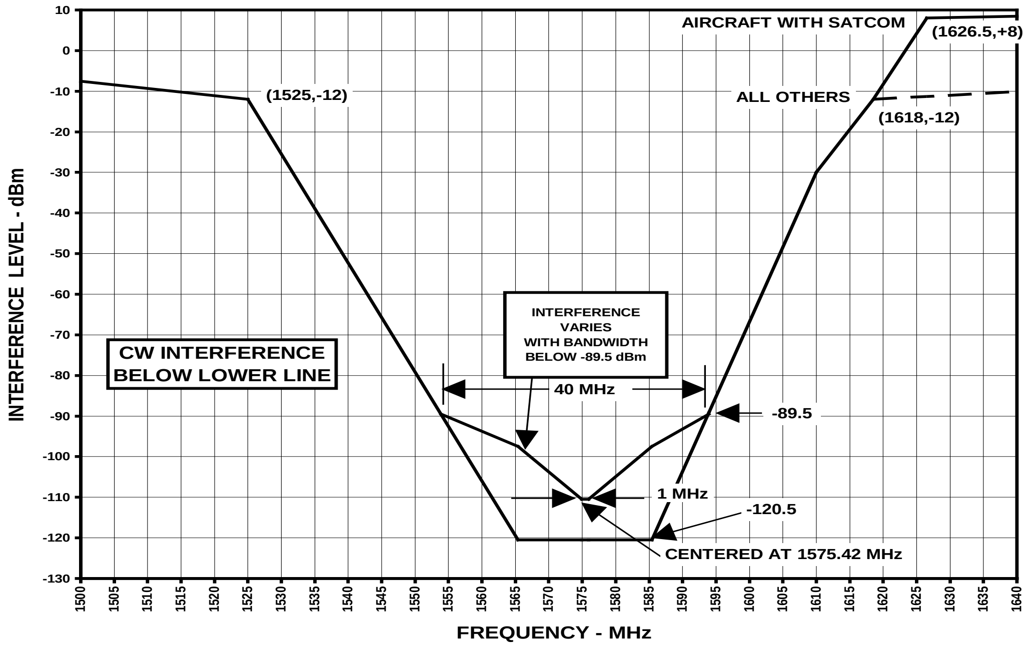

Figure 5-2: CW Interference Susceptibility vs. Frequency, Tracking Mode

To preserve the aeronautical safety margin, the maximum mean aggregate RFI power must be kept at least 6 dB below the curves at any center frequency point[8]. An additional constraint on the aggregate RFI is that the probability the received RFI exceeds a value 2 dB below the limit curve is less than 10^{-6}/hour. The 10^{-6}/hour probability represents a 1/10 portion of the overall continuity requirement for aircraft operations from en route to non-precision approach[9]. This 10^{-6}/hour limit is understood as the probability of a single disruptive RFI event. As with previous analyses, the frequency point for limit determination is the emission center frequency. For any aircraft attitude under study, the aggregate mean and rare (10^{-6}) limits apply simultaneously. A limit computed at one center frequency can be converted to the corresponding limit at a different center frequency by using Figure 5-2 and the appropriate mask slope. For example, the slope between 1525 MHz and 1565.42 MHz is -2.6843 dB/MHz.

5.1.2.2 Receiver Acquisition Limit Criteria for Adjacent-Band RFI

Another consideration is the ability for the aviation receiver to acquire GPS satellite signals. Acquisition is normally accomplished prior to takeoff and, under ideal circumstances, GPS acquisition is not necessary during flight. However, power interruptions on the aircraft or loss of GPS due to aggregate RF interference require that the aircraft be capable of GPS acquisition while airborne. Since acquisition is more demanding than tracking, the receiver standards

---

[8] This safety margin applies for aircraft airborne and ground operations.

[9] The reliability of the positioning service is specified in terms of continuity (see Section 2.3.3 of the WAAS Performance Standard [13]) The more stringent requirement is for en route through non-precision approach where the service is defined from the surface of the earth to 100,000 feet. The associated continuity requirement is 10^{-5} per hour.

specifications require operation with a 6 dB lower interference test condition than in the tracking case. As a result, the acquisition test threshold is -34.1 dBm (-64.1 dBW) and applying a safety margin would then result in an interference threshold at -70.1 dBW.

Rather than apply this limit directly, the FAA previously determined in the 2012 Interim FAA Study Report [7] that the analysis should account for a maximum probability of 10^{-3} that the interference exceeds -64.1 dBW. While this approach discounts the additional risk to acquisition that occurs during banking or other real-world effects, it does recognize that acquisition would likely become possible at some point as the aircraft continues to fly out of the area of peak interference. For the assessment in this Report this particular threshold was not the limiting condition, so for all the certified aviation use cases/interaction scenarios in this analysis only the tracking mode was considered.

5.1.2.3 Receiver Tracking Limit Criteria for Broadband Handset RFI In-band to GPS

In this Report, all the scenarios associated with new broadband handset unwanted RFI to certified GPS aviation receivers assume operation in the presence of a baseline non-aeronautical noise-like RFI environment within the receiver passband (i.e., in-band RFI to the receiver). As stated in [8], the in-band susceptibility for broad bandwidth non-aeronautical RFI is specified (e.g., in RTCA DO-229 Appendix C, Table C-2 [9]) as -110.5 dBm/MHz (-140.5 dBW/MHz) in a ±10 MHz band centered on 1575.42 MHz. As with the adjacent band susceptibility, this limit represents an airborne receiver test condition limit and, for aviation safety considerations, the mean environment aggregate RFI power spectral density (PSD) must be kept at least 6 dB below the test limit. Recent studies (e.g. [8]) have shown that an existing baseline environment results in an aggregate received RFI whose probability distribution tail essentially reaches the operational probability limit for precision approach. As such, any additional aggregate impact from new broadband wireless source unwanted emission will need to be well below that of the baseline environment. The limit used for these analyses is that the aggregate effect from additional in-band RFI does not increase the exceedance probability by more than 6% [10].

5.1.3 Transmitter and Receiver Component Assumptions

The transmitter portion is intended to be a single description for the full DOT ABC study. Regarding the receiver, the primary assumptions are the interference threshold (above) and the receiver antenna gain model. However, the “transmitter” material in this section describes important assumptions used in the FAA certified aviation receiver analyses; some of which may be different than in the other DOT analyses.

5.1.3.1 GPS Receive Antenna Gain

An FAA Federal Advisory Committee, RTCA Special Committee (SC-159), has developed a representative lower hemisphere antenna gain pattern model for the GPS receive antenna mounted on the top of the aircraft fuselage. The vertical and horizontal polarization pattern models are assumed to be azimuthally symmetric and dependent solely on the elevation angle from the aircraft horizon and represent the maximum gain for the particular RFI signal polarization. The gain pattern model is dependent on the approach category for which the aircraft is certified.

The lower hemisphere aircraft receive antenna pattern model in terms of gain versus elevation angle (angle between the aircraft horizon and the line joining aircraft and RFI source) is illustrated in Figure 5-3. This pattern is used for the broadband handsets and base stations unwanted emission analyses when those source antenna heights are below the aircraft antenna height.

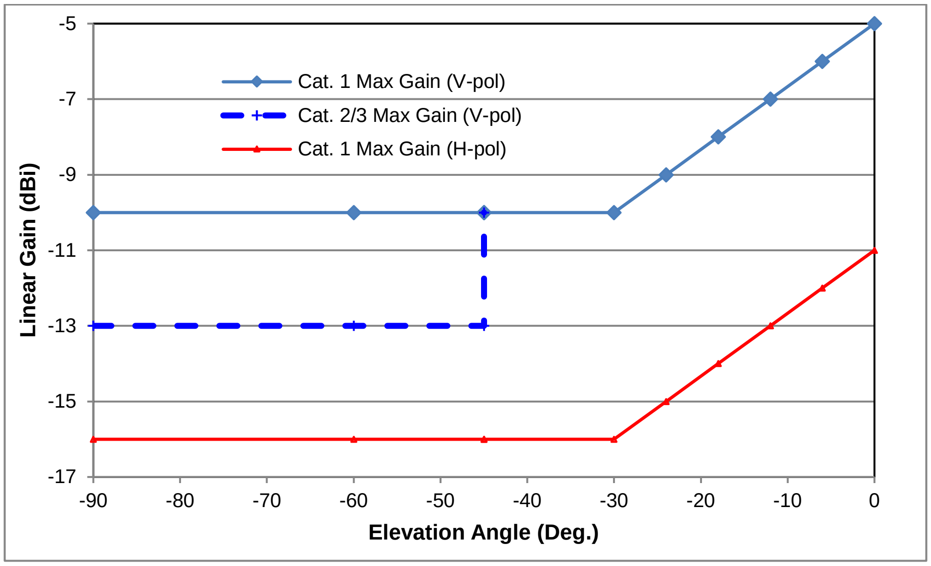

Figure 5-3: Lower Hemisphere Installed V-pol and H-pol Receive Antenna Patterns Max. Gain vs. Elevation Angle

(Cat.I GVPOL = -10 dBi for $-90° \leq el < -30°$; = $-10 + (5 + el/6)$ for $-30° \leq el \leq 0°$)
(Cat. II/III GVPOL = -13 dBi for $-90° \leq el < -45°$; = Cat. I GVPOL for $-45° \leq el \leq 0°$)
(GHPOL = -16 dBi for $-90° \leq el < -30°$; = $-16 + (5 + el/6)$ for $-30° \leq el \leq 0°$)

The upper hemisphere aircraft installed receive antenna maximum gain pattern model for linear vertical polarization is shown in Figure 5-4. This pattern is used in cases where the source antennas are at, or above, the height of the aircraft antenna.

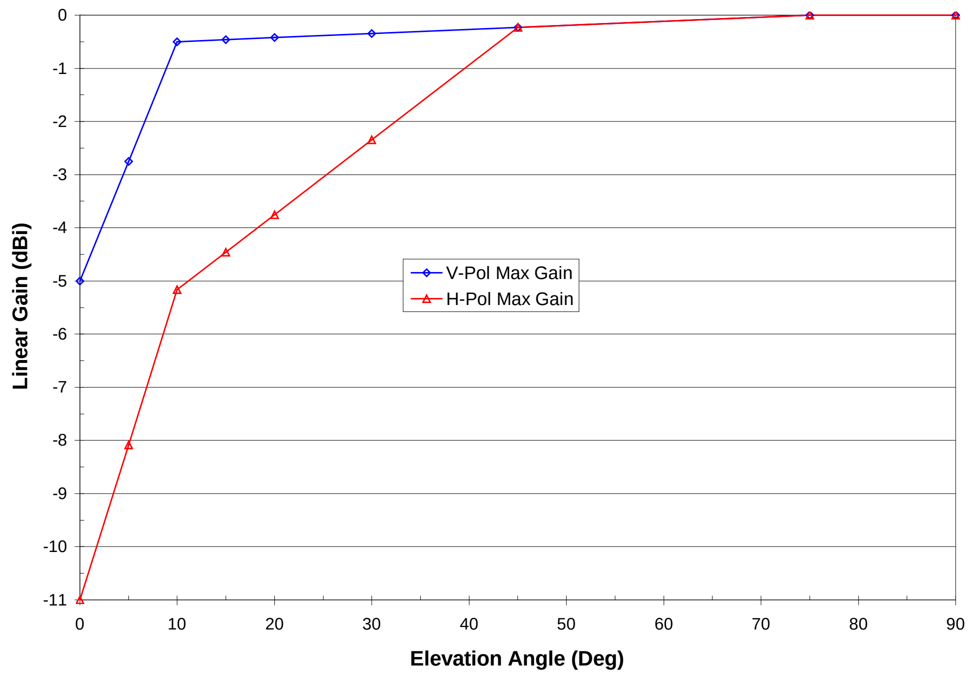

Figure 5-4: Upper Hemisphere Installed V-pol. And H-pol. Receive Antenna Patterns Max. Gain vs. Elevation Angle

(GVPOL = 0 dBi, 75°≤ el; = -0.5+0. 0077(el-10), 10°≤ el ≤ 75°; = -5+0.45•el, 0 ≤ el < 10°)
(GHPOL = GVPOL, 45°≤ el ≤ 90; = GVPOL – (6*(45-el)/45), 0°≤ el ≤ 45°)

In the analyses that follow, the aircraft antenna is either assumed to be boresighted at zenith (for an aircraft in level flight) or banked (for a banking aircraft) at a particular angle towards a particular azimuth bearing.

5.1.3.2 Broadband Wireless Base Station and Mobile Handset Characteristics

5.1.3.2.1 Broadband Wireless Base Station Characteristics

The broadband wireless base stations used in this analysis are assumed to utilize a 3-lobed transmit antenna pattern with a narrow beam elevation plane shape and a broader beam azimuth plane shape. The three lobes are assumed to be centered nominally 120° apart and down-tilted slightly in elevation (see Appendix G for antenna pattern details). The base station signal radiation is assumed to be either vertically polarized or +/-45 degree cross-polarized. This cross-polarized signal is equivalently modeled for GPS RFI analyses as a dual, equal amplitude vertically and horizontally polarized signal. The antenna lobes are each assumed to transmit an equal effective isotropic radiated power (EIRP) relative to beam-center. Determination of that EIRP value for compatibility with aviation GPS operation is the goal of the study. The necessary emission bandwidth is assumed to be 10 MHz at a 1531 MHz center frequency though other possible center frequencies were considered.

The analyses used two different strategies for the key base station parameter of antenna height above terrain: one, a fixed height for all antennas; or two, a set of heights specified by a representative deployment over a wide area. The antenna towers were either at specific deployment locations (e.g., a hexagonal grid of locations with fixed grid spacing) or a random distribution of locations with a given average surface concentration.

5.1.3.2.2 Broadband Wireless Mobile Handset Characteristics

In order to perform the certified avionics assessment versus broadband wireless mobile handsets operating above 1610 MHz, a worst-case approach was used. Broadband wireless handsets in these analyses are assumed to have a similar necessary emission bandwidth as the base station but with a center frequency at or above 1616 MHz. Maximum fundamental power was assumed to be less than 1 Watt (0 dBW). The assumed handset antenna height above terrain is 1.8 meters unless otherwise noted and has an omnidirectional antenna pattern. The handset is assumed to have a specified unwanted effective isotropic radiated power spectral density limit (less than -95 dBW/MHz) within the GPS receiver band (1565.42 – 1585.42. MHz). For one scenario, ground-based handsets were assumed to be randomly distributed with an average surface concentration of up to 180 per square kilometer. Other scenarios utilized a different distribution.

5.2 Transmit Power Level Calculations

The following material discusses various scenarios and conditions used for the analyses in this Report. Table 5-1 summarizes these activities.

Table 5-1: Analysis Scenarios and Conditions

Scenario	Conditions
Inflight Aircraft / Ground-based Handset	Final Approach Fix (FAF) Waypoint (WP) Cat. I Decision Height (DH) Cat. II DH
Inflight Aircraft / Ground Base Station	Random and discrete tower locations, Specified aircraft locations and altitudes, flight attitudes: -25^{o}, 0^{o} banking
Inflight Aircraft / Onboard Handset	10K ft altitude
Aircraft on Ground / Onboard Handset	Aircraft antenna at 4 m
Aircraft at Gate / Single Handset Source on or near Boarding Stairs or Jetway	0 dBW @ 1616 MHz

Aircraft at Gate/Users Inside Airport	Random distribution of thirty handsets
TAWS / HTAWS Scenarios with Ground-based Mobile Broadband Handsets	Three handset surface concentrations(30, 75, 180 per sq. km), with -95 dBW/MHz in the GPS L1 receiver passband, Two aircraft antenna heights (25.9 & 53.3 m)
TAWS and HTAWS Scenarios with Broadband Base Station	Base stations located on a grid with 433m or 693m inter-station distance. Base station heights of 6, 10, 15 and 25 m were considered, with 2, 4, 6, and 8 degree antenna down tilt. Aircraft was assumed at the worst-case location on the assessment zone, both level flight and 25 degree bank toward the base station[10]. Additional parameters including sloping ground were utilized as part of a sensitivity analysis as described in 5.3.3.8.

5.2.1 Use Case/Interaction Scenario Development

The certified aviation assessment considered five use cases or interaction scenarios. In all scenarios, the key parameters of interest were aircraft and source antenna heights and orientation, number and relative location of the sources with respect to the aircraft, and the aircraft GPS receiver operation under assessment. The results for these scenarios are summarized below and additional information can be found in the FAA GPS Adjacent-Band Compatibility Study Methodology and Assumptions with RTCA SC-159 [10].

5.2.1.1 Inflight Aircraft/Ground-Based Source Scenario Set

As noted above, for all the interaction scenarios the GPS receivers are assumed to operate in the signal tracking mode. Four sub-cases were considered within this set: Handsets, discretely-located base stations, randomly-located base stations and TAWS/HTAWS/low-altitude scenarios.

5.2.1.1.1 Inflight Aircraft/Ground-Based Handset Cases

The geometric parameters for this group of cases (Final Approach Fix waypoint (FAF WP), Category I decision height and Category II decision height) were developed from previous studies. The FAF WP case was also used to represent airborne terminal area operations, while the other 2 cases represent limiting cases on aircraft precision approaches. The mobile broadband

[10] These parameters focus on a “small cell” topology for the broadband wireless base stations.

ground-based handsets in these cases were assumed to have a 1.8 meter antenna height and randomly located in a uniform distribution at one of three different surface concentrations (30, 75, 180 per sq. km) extending to the radio horizon (except where excluded from annular sector zones). The assumed unwanted EIRP level for these handsets was -95 dBW/MHz in the GPS L1 receiver passband.

5.2.1.1.2 Inflight Aircraft/Ground-Based Base Station Cases

The interference analysis methodology for the ground base station cases used a representative scenario encompassing three different aircraft waypoint locations (JTSON, WIRSO, FIROP) on the RNAV (RNP 0.11) approach to DCA Runway 19. Corresponding antenna heights (548.6 m, 125.64 m, 67.52 m) were used to represent points on a typical aircraft approach to a landing. The aircraft was either in level flight or in a 25° bank toward the worst-case direction. These cases were assessed under discrete and random base station location scenarios.

5.2.1.1.3 Inflight Aircraft / Discretely-located Ground Base Station Cases

For the discretely located case, base stations are at different radii and typically have a varying height distribution. In the discrete propagation model the effective antenna height of a given tower was generally the tower height above the ground at its base (taken from representative deployment data) added to a correction term that accounts for the average height of the tower base above mean sea level (MSL). The local ground height at the tower base was determined from The National Map of the United States Geological Survey (USGS). This data is available at "https://nationalmap.gov/elevation.html". The aircraft antenna height was adjusted for the same average base ground height. This correction feature accounted for the first order effect the terrain variation on the path loss and also provided accurate antenna pattern angles needed for a "flat earth" analysis. Additional correction was used for situations where the terrain exhibits a significant slope in the direction toward the aircraft in addition to undulation.

5.2.1.1.4 Inflight Aircraft / Randomly-located Ground Base Station Cases

The randomly located base station case is included in the analysis only for comparison with results from the discrete scenario. Based on prior analysis [10], and even though this case may under-bound the resultant power emission limit computation, these results serve as a check on the discrete case result. Randomly located analysis was also used to address the relative impact for higher concentrations of base stations with correspondingly smaller radius cells.

5.2.1.2 TAWS/HTAWS and Low Altitude Positioning and Navigation Scenarios

The encounter scenarios for TAWS and HTAWS are premised on aircraft operations at low altitude relative to the terrain while using the installed GPS receiver to determine position/velocity data for comparison with a terrain and obstacle data base. The aircraft may be in level flight or banking up to a given angle (aircraft- and operation-dependent).

The same TAWS/HTAWS encounter geometries were also assumed to hold for low altitude aircraft Positioning/Navigation (Pos/Nav) operations. The principal difference in Pos/Nav operations is that the GPS receiver position/velocity output is used to determine aircraft flight control signals (e.g., a helicopter on a point-in-space approach) or attitude determination (e.g., UAS attitude and heading reference system [AHRS] applications).

5.2.1.2.1 TAWS / HTAWS and Pos/Nav Scenarios with Ground-based Mobile Broadband Handsets

In a previous analysis [7], the mobile broadband handset aggregate unwanted emissions were determined to be most significant for the Cat II DH scenario where the aircraft antenna was 25.9 m above the ground. In that analysis, assessment zones were assumed where mobile handsets could NOT be operated (e.g., within the airport runway object-free area, obstacle clearance zone, etc.).

For this analysis the mobile broadband handsets were assumed to be randomly distributed at one of 3 different surface concentrations (30, 75, 180 per sq. km). Their assumed unwanted emission level was -95 dBW/MHz in the GPS L1 receiver passband. At these surface concentration values, the fundamental emission effects were insignificant. The two different aircraft antenna height cases analyzed were 25.9 m and 53.3 m.

5.2.1.2.2 TAWS and HTAWS Scenarios with Broadband Base Stations

The hexagonal cellular system for this scenario consists of a central tower plus 19 concentric hexagonal rings of towers, all at a particular inter-site distance (ISD) (i.e., distance between towers) for a total of 1,141 towers with a grid maximum radius of 8.2 km. The aircraft (in this case a helicopter) is assumed to 250 feet (76.2 m) from the central tower at an azimuth bearing of 30 degrees. This is the same azimuth as that of the main lobe of one of the three antennas on the central tower, the three being equally spaced 120 degrees apart. Transmissions are assumed to be equal power vertically and horizontally polarized so both the vertical and horizontal polarization attenuation curves of the aircraft GPS antenna were used. Both flat ground and sloping ground scenarios were examined. The nominal emitter antenna down tilt was 6 degrees.

5.2.1.3 Handset Sources on Board Aircraft

5.2.1.3.1 Onboard Handset Operation for Aircraft Inflight

In this scenario, the broadband wireless handsets were assumed to be operating with an on-board WiFi access point when the aircraft is above 10,000 feet (AGL) altitude. The handsets were expected to exhibit similar unwanted emissions in the GPS L1 band as in their wideband communication mode on the ground. Emissions in the WiFi transmit band (2.45 GHz) were expected to be similar to a standard mobile WiFi transceiver. If that assertion is correct, then these handsets would not present a special RFI compatibility issue on the aircraft where WiFi device operation is already permitted.

5.2.1.3.2 Onboard Handset Operation for Aircraft on Ground

In contrast to the inflight scenario, when the aircraft is taxiing toward the gate the onboard broadband handsets were assumed to communicate through a standard ground base station outside the aircraft. Because of the partial shielding provided by the aircraft fuselage, the handsets were assumed to operate at full transmit power for their necessary emission. The aircraft antenna height was assumed to be 4 m above ground and at a representative location at the start of the taxiway and the aircraft GPS receiver was assumed to be in the signal tracking mode. Propagation of handset emissions to the aircraft GPS antenna were characterized by the model in RTCA/DO-235 [5.3-3] Appendix E.6.2.

For the unwanted emission analyses, the GPS receiver was assumed to operate in the presence of a baseline level of RFI emanating from other randomly-distributed sources outside the aircraft. The analysis uses a 3x3 cabin configuration (i.e., three seats per window) meaning that there are three seats per window location on each side of the aircraft, resulting in a total of 189 seats. The handsets were distributed in a random assortment of discrete locations throughout the passenger cabin for a few representative values of total handset count. Path loss values at possible locations were taken from [5.3-3] Appendix E, Table E-10.

5.2.1.4 Aircraft at Gate Scenarios

5.2.1.4.1 Aircraft at Gate / Single Handset Source on or near Boarding Stairs or Jetway

This scenario used a single broadband wireless handset operating at full emission power and the signal propagation was assumed to be far field free-space. Handset location relative to the GPS aircraft antenna was assumed such that the receive antenna gain was -5 dBi. Given the propagation conditions and a single source, the result is deterministic. In this case for a single handset with 0 dBW EIRP operating at 1616 MHz, the minimum handset antenna separation distance for compatibility is 3.5 m. This separation might be assured by aircraft fuselage size and geometry. The unwanted handset RFI analysis was also included in the baseline RFI effect as well as the effect of unwanted RFI from a concentration of general sources inside the airport terminal.

5.2.1.4.2 Aircraft at Gate/30 Users Inside Airport

This scenario was comprised of 30 wireless broadband handsets operating in an airport terminal gate area that generate RFI to a GPS receiver on an aircraft located outside the terminal in front of the gate area. The scenario is well documented in [10]. The key factors for this analysis were as follows.

1) The aircraft GPS antenna height is assumed to be 4 meters above ground and 34 meters from front edge of terminal area.
2) The handset antenna heights are all 3 m above the aircraft antenna level (2 m above terminal floor).

3) The terminal area is assumed to be symmetrically spaced in front of the aircraft with a 20 meters average depth and 50 meters width.
4) 30 handsets are assumed to be uniformly distributed throughout the 1000 sq. m. area.
5) Handsets are assumed to be operating in the 1610-1656.5 MHz band with -95 dBW/MHz unwanted EIRP in the GPS L1 band.
6) The median path loss model was two-ray free-space at these distances but with additional building loss incorporated as follows: 20% of handsets incur an additional 20 dB loss, 60% an additional 15 dB loss, and 20% an additional 10 dB loss (excess loss assigned relative to decreasing distance from front terminal wall).

5.2.2 Propagation Models

The RFI propagation path loss models used for the certified aviation assessment are based on the flat-earth approximation. In other words, the ground under the aircraft is assumed to be essentially smooth and flat out to a radio horizon from the point on the ground directly under the aircraft. In line-of-sight propagation conditions at radio frequencies near that of the GPS carrier, this radio horizon value generally depends on the aircraft GNSS and RFI source antenna heights and the amount of atmospheric refraction along the propagation path. A 4/3 Earth radius approximation for the refractive effect on the radio horizon is used in all propagation models.

The propagation models used in this analysis can be categorized as two different types: (1) those scenarios where diffuse scattering, diffraction, and blockage were factors analyzed using probabilistic path loss; and (2) clear line-of-sight scenarios which were analyzed using deterministic free space path loss. For this assessment, the point above which free space path loss is used generally occurs at an aircraft antenna height above ground of 550 meters. Above 550 meters, various parameter limits associated with the probabilistic models are exceeded thus making their use problematic. Also at these aircraft heights, line-of-sight conditions generally prevail which means that use of free space path loss was most appropriate.

5.2.2.1 Single Path Propagation Model

For free space propagation, the signal power loss over a single path is given by the well-known inverse square law propagation model. For probabilistic propagation, the models developed by the cellular radio community are generally applicable. These models have one feature in common; the probabilistic nature of the path loss is very well approximated by the product of a slow fading process and a fast fading process (as a consequence, this is also true for the single path received interference power/power density). The slow fading process is approximated by a log-normal distribution while the fast fading process is described by a non-central chi-squared distribution. The log-normal component is completely determined by two parameters, μ and σ and the chi-squared process by the parameters, L, ψ_0 and ρ_0. The range-dependent median path loss between the GPS antenna and the interference source determines the primary component in the parameter μ while the remaining parameters vary with range depending on the scenario.

A principal component in the slow-fade parameter, μ, is the single path-median isotropic path loss. For this analysis, the median isotropic path loss was modelled using a continuous set of three basic deterministic range-dependent segments. For short ranges, a two-ray path loss model was used for distances less than the first breakpoint distance "r_1." For long ranges, a Hata-Okumura path loss model was used for distances greater than the second breakpoint distance "r_2." At intermediate ranges, at distances greater than r_1 but less than r_2, the path loss model depended on antenna heights contained in a given scenario. A modified Erceg/Greenstein model was used as the intermediate range model for most handset scenarios (aircraft antenna height ≤ 80 m, source antenna ≤ 2 m). In all other scenarios the intermediate range path loss model used an exponential fit between the short and long range models (log-linear interpolation (on path loss) versus range between the r_1 and r_2 values). In some scenarios a moderate amount of effort was required to determine the appropriate breakpoint distances. Additional details on path loss models and the calculation of breakpoint values and other model parameters are provided in Appendix F.

5.2.2.2 Aggregate Effects Model

For uniformly distributed, randomly-located interference sources, once the single path interference characteristics have been determined, it is possible to determine analytically the mean, standard deviation, and cumulative probability distribution associated with aggregate received interference power. In this case, the received power from a randomly located interfering emitter was modeled as the product of a slow fading process (log-normally distributed) and a fast fading process having a non-central chi-squared distribution with the parameters described above.

For sources having a known discrete distribution (i.e. the location and height parameters associated with each source are known), two possible approaches may be used to determine the aggregate interference power, the mean value and the cumulative distribution function. The single source received interference power in this case is also a random variable and is described by the product of a slow fading process and a fast fading process. Thus the aggregate interference power, its mean value and cumulative distribution can be determined using an analytic approach. Alternatively, it is possible to use a Monte Carlo simulation to determine both the mean aggregate interference power and cumulative probability distribution for the discrete source distribution case. Appendix F contains details of the aggregate statistics computation. The analysis of received aggregate interference from handset sources assumes that handsets are uniformly distributed over some area at an unknown random distance from the aircraft GPS receiver. Exceptions to this assumption include scenarios where the aircraft is located at the gate with handsets located within the terminal or on a stairway about to enter the aircraft. In these exception cases, a discrete distribution of handsets was assumed. For interference from base station sources, both a discrete and a random distribution of base stations were assumed.

5.2.3 Tolerable Transmit Power Calculation Results and Sensitivity Analysis

The spectrum engineering assumptions and path loss models described above were used to perform inverse transmit power calculations. Generally, this type of calculation first aggregated at one location the RFI from all emitters contained in the given scenario then calculated the single common EIRP transmission limit that satisfied the tolerable RFI constraint. Both mean based and rare event based type constraints are applicable though variations on this general method are possible and are described below.

5.2.3.1 Tolerable Transmit Power Calculation Method Overview

Two major basic types of tolerable transmit power calculations are used in this certified aviation receiver assessment. In the broadband base station calculation method, the station fundamental (adjacent band) EIRP is not known a priori and is the goal of the analysis. The tolerance criteria are simple receiver-based limits (see Sec. 5.1.2.1). In contrast for the associated broadband wireless handsets, the unwanted handset EIRP (in-band to the GPS receiver) is assumed to be at a specified limit and baseline in-band RFI is also present. Additionally, the tolerance criterion is different (see Sect. 5.1.2.3) in that the growth in exceedance probability of the composite RFI is limited to a percentage above the baseline case.

5.2.3.1.1 Tolerable Transmit Power Calculation Method – Base Station Cases

The transmit power calculation method for the base station cases assumed that each of the three antenna beams on a base station tower transmit with a normalized (unity) EIRP. A mean aggregate power factor (AF) is then computed at a desired aircraft location such as a waypoint by combining the RFI from all base station sources using the probabilistic path loss and probabilistic models described above (Sec. 5.2.2). In linear units, the AF is the received power divided by the EIRP. The analytic transmit power calculation method for the base station cases has two major steps[11]. The mean AF is computed first and then the CDF of the AF is computed. The random variable Z is the normalized AF, defined as AF/(mean AF). The CDF P(z) is defined as the probability that Z is less than or equal to z.

The corresponding mean based and rare event EIRP limits for an antenna are computed using equations (5-1) and (5-2), respectively. These equations were derived from the information provided in paragraph 5.1.2 and the spectrum mask information of Figure 5-2. The parameter “Zcrit” in equation (5-2) is the argument of the AF CDF that corresponds to a threshold exceedance probability of 10^{-6}.

$$Mean\_Based\_EIRP\_Limit = -64.11\ dBW - 10 * log_{10}(Mean\ AF) \quad \textbf{(5-1)}$$

$$Rare\_Event\_EIRP\_Limit = -60.11\ dBW - 10 * log_{10}(Zcrit) \quad \textbf{(5-2)}$$

The more stringent of the two results from

[11] In the alternative Monte Carlo method, the mean AF and the AF CDF are determined together in a single computation.

equations (5-1) and (5-2) is then the applicable limit for the particular case under study.

All the RFI calculations for the base station cases assumed the emitter has a center frequency of 1531 MHz with a 10 MHz emission bandwidth. Equations (5-1) and (5-2) are specific for a center frequency of 1531 MHz. Examples of how to convert from the 1531 MHz based EIRP limit calculated in this analysis to the corresponding limit at a different frequency are shown in section 5.2.3.7.

5.2.3.1.2 Tolerable Transmit Power Calculation Method – Handset Cases

The method for evaluating the impact of ground based broadband wireless handsets is different and more indirect than that of evaluating the RFI impact of base station emitters. Analysis has shown that the fundamental emission of the broadband wireless mobile handsets, at least up to the assumed 0 dBW maximum power and operation above 1616 MHz, are not of concern for certified avionics. As a result, rather than determining an unknown fundamental power level of the base stations as described above, the broadband wireless handsets are assumed to operate with a specified unwanted emission limit (-95 dBW/MHz) within the aviation GPS receiver passband. For certain scenarios, various values for the average number of handsets per unit area (randomly distributed) are also assumed up to a maximum. The tolerability criterion for the handset cases (5.1.2.3) is a limit on the percentage growth in RFI impact for the addition of new handset sources to the baseline RFI condition. For handset cases the RFI impact is quantified by the probability of the aggregate RFI power density exceeding the certified aviation receiver MOPS test threshold (-140.5 dBW/MHz). Appendix F has details on computing the aggregate RFI cumulative probability distribution.

5.2.3.2 Results for Inflight Aircraft/Ground-based Handset Cases

Details of the baseline RFI impact computation are given in [8]. In summary the baseline condition is developed by a random distribution of sources (1.8 m antenna height) out to the radio horizon at an average concentration of 100 per square kilometer with an individual unwanted emission of -81.1 dBW/MHz. The limiting case baseline scenario geometry in [8] is the Category II DH waypoint (25.94 m aircraft antenna height). Table 5 of [8] shows the aggregate received RFI power density exceeds the MOPS test threshold (-140.5 dBW/MHz) at a probability of 3.0144×10^{-4} as predicted by the generalized model.

The RFI impact of the composite of broadband wireless handsets with the baseline RFI is analyzed in two steps. First a random distribution of only the broadband wireless handsets is analyzed with the same scenario geometric constraints as in the baseline RFI case. The handsets (1.8 m antenna height, 180 per sq. km. average) are assumed to emit -95 dBW/MHz unwanted power density in the GPS receiver passband (1575.42 ± 10 MHz). The desired analysis results are the handset-only statistics (mean and CDF). Then these statistics are combined with those of the baseline to form the composite statistics (computation details in Appendix F).

The handset scenario baseline and composite statistical results are shown in two CDF (1-P(z)) curves (Figure 5-5). The dashed (baseline) curve is based on an average concentration of 100 baseline emitters per square kilometer. The solid (composite) curve is based on 280 total emitters per square kilometer. In Figure 5-5, the Z value (x-axis point)[12] at which the baseline curve exceeds the MOPS test limit is 16.4722. The associated y-axis (1-P(z)) value is 3.0144×10^{-4}. Since the composite case (baseline + handsets) mean value is somewhat higher, the composite curve Z value is 15.34512 at the MOPS threshold and the associated probability on the red solid curve is 3.06224×10^{-4}. This 1.59% probability increase from the baseline probability is below the maximum tolerable increase of 6%. Thus, this scenario is assessed as not a critical or limiting scenario based on the assumed handset-related parameters.

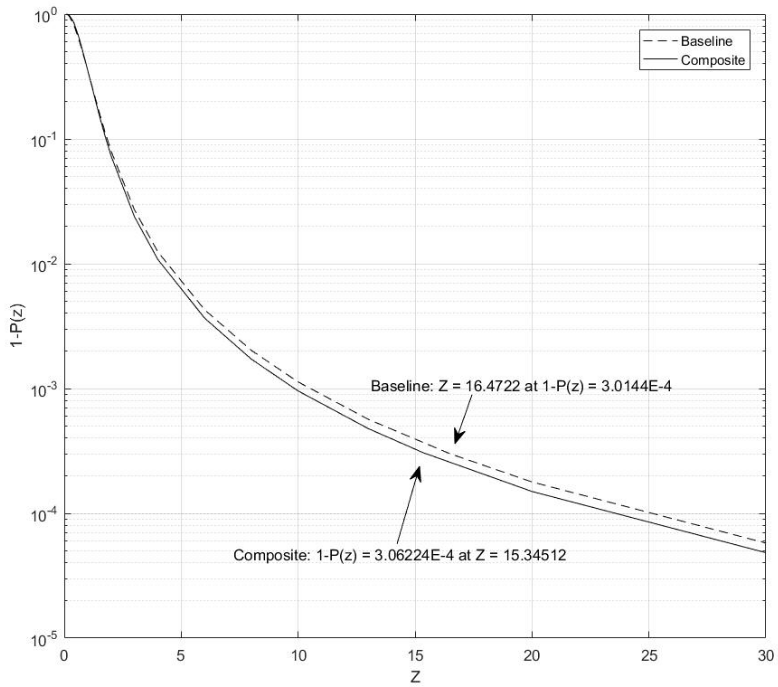

Figure 5-5: Handset Scenario Probabilities

5.2.3.3 Results for Inflight Aircraft / Ground Based Base Station Cases

Results presented here were obtained for the WIRSO case discussed in Section 5.2.1.1.2. This specific waypoint places the aircraft nadir axis at 38.8816° North latitude and 77.046° West longitude with the GPS antenna at an altitude of 125.64 meters above Mean Sea Level (MSL). The aircraft was located over the Potomac River near the Tidal Basin in Washington DC.

---

[12] As defined earlier, the x-axis parameter Z is the algebraic ratio of the aggregate power density to the mean aggregate power density. Thus the point Z=1 corresponds the mean aggregate power density.

The analysis was performed assuming each interfering base station operates in the adjacent band just below the GPS L1 band with an emission bandwidth of 10 MHz. While analyses for three different base station center frequencies was initially intended, the results herein were completed only for the frequency 1531 MHz. Extension to other frequencies can be performed as described in Section 5.1.2 of this Report. The base station key operational parameters are described in Section 5.1.3.2.

The propagation model used in the analysis was that described above in Section 5.2.2.1. As discussed, this model incorporated a median path loss component between the GPS antenna and the interference source which, along with the normalized base station and GPS antenna gains, determined the log normal distribution parameter, μ . The single path median isotropic path loss, PL(r), is composed of three range dependent segments. The WIRSO median isotropic path loss model used a two-ray model for short ranges ($r< r_1$), an exponential fit model for intermediate ranges ($r_1 \leq r \leq r_2$), and the Hata-Okumura model for longer ranges ($r> r_2$). The detailed definition of these models is contained in Appendix F.

As a further refinement, the WIRSO interference scenario analysis also included a terrain dependent slope correction factor which was incorporated into the Hata-Okumura long range median path loss model [10]. To accurately model the scenario terrain slope, the area surrounding the aircraft location was divided into 12 azimuth sectors of nominally 30° angular width. (See Appendix F for additional details.)

Table 5-2 lists transmission power limits computed using the WIRSO scenario. The results of this table were obtained using both the Analytic Statistical method and the Monte Carlo method and there is good agreement between the results of the two methods. The Mean Power Based EIRP Limit value in the table is based on the mean limit of -64.1 dBW at 1531 MHz while the Rare Event Based EIRP Limit value is based on the -60.1 dBW limit. These results apply for both flight attitudes.

Table 5-2: WIRSO Scenario Based Limits from Two Methods

Method	Flight Attitude	Mean Agg. Power Factor (dB)	Mean Power Based EIRP Limit (dBW)	Zcrit	Rare Event Based EIRP Limit (dBW)
Analytic Statistical	Level Flight	-97.85	33.75	3.0974	32.84
Monte Carlo	Level Flight	-97.89	33.79	3.0205	32.99
Analytic Statistical	Banking, -25 deg.	-94.41	30.31	3.3547	29.06
Monte Carlo	Banking, -25 deg.	-94.47	30.37	3.5300	28.89

The results listed in Table 5-2 include values for "Zcrit", the Z value (as defined earlier Z is the aggregate interference factor (AF)/mean AF) for which the probability of the corresponding CDF curve is $1x10^{-6}$. Figure 5-6 consists of two curves for the WIRSO banking scenario which overlap for low values of Z but diverge at Z values of about 3.35 and higher. This figure provides an indication of the solution sensitivity to the solution method. The ordinate of each curve is plotted as "1 - CDF" (i.e., "1 – P(z)") instead of as a traditional CDF for the sake of convenience. The curves shown correspond to the bottom two rows of Table 5-2. While the precision of the Monte Carlo results for higher Z values could be improved if more time-consuming calculations were made, that exercise is unnecessary given Z values for 1-P(z) values below $1x10^{-6}$ are not needed.

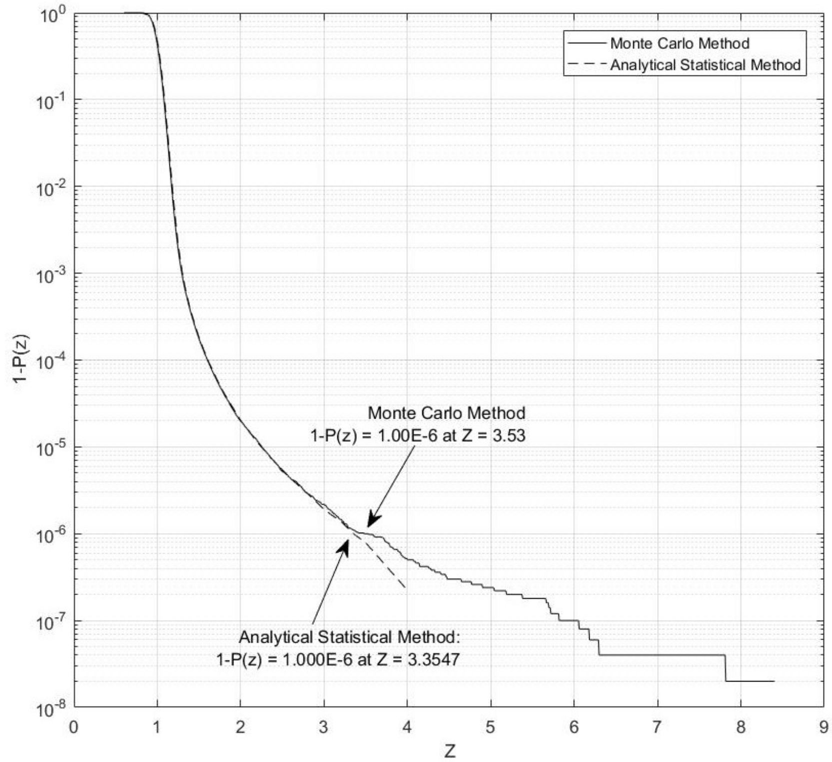

Figure 5-6: WIRSO Banking Scenario 1 – P(z) values Using Two Methods

The WIRSO scenario results were also computed using a third method. The WIRSO limits computed using the random location method are shown in Table 5-3. A random location model scenario result was computed for each limit type because the underlying assumptions used to model the tower locations were adjusted.

Table 5-3: WIRSO Scenario Based Limits from Random Method

Random Model Scenario	Flight Attitude	Mean Agg. Power Factor (dB)	Mean Power Based EIRP Limit (dBW)	Zcrit	Rare Event Based EIRP Limit (dBW)
1	Level Flight	-97.45	33.35	2.497	33.37
2	Banking at -25deg	-95.48	31.38	2.497	31.41

A comparison of the EIRP limits computed using the Analytical Statistical discrete and random location methods (random-discrete result) is shown in Table 5-4. The comparison shows relatively good agreement for the level flight scenario mean power based limit but there are larger differences for the banking scenario and for the rare event based limits. These differences arise from the same fundamental issue, i.e., the highly asymmetrical distribution of the towers with respect to azimuth and distance. The analytical statistical method uses actual tower locations while the random method used random assignment based on an approximation of the tower locational distribution. Of more significance, the analytical statistical method computes a cumulative distribution function directly from a characteristic function which was computed using actual tower locations. In theory the analytical statistical method will more accurately capture the probabilistic impact of the asymmetric tower distribution. The primary purpose of the random method in this instance was to serve as a reasonableness check for the analytical statistical method solution. As a result, the analytical statistical method based limits of Table 5-2 are cited as the WIRSO results.

Table 5-4: Comparison of Two Methods for WIRSO Scenario Based Limits

Flight Attitude	Method Delta - Mean Power Based EIRP Limit (dBW)	Method Delta - Rare Event Based EIRP Limit (dBW)
Level Flight	0.40	-0.53
Banking at -25deg	-1.07	-2.35

5.2.3.4 Results for Onboard Handset Operation for Aircraft on Ground

The locations of the handsets are the random variables selected in each realization within the Monte Carlo simulation. This effort distributed handset locations uniform randomly throughout the cabin and computed the normalized aggregate personal electronic device (PED) power factor ($F_{AGG,PED}/IPL_{MIN}$) which is independent of PED EIRP. Although biasing handset locations toward the front of the aircraft (lower path losses) where potentially more first-class passengers would operate a handset was considered, the Monte Carlo results in Figure 5-7 suggest such a constraint is unnecessary. The difference between the maximum and mean aggregate power factor indicates that the handset locations need not be biased toward the front. With more than approximately 20 handsets, the difference between the maximum and mean power factor is less than 3 dB.

Assuming 100 of the 189 possible handsets[13] are operating simultaneously indicates mean aggregate signal loss of approximately 52 dB. Using this loss with a fundamental handset power of 0 dBW gives a power at the aircraft antenna of -22 dBm. This fundamental power is essentially at the aviation mask with 6 dB safety margin for the 1616 MHz frequency. Considering the emissions level of -95 dBW/MHz, this level leads to unwanted emissions in the GPS L1 band of -147 dBW/MHz. At the limit of all 189 handsets operating, the

[13] During the scenario development, the number of users were chosen to provide an overbound/stress case to support the stated conclusion that no interference to certified avionics is expected from handsets with the postulated technical characteristics.

aggregate signal loss is 48 dB which results in slight exceedance of the aviation mask with safety margin included. The scenario of all 189 devices operating simultaneously at exactly their maximum levels for both fundamental and unwanted emissions is considered very conservative so this is not deemed a limiting case. These results indicate that no further assessment was required. If a further assessment were to be performed, it should also include computation of a baseline RFI condition without broadband wireless handsets as stated in Section 5.2.1.3.2.

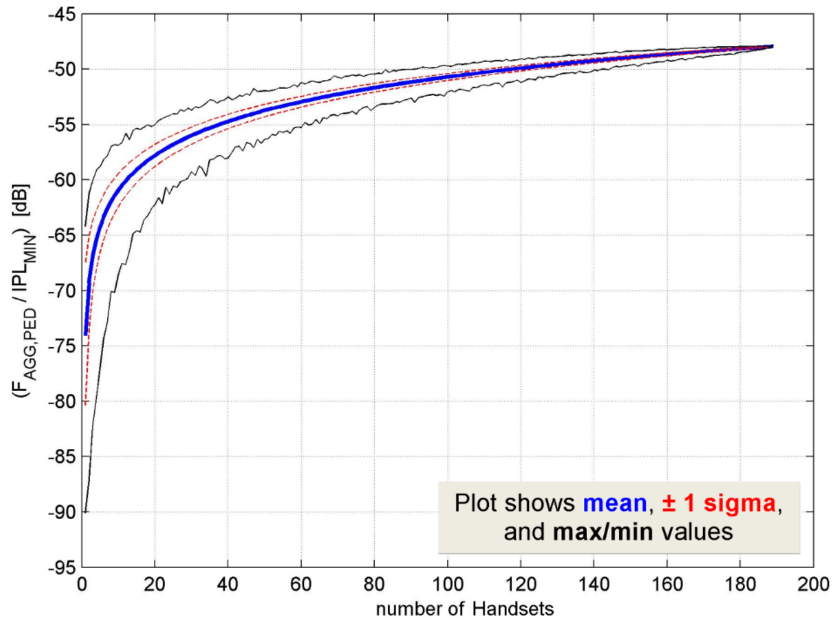

Figure 5-7: Aggregate Handset Signal Loss

5.2.3.5 Results for Aircraft at Gate/30 Users Inside Airport

Computations from RTCA DO-235B Appendix E, Equations E-1 and E-2 were again applied to compute the aggregate power factor and normalization factor. The scenario can be visualized as shown in Figure 5-8.

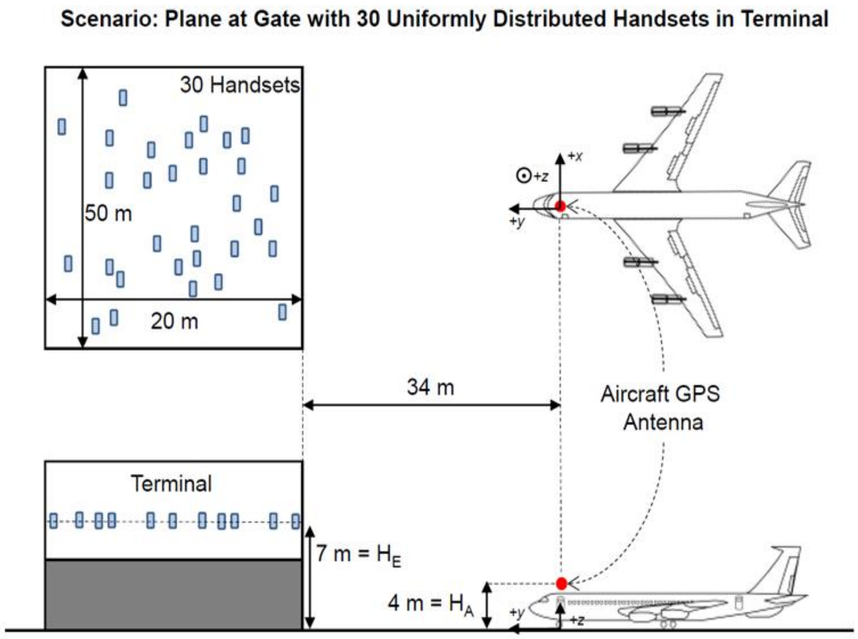

Figure 5-8: Aircraft at Gate with Thirty Uniformly Distributed Handsets in Terminal

Figure 5-9 shows the normalized factor as function of the number of handsets. (To compute the aggregate RFI power, add the handset EIRP to the abscissa. For example, 30 handsets with unwanted emissions at -95 dBW/MHz and 60 handsets[14] with unwanted emissions at -81 dBW/MHz result in a mean received aggregate interference power of -145.9 dBW/MHz.) These results indicate that no further assessment was required. If a further assessment were to be performed, it should also include computation of a baseline RFI condition (general sources inside and outside the terminal) without broadband wireless handsets as stated in Section 5.2.1.4.1.

[14] During the scenario development, the number of users were chosen to provide an overbound/stress case to support the stated conclusion that no interference to certified avionics is expected from handsets with the postulated technical characteristics.

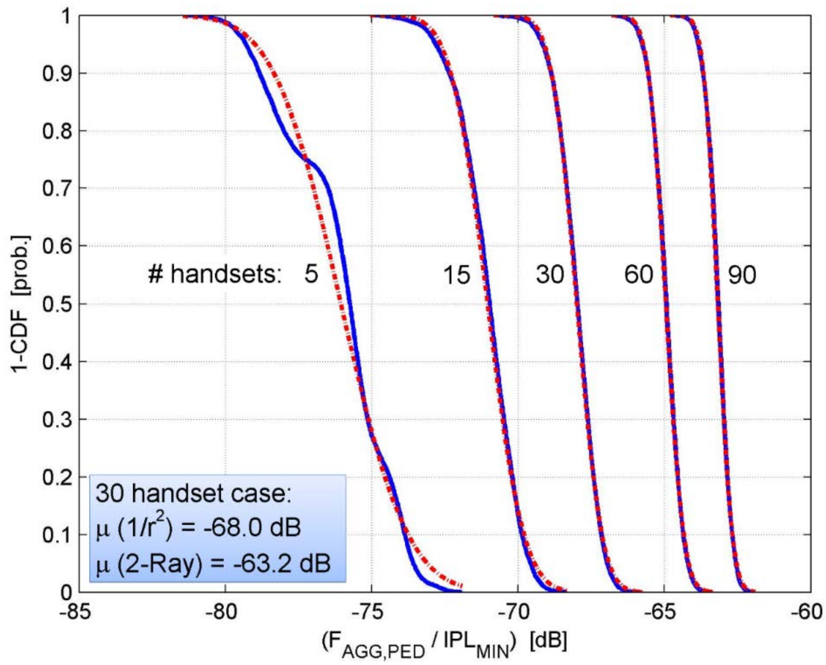

Figure 5-9: (1-CDF) Aggregate Power Factor

5.2.3.6 Results for Inflight Aircraft TAWS/HTAWS and Low Altitude Pos/Nav

The limiting EIRP for the emitters used in this scenario was evaluated using a different distribution of towers and a different relative aircraft location than the evaluation at the WIRSO waypoint described above. The hexagonal cellular system of this scenario consists of a central tower plus 19 concentric hexagonal rings of towers, all at a particular inter-site distance (ISD) for a total of 1,141 towers with a grid maximum radius of 8.2 km. The helicopter is assumed to 250 feet (76.2 m) from the central tower at an azimuth bearing of 30 degrees. This is the same azimuth as that of the main lobe of one of the three antennas on the central tower, the three being equally spaced 120 degrees apart. Transmissions were assumed to be equal power vertically and horizontally polarized so both the vertical and horizontal polarization attenuation curves of the aircraft GPS antenna were used. Both flat ground and sloping ground scenarios were examined.

The nominal emitter antenna down tilt was 6 degrees. Sensitivity analysis for this scenario included varying the degree of down tilt and the aircraft distance from the central tower keeping in mind the importance of having the helicopter located in the center of a main lobe of a central tower antenna. Other parameter sensitivity variations included using vertical polarization-only type transmissions, varying the ISD and "rounding out" the perimeter of the hexagonal grid system into a circle (thereby increasing the number of towers to 1,345).

In this scenario, the dual polarization nature of the RF signal makes the calculation of the r_1 breakpoint more complex. This breakpoint was set to be the closest radius at which the vertical and horizontal polarization path losses are equal just beyond the point at which the vertical polarized ray is at its critical grazing angle (at approximately 112.5 m). Also different in this study is that the Hata r_2 breakpoint was set to be 1,000 m in all scenarios.

A consistent result of all the parameter variations studied is that more that 90% of all RFI comes from the central tower. While this is not surprising due to the distances involved, a consequence is that the two-ray model becomes the primary path loss model, whereas in the WIRSO scenario all towers were beyond the r_1 breakpoint. The scenario primacy of the two-ray model in combination with the sensitivity of the aircraft antenna to polarization type and elevation angle meant that an additional level of detail to the RFI calculation procedure was needed. The two-ray path loss calculations were modified to account for the direct and reflected rays entering the helicopter antenna at different elevations and hence attenuated differently. The two-ray path loss model also computes different reflection coefficients (magnitude and phase) for vertically and horizontally polarized waves.

This scenario used a different antenna pattern than the WIRSO scenario. The transmit antenna models for both scenarios are functions of azimuth and elevation but in this scenario the central tower antenna oriented at an azimuth of 30 degrees had a minimum gain of -15 dB imposed for elevations lower than -22 degrees in order to account for a lack of symmetry. Details for the base station antennas are contained in Appendix G.

The EIRP limits computed using both the Monte Carlo and Analytic Statistical methods are shown in Table 5-5. The results show good agreement between the two methods. Some parameter combinations were Not Computed (NC) because they obviously would not constitute a limiting condition and are thus rendered moot. The assumptions used to calculate the results of Table 5-5 include a helicopter located 76.20 m (250 ft.) from the central tower with all tower heights of 25 m for flat ground scenarios. The sloping ground scenarios assume a funnel shaped terrain with an upward slope of 10 milliradians with the central tower at the bottom of the funnel. In the sloping ground scenario the height above local ground for all towers remains 25 m but the effective tower height with respect to the aircraft increases with the rising ground.

Table 5-5: Hexagonal Grid Power Limits Computed Using Two Methods

Scenario Number	Inter Site Distance (m)	Aircraft Bank Angle (deg)	Terrain Slope (milli-radians)	Tower Antenna Down Tilt (deg)	Aircraft Height (m)	Mean Based Limit (dBW)		Rare Event Based Limit (dBW)	
						Monte Carlo	Analytic Statistical	Monte Carlo	Analytic Statistical
#1	693	0	0	6	16.99	13.35	13.34	13.37	NC
#2	433	0	0	6	16.99	13.31	13.3	13.36	NC
#3	693	0	10	6	16.99	13.30	13.26	13.32	NC
#4	433	0	10	6	16.99	13.21	13.11	13.29	13.06
#5	433	25	10	6	16.99	10.28	10.27	10.34	10.18
#6	433	25	10	8	14.29	10.16	10.36	10.19	NC

Results were computed for other hexagonal grid scenarios using the Monte Carlo method. These results are shown in Table 5-6. The results were computed using the same general assumptions listed for Table 5-5. None of the results contained in Table 5-6 indicate a more stringent limit than that indicated by Table 5-5.

Table 5-6: Hexagonal Grid Power Limits Computed Using 433m ISD Flat Earth Scenario

GPS Rx antenna height at Max EIRP (m)	Max Tx EIRP (Multiple Towers) (dBW)					
	No Banking				25° Banking	
	6m Base Station Tower with 2° Down Tilt	10m Base Station Tower with 4° Down Tilt	15m Base Station Tower with 6° Down Tilt	25m Base Station Tower with 8° Down Tilt	15m Base Station Tower with 6° Down Tilt	25m Base Station Tower with 8° Down Tilt
4	24.90	20.45	16.19	13.26	14.13	11.80
6	23.84	19.83	15.60	12.96	12.92	11.72
8	22.95	19.62	15.28	12.17	11.97	10.71
10	22.51	19.61	15.37	11.79	11.44	10.40
12	22.18	19.24	15.89	11.78	11.34	10.38
14	22.41	19.59	16.75	12.36	11.60	10.37
16	*	19.91	17.81	13.06	12.45	10.45
18	*	20.31	18.46	13.90	12.63	10.68
20	*	*	19.78	14.86	13.90	11.05
22	*	*	21.02	15.98	15.09	11.50
24	*	*	22.53	17.31	16.36	12.10
26	*	*	*	18.45	*	13.09
28	*	*	*	19.62	*	13.96
30	*	*	*	20.73	*	15.25
32	*	*	*	22.17	*	16.58
34	*	*	*	23.63	*	18.03

*Not assessed

EIRP limits were also computed for a helicopter on the ground. These results are shown in Table 5-7 and none of the results contained in this Table indicate a limit more stringent that that indicated by Table 5-5.

Table 5-7: Power Limits for Landed Helicopter at Various Separation Radii from Central Tower

Separation Radius from GPS Rx to Central Tower (ft)	Base Station Antenna height (m)	Base Station Antenna down tilt (deg)	GPS Rx antenna height at Max EIRP (m)	Max Tx EIRP (Multiple Towers) (dBW)
50	25	8	4	14.59
100	25	8	4	18.31
200	25	8	4	13.82
250	25	8	4	13.26

Power limits obtained from a wide range of additional scenarios were computed using the randomly distributed base station method. The results are shown in Table 5-8. Note that some of the limits in this table are much lower than the 10 dBW limit recommended in this section. All limits below 10 dBW were computed using an aircraft to tower distance of only 100 ft. instead of the cylinder radius of 250 ft. used in Table 5-5. Further, the values in this table were read from the minimum points along a series of curves, so the aircraft height and EIRP values do not have the same high precision as the results reported in the other tables.

Table 5-8: Hexagonal Grid Scenario Based Limits from Randomly Located Base Station Method

Aircraft Lateral Separation Distance to Center Tower (ft.)	Flight Attitude	Center Tower Height (m)	Aircraft Antenna Height (m)	Mean Power Based EIRP Limit (dBW)	Tower Antenna Downtilt (deg)
250	Level	10	7.5	17.6	2
250	Level	15	12	14.8	2
250	Level	20	10	12.6	8
250	Level	25	12.25	14	8
100	Level	10	6	5	8
100	Level	15	14	6	2
100	Level	20	16	4	8
100	Level	25	20	4	8
250	Banking	10	8	14	2
250	Banking	15	12 to 16	12	2
250	Banking	20	14 to 16	11.5	4
250	Banking	25	20	10.4	4
100	Banking	10	8	2.8	4
100	Banking	15	14	2.5	2
100	Banking	20	16	2.6	8
100	Banking	25	24	2	2

5.2.3.7 Frequency Dependencies

Using the slope of the spectrum mask of Figure 5-2 allows an EIRP transmit power limit computed at one frequency to be converted to an equivalent limit at a different frequency. For example, the spectrum mask shows the permissible interference level decreasing from -12.0 dBm at 1525.0 MHz to -103.267 dBm at 1559.0 MHz, a slope of -2.68432 dB/MHz. It then follows that a transmit limit such as 10 dBW at 1531 MHz corresponds to a limit of -16.84 dBW at 1541 (i.e., 10 dBW + (-2.68432 x (1541 – 1531) dB)) and a limit of -43.69 dBW at 1551 MHz (i.e., 10 dBW + (-2.68432 x (1551 – 1531) dB)). These examples apply for frequencies between 1525 MHz and 1565 MHz where the slope of the spectrum mask is the same.

5.2.3.8 Sensitivity Analysis Results

The HTAWS case presents the most restrictive limits so solution sensitivities to various parameters are best demonstrated using examples from this case. An important interplay between the parameters focuses on placing the aircraft in the center of the main lobe of the RFI emitter antenna beam. The relationship of the aircraft and the emitter main lobe varies with both antenna heights, the degree of the emitter antenna down tilt and the distance between the antennas. Banking (vs. level flight) also has a significant impact because the aircraft antenna gains vary with elevation angle and banking changes the effective elevation angle. Sloping (vs. flat) ground has a noticeable impact because the Hata path loss model contains a slope dependent parameter and the total height of all towers, except the central one, increases with radius. The computed limit is also sensitive to the emitter polarization because, at some elevations, the aircraft antenna gains are larger for vertically than for horizontally polarized signals. All analyses in this Report assume either vertically polarized radio waves or an equal power combination of vertically and horizontally polarized waves (i.e., dual polarization).
The parameters varied during the HTAWS case study are listed below and after each parameter type the range of values explored are listed in parentheses. The computed maximum limit is sensitive to the following parameters and the interplay between these parameters:

- The heights of the emitter (10, 15, 20, 25 meters) and aircraft antennas (4 to 35 meters)
- The down tilt angle of the emitter antenna (2, 4, 6, 8 degrees)
- The ground distance between the two antennas (100 feet vs. 250 feet and vicinity)
- Flat ground vs. Sloping ground (upward with a 10 milliradian slope)
- Level flight vs. banking (at 25 degrees)
- Vertical vs. dual polarization (equal power vertical and horizontal polarization)

Figure 5-10, Figure 5-12, and Figure 5-14 depict how a computed mean based limit is sensitive to various parameter changes. Figure 5-11, Figure 5-13, and Figure 5-15 show the corresponding “1-CDF” (i.e., “1-P(z)”) curve based on parameter set of the most restrictive mean based limit of the preceding figure. Each of these three mean based limit figures contains four curves with different amounts of antenna down tilt. Each abscissa varies the aircraft (AC) antenna height and the ordinate displays the resultant limit values. Figure 5-10, Figure 5-12, and Figure 5-14 show an ordered pair of numbers for the abscissa and ordinate values that correspond to the most restrictive mean based limit. All these figures used an assessment zone radius of 250 feet. Calculations were also performed for a standoff radius of 100 feet, which results in lower limits (not shown). Figure 5-10 and Figure 5-12, are for dual polarization while Figure 5-14 is for vertical polarization. Figure 5-10 uses a 20 m height emitter while Figure 5-12 uses a 10 m height emitter and Figure 5-14 uses a 25 m height. Figure 5-10 shows a limit of 9.948 dBW, the lowest mean based limit computed with dual polarization. The corresponding rare event based limit is 9.869 dBW, as computed with Equation 5.3-2 using the Zcrit value of 2.558 taken from Figure 5-11.

Figure 5-14 presents an even lower mean based limit of 7.945 dBW with vertical polarization only. The corresponding rare event based limit computed with Equation 5.3-2 using the Zcrit value of 2.530 from Figure 5-15 is slightly lower at 7.9138 dBW. Thus Figure 5-14 and Figure 5-15 demonstrate the importance of wave polarization type on the computed limit.
The rare event limit of 9.869 dBW for dual polarization is lowest limit computed at the 250 ft. (76.2 m) assessment zone radius. The one single limit value of 9.8 dBW cited in this Report is derived from rounding down the computed result. This rounding allows for the additional effect of a random distribution of base station emitters, as in [10] Section.3.5.2, that extends beyond the central hexagonal grid sources out to the radio horizon at a decreasing surface concentration. It is very important to note that this result assumes (equal power split) dual polarization and highlights that a requirement for cross-polarization emissions from the base stations must be captured in any license application or issuance. A vertical polarization (only) based limit must be significantly lower than 9.8 dBW.

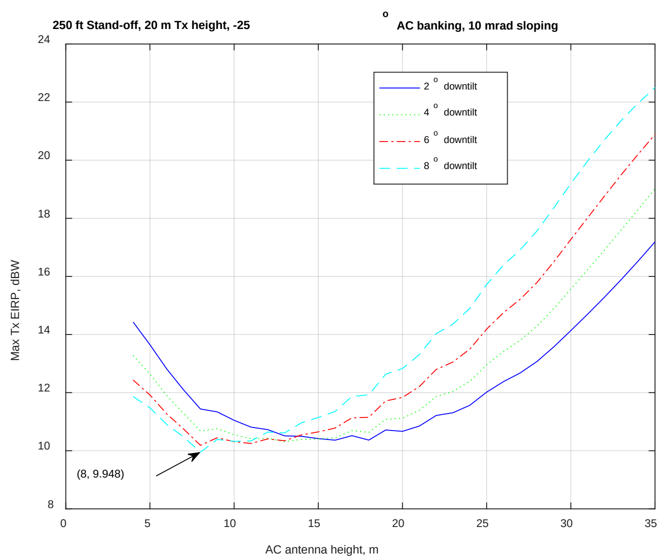

Figure 5-10: HTAWS Dual Polarization 20 m Emitter Antenna-Mean Limits

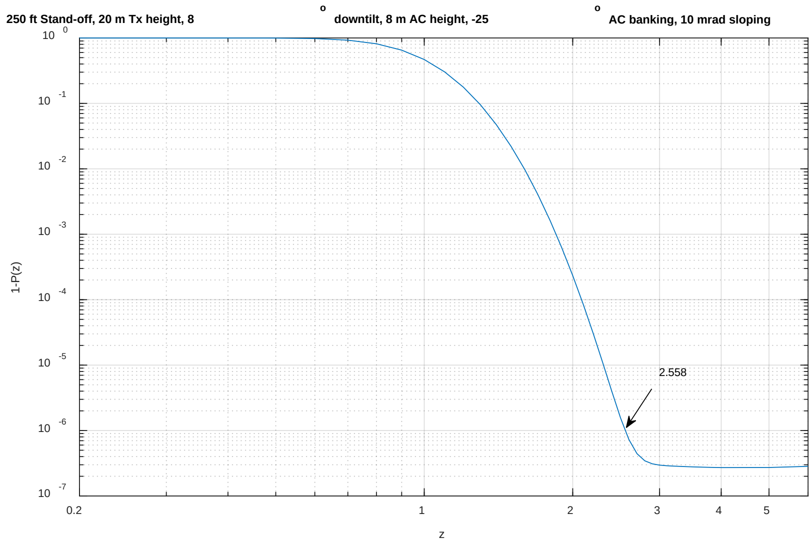

Figure 5-11: (1-CDF) for Most Restrictive Mean Limit Condition of Figure 5-10

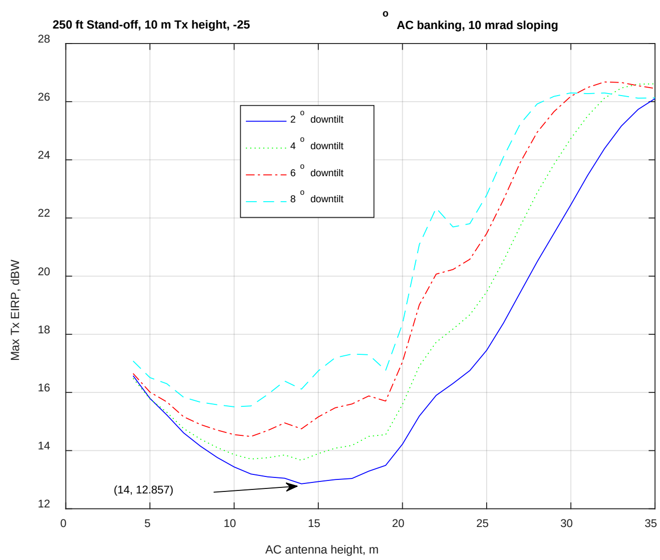

Figure 5-12: HTAWS Dual Polarization 10 m Emitter Antenna-Mean Limits

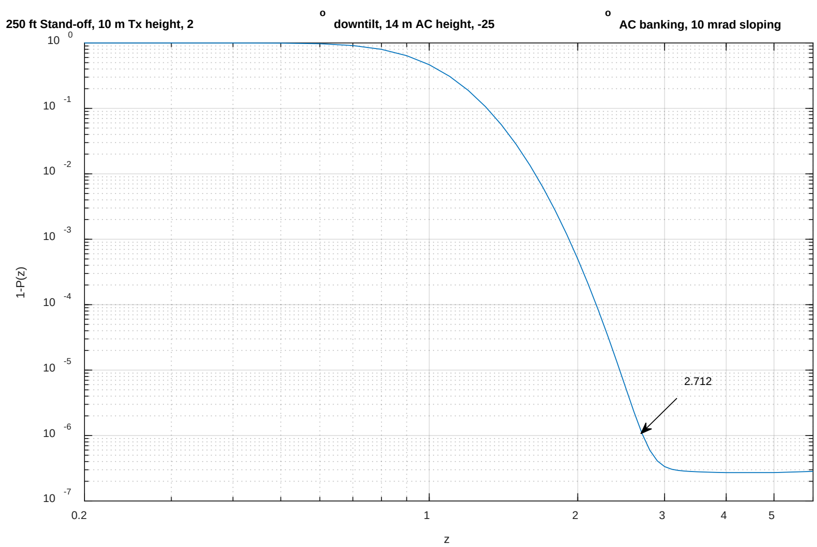

Figure 5-13: (1-CDF) for Most Restrictive Mean Limit Condition of Figure 5-12

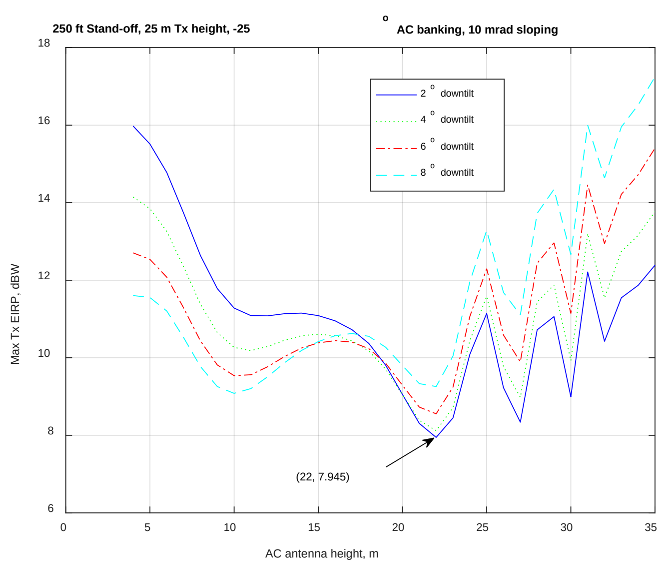

Figure 5-14: HTAWS Vertical Polarization 25 m Emitter Antenna-Mean Limits

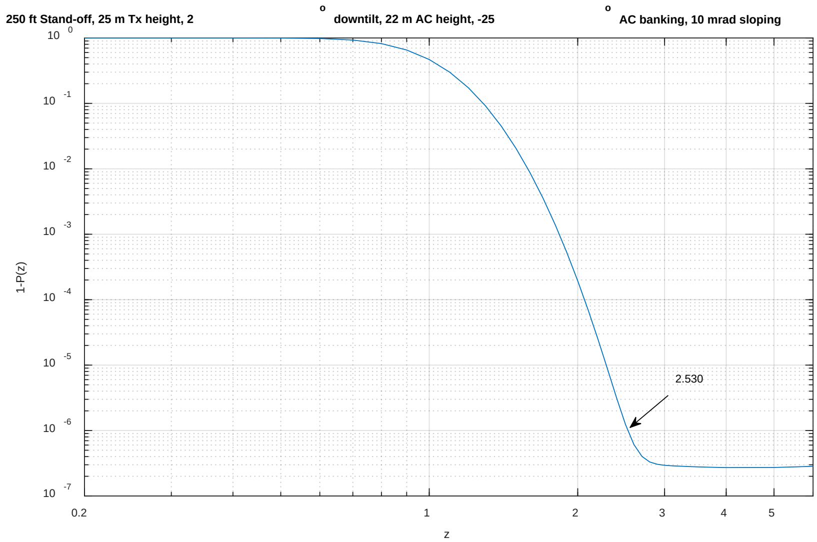

Figure 5-15: (1-CDF) for-Most Restrictive Mean Limit Condition of Figure 5-14

5.2.3.9 Certified Aviation Receiver Analysis Results Summary

RFI degradation calculations for a variety of scenarios have been performed by the FAA in order to determine a maximum tolerable power transmission level for usage of frequencies near the GPS L1 band. All analyses were conducted in accordance with the procedures recommended in the applicable RTCA [10] and FAA Technical Center [8] reports with the procedures refined when necessary. A summary of these results from the performed analyses is provided in Table 5-9.

The "Handset" cases assessed showed these do not present a limiting case or scenario for certified aviation receivers. The "Ground Station" analyses computed aggregate RFI power assuming an aircraft was located at the WIRSO waypoint in Washington, DC (i.e., near Reagan National airport over the Potomac River). This analysis used a realistic set of 1,068 towers as well as extensive modeling of the surrounding terrain so that the impact of slope on the Hata-Okumura path loss model could be ascertained. The "HTAWS" analyses assumed towers are deployed in a symmetrical hexagonal grid pattern with the aircraft located 76.2 meters (i.e., 250 feet) from the central tower. Terrain modelling for this analysis assumed either flat ground or an idealized symmetrical funnel shaped terrain with a slope of 10 milliradians in all directions.

Different transmit antenna patterns were used by the Ground Station and HTAWS analyses. In addition to tower deployment, terrain modeling and transmit antenna patterns, another major difference between these two analyses is signal polarization. As recommended in [10], the Ground Station analysis set assumed all radio transmissions were vertically polarized only.

However, to evaluate the HTAWS case, the FAA RFI analysis methodology evaluated vertical polarization only, as well as dual polarization consisting of equal power vertical and horizontal polarized transmissions. The issue of radio polarization type is significant because the aircraft GPS antenna gain varies according to signal elevation and polarization. The Ground Stations analysis simulated the RFI encountered by an aircraft at an altitude of 125.64 m at an actual waypoint over the Potomac River found an EIRP limit of 28.9 dBW. The HTAWS analysis simulated a helicopter flying within 76.2 meters of a cellular system tower of a hexagonal grid system dictates a significantly lower limit of 9.8 dBW.

The two cases yielded such different limits due to differences in the lateral separation distance from the aircraft to the closest tower. The distance from aircraft nadir to the closest tower base for the WIRSO scenario is a relatively large 1,396 m while the minimum separation distance in the hexagonal grid scenario is 76.2 m. Assuming for a moment a simple free space path loss model, this difference in separation distance would result in a 25 dB difference in path loss to the closest tower. The actual delta path loss to the closest tower between the two analyses is larger because 76.2 m is within the zone of a two-ray path loss model but no tower in the WIRSO scenario was within the two-ray zone. In all the hexagonal grid scenarios examined the central tower provided at least 90% of the scenario total aggregate RFI power (in some scenarios much more). Further, the hexagonal grid scenario with an Inter-Station Distance (ISD) of 433 m had 37 towers within 1,396 m, and even a grid with an ISD of 633 m has 14 towers inside the radius of the closest WIRSO tower. Though the evaluation of the RFI at other waypoints was suggested by the RTCA document [10], it is unlikely that these would include an aircraft flying within 76.2 meters of a tower.

These analyses indicate that protection of certified avionics, operating under the assumption of the described 250 foot (76.2 m) radius assessment zone, requires that the Ground Station transmission EIRP not exceed 9.8 dBW (cross-polarized) at 1531 MHz. This limit is obtained from the HTAWS scenario which was found to be the most restrictive of the scenarios examined. The limit from the Discrete Tower scenario at the WIRSO waypoint was found to be 28.9 dBW with considerably larger Ground Station ISD. Limit values at other frequencies can be computed as described in section 5.2.3.7 using the spectral mask slope of Figure 5-2.

Table 5-9: Summary of Scenarios and Findings

Scenario	Conditions	Comments
Inflight Aircraft / Ground-based Handset	Final Approach Fix & Waypoint, Cat. I & Cat. II Decision Height	Cat. II determined as most stringent case; Assessed, <6% threshold increase, not deemed a critical or limiting scenario (see 5.2.3.2)
Inflight Aircraft / Ground Base Station	Random and discrete tower locations, Aircraft level & banking	Assessed 1531 MHz at WIRSO location 125.64 m altitude. Differences between 0^{o} , 25^{o} attitude as well as rare event attributed to tower distributions (see 5.2.3.3)
Inflight Aircraft / Onboard Handset	Aircraft at 10K ft. altitude	Assessment premised on handset exhibiting characteristics of WiFi at 2.45 GHz, no further assessment required (see 5.2.1.3.1)
Aircraft on Ground / Onboard Handset	Aircraft antenna at 4 m	Assessed, not deemed a critical or limiting scenario (see 5.2.3.4)
Aircraft at Gate / Single Handset Source on or near Boarding Stairs or Jetway	0 dBW @ 1616 MHz	Assessed, 3.5 m minimum separation distance (see 5.2.1.4.1)
Aircraft at Gate/Users Inside Airport	Random distribution of thirty handsets	Assessed, not deemed critical or limiting scenario (see 5.2.3.5)
TAWS / HTAWS Scenarios with Ground-based Mobile Broadband Handsets	Three handset surface concentrations with -95 dBW/MHz in the GPS L1 receiver passband, Two aircraft antenna heights	Assessed, found fundamental emission effects insignificant, no further assessment required (see 5.2.1.2.1)
TAWS and HTAWS Scenarios with Broadband Base Station	Base stations located on a grid with 433 m or 693 m inter-station distance. Base station heights of 6, 10, 15 and 25 m were considered, with 2, 4, 6, and 8 degree antenna down tilt. Aircraft was assumed at the worst-case location on the assessment zone, both level flight and 25 degree bank toward the base station. Additional parameters including sloping ground were utilized as part of a sensitivity analysis as described in 5.2.3.8.	Fixed location base stations in hexagonal grid with 433 m and 693 m ISDs, flat earth and funnel terrain, aircraft lateral distances of 15.2-76.2 m, 25^{o} and 0^{o} banking. Both Monte Carlo and Analytic Statistical methods used for assessment (see 5.2.3.6) Assessment found HTAWS the most restrictive scenario (see 5.2.3.8)

6. SUMMARY

This report describes DOT's efforts to evaluate the adjacent band radiofrequency band power levels that can be tolerated by GPS and GNSS receivers. The assessment described in this report addresses transmitters in bands adjacent to the 1559-1610 MHz radionavigation satellite service (RNSS) band used for GPS L1 signals that are centered at 1575.42 MHz.

Results from GNSS receiver testing conducted in the ARL anechoic chamber facility at WSMR to assess their sensitivity to adjacent band interference in the range 1475 to 1675 MHz are presented in this report for the six categories of receivers tested. The radiated GNSS signals included GPS, SBAS, GLONASS, BeiDou, and Galileo signals. The radiated interference waveforms included 1 MHz AWGN and 10 MHz LTE signals (referred to as Type-1 and Type-2). The GNSS and interference signals were radiated through separate and collocated antennas as shown in the chamber layout diagram.

The collected test data capture the performance degradation of each device through the CNR which decreases as the interference power increases and the signal power stays fixed. In this report, the main analysis of GNSS receiver susceptibility to adjacent band interference refers to the interference power level at which the average CNR for a device drops by 1-dB from its baseline (interference-free) value. The resulting interference power level vs. interference frequency is referred to as the Interference Tolerance Mask for that device. The test data were also used for a secondary analysis of receiver susceptibility to determine the interference power level at which a receiver assembly loses signal tracking (referred to as Loss of Lock).

These bounding ITMs per receiver category and the GPS/GNSS antenna characteristics were the primary inputs to use case scenario assessments to determine the maximum Effective Isotropic Radiated Power that could be tolerated in the adjacent radiofrequency bands for each GPS/GNSS receiver category. Space-based applications are different from other GPS/GNSS applications considered, primarily due to the need to account for aggregation effects of multiple transmitters visible in orbit. Although OST-R derived ITMs for space-based receivers, along with other GPS/GNSS receiver types, OST-R deferred to NASA for assessing adjacent-band transmitter power levels that can be tolerated for this receiver category.

The L1 C/A bounding ITM is the lowest interference power at a given frequency that resulted in a 1 dB CNR reduction for at least one receiver in the category (for each receiver category). Most sensitive categories are the high precision and space-based receivers. The least sensitive category is the cellular category.

The Loss of Lock power levels for high elevation angle satellites (nominal signal power -128.5 dBm) were typically 15 – 25 dB higher than the ITM levels. The loss of Lock Interference power levels for low elevation angle satellites (signal power -138.5 dBm) were typically 5 – 15 dB higher than ITM levels as would be expected since the low elevation were emulated by a 10 dB reduced power levels from the nominal signal power to account for change of receiver antenna gain at low elevations.

During July 2016, 14 GNSS receivers were tested for further ABC assessment in a laboratory setting at Zeta Associates Inc. in Fairfax, VA. The test objectives were: (1) evaluation of the impact of adjacent-band interference on signal acquisition, (2) comparison between wired and radiated receiver susceptibility to adjacent band interference with 1 MHz bandpass noise and 10 MHz LTE, and (3) assessment of adjacent band transmitter OOBE impacts.

The ITMs from the wired test exhibited good agreement with the radiated results when the same active antenna was used or when the bypassed active antenna components were properly considered in the comparison. The wired test also showed that the FCC OOBE limits (base station and handset limits) have the potential to impact ITMs as does one entrants' proposed OOBE limits for handsets at separation distances less than 2 meters.

The results of these tests indicate that the 1-dB CNR degradation level is a good indicator of the region where acquisition starts to be impacted for some receivers. This is especially noticeable for the lower power GNSS signals emulating low elevation satellites or attenuated GNSS signal due to foliage or other environmental factor.

The approach to determine tolerable EIRP levels for a given standoff distance (inverse modeling), as well as the one to determine minimum standoff distance for a given EIRP value (forward modeling) were described in the approach section. Interference source (transmitter) characteristics were primarily obtained from M.2292 and proposals to FCC for adjacent band network applications.

Antenna Measurements for each one of the 22 frequencies used in the WSMR tests were done to determine the appropriate antenna pattern to use for each category of receivers. Parabolic fits to these measurements were ultimately used as inputs to the forward and inverse modeling calculations. The propagation loss was estimated through the Free-Space Path Loss model and the Two-ray model. Since the Irregular Terrain Model is expected to have the same properties as FSPL for distances up to 100 meters it is indirectly considered as part of the FSPL analysis.

Understanding GPS/GNSS receiver use cases scenarios are important so that the geometric parameters, specifically a receiver height and lateral offset from a transmitter can be determined. Also, it is important that use cases representative each receiver category and can provide a worst-case scenario so most, if not all, receivers in that category are protected. In addition, use cases are needed in conjunction with ITMs, propagations models, and transmitter scenarios to determine what power levels can be tolerated adjacent to GPS/GNSS signals.

Use cases were compiled through substantial outreach with DOT federal partners and agencies. Members of the working group were provided a template that contained questions related to how their organizations use GPS/GNSS receivers to support their mission. In particular, questions included identifying height, speed, terrain, antenna orientation and integration, and urbanization areas.

The use case analysis has shown that receiver heights extends to at and above the height of a base station in all categories and therefore the tolerable EIRP as a function of standoff distance can be found by taking the minimum along heights up to and above base station heights. The extent of the impact region for a high precision receiver is >10 km from the transmitter for an EIRP of 29 dBW and 1.8 km for EIRP of 10 dBW.

In the area of impact, the behavior of the GPS/GNSS receiver can become unreliable in its ability to meet the accuracy, availability, and integrity requirements of its intended function, impacting safety-critical applications such as transportation, the earthquake early warning system, and space-based missions using GPS/GNSS receivers, as well as high precision users such as precision agriculture, machine control, and surveying.

Tolerable EIRP levels to protect all tested receivers processing the L1 C/A signal are shown in at standoff distances of 10 and 100 meters for two different deployments. For L1 C/A signals and macro-urban networks, the tolerable EIRP decreases monotonically from about -24 dBW (4 mW) at 1475 MHz, to -42 dBW (< 0.1mW) at 1530 MHz, to -62 dBW (<1 μW) at 1550 MHz; for micro-urban networks the results increase by a fraction of a dB. For all GNSS signals, the above values decrease by a few dB.

For certified GPS avionics, the FAA analyzed a number of scenarios including:

1) Inflight Aircraft with a Ground-based Handset
2) Inflight Aircraft with a Ground Base Station
3) Inflight Aircraft with an Onboard Handset
4) Aircraft on the ground with an Onboard Handset
5) Aircraft at Gate / Single Handset Source on or near Boarding Stairs or Jetway
6) Aircraft at Gate/Users Inside Airport
7) Terrain Awareness Warning System (TAWS) / Helicopter TAWS (HTAWS) Scenarios with Ground-based Mobile Broadband Handsets
8) TAWS and HTAWS Scenarios with Broadband Base Station

The analysis is based on the concept of an "assessment zone" inside of which GPS performance may be compromised or unavailable. In this region GPS based instrument flight rules (IFR) operations will be restricted due to the elevated levels of RFI. Different transmit antenna patterns were used by the Ground Station and HTAWS analyses. In addition to tower deployment, terrain modeling and transmit antenna patterns, another major difference between these two analyses is signal polarization. The Ground Station analysis set assumed all radio transmissions were vertically polarized only. However, to evaluate the HTAWS case, the FAA RFI analysis methodology evaluated vertical polarization only, as well as dual polarization consisting of equal power vertical and horizontal polarized transmissions.

The issue of radio polarization type is significant because the aircraft GPS antenna gain varies according to signal elevation and polarization. The Ground Stations analysis simulated the RFI encountered by an aircraft at an altitude of 125.64 m at an actual waypoint over the Potomac River found an EIRP limit of 28.9 dBW. The Helicopter Terrain Awareness Warning System (HTAWS) analysis simulated a helicopter flying within 76.2 meters of a cellular system tower of a hexagonal grid system dictates a significantly lower limit of 9.8 dBW. A very important difference between the two case analyses is simply the lateral separation distance from the aircraft to the closest tower. The distance from aircraft nadir to the closest tower base for the WIRSO scenario is a relatively large 1,396 m while the minimum separation distance in the hexagonal grid scenario is 76.2 m.

This limit is obtained from the HTAWS scenario which was found to be the most restrictive of the certified aviation scenarios examined. The FAA analysis of certified aviation indicate that protection of certified avionics, operating under the assumption of the described 250 foot (76.2 m) radius assessment zone, requires that the ground station transmission not exceed 9.8 dBW (10W) (cross-polarized) at 1531 MHz. Based on the results of the OST-R testing and analysis of the other categories of receivers, the transmitter power level that can be tolerated by certified aviation may cause interference with, or degradation to, most other categories of GPS/GNSS receivers including those used for General Aviation and drones.

ACRONYM LIST

ABAS	Aircraft-Based Augmentation System
ABC	Adjacent Band Compatibility
AC	Aircraft
ACLR	Adjacent Channel Leakage Ratio
ADS-B	Automatic Dependent Surveillance-Broadcast
AF	Aggregate Factor
AFSS	Autonomous Flight Safety System
AFTS	Automated Flight Termination System
AFTU	Automated Flight Termination Unit
AGL	Above Ground Level
AHRS	Attitude and Heading Reference System
ARL	Army Research Laboratory
ATC	Ancillary Terrestrial Component
ATIS	Alliance for Telecommunications Industry Solutions
AWGN	Additive White Gaussian Noise
AZ	Azimuth
CAR	Certified Aviation Receiver
CAT	Category
CDF	Cumulative Distribution Function
CEL	Cellular
CNR	Carrier-to-Noise density Ratio
COSMIC	Constellation Observing System for Meteorology, Ionosphere and Climate
CR	Cell Radius
CSV	Comma Separated Variable
CW	Continuous Wave
CYGNSS	Cyclone Global Navigation Satellite System
dB	decibel
dBi	decibel isotropic
dBic	decibel isotropic circular
dBm	decibel-milliwatt
dBW	decibel-watt
DORIS	Doppler Orbitography by Radiopositioning Integrated on Satellite
DOT	U.S. Department of Transportation
DUT	Device Under Test
DSAC	Deep Space Atomic Clock
EDP	Electron Density Profile
EIRP	Effective Isotropic Radiated Power
EL	Elevation
BS	Base station
ETSO	European Technical Standard Order
EMVAF	Electromagnetic Vulnerability Assessment Facility
FAA	Federal Aviation Administration

FAF	Final Approach Fix
FCC	Federal Communications Commission
FMS	Flight Management System
FSPL	Free-Space Path Loss
GAV	General Aviation
GBAS	Ground-Based Augmentation System
GEO	Geostationary
GHz	gigahertz
GLN	General Location and Navigation
GM	General Motors
GNSS	Global Navigation Satellite System
GNSS-R	GNSS Reflectometry
GPS	Global Positioning System
GRACE	Gravity Recovery and Climate Experiment
GUST	Geostationary Uplink System Type-1
HITL	Human-in-the-Loop
HPA	High Power amplifier
HPOL	Horizontal Polarization
HPR	High-Precision Receiver
HTAWS	Helicopter Terrain Awareness Warning System
Hz	hertz
ICAO	International Civil Aviation Organization
ICD	Interface Control Document
IFR	Instrument Flight Rules
IGOR	Integrated GPS Occultation Receiver
IMT	International Mobile Telecommunication
IP	Interference Power
IPC	Interference Protection Criteria
ISD	Inter-Site Distance
ISS	International Space Station
ITM	Interference Tolerance Mask
ITU-R	International Telecommunications Union Radiocommunication Sector
JPL	Jet Propulsion Laboratory
K	kelvin
kHz	kilohertz
km	kilometer
KPI	Key Performance Indicator
L1 C/A	GPS L1 Course Acquisition
LEO	Low Earth Orbit
LNA	Low Noise Amplifier
LOL	Loss of Lock
LPV	Localizer Performance with Vertical Guidance
LTE	Long Term Evolution
m	meter
M&S	Modeling and Simulation
MATLAB	Matrix Laboratory

MHz	megahertz
MOPS	Minimum Operational Performance Standard
MSL	Mean Sea Level
MSS	Mobile Satellite Service
mW	milliwatt
NaN	Not a Number
NAS	National Airspace System
NASA	National Aeronautics and Space Administration
NC	Not Computed
NCO	National Space-Based PNT Coordination Office
NDA	Non-Disclosure Agreement
NET	Networks
NI	National Instruments
NISAR	NASA-ISRO Synthetic Aperture Radar
NMEA	National Maritime Electronics Association
NOAA	National Oceanic and Atmospheric Administration
NTIA	National Telecommunications and Information Administration
OFDM	Orthogonal Frequency Division Multiplexing
OOBE	Out of Band Emissions
OST-R	DOT Office of the Assistant Secretary for Research and Technology
PBN	Performance-Based Navigation
PF	Power Factor
POD	Precise Orbit Determination
Pos/Nav	Positioning/Navigation
PRN	Pseudorandom Noise
PSD	Power Spectral Density
QZSS	Quazi-Zenith Satellite Service System
RAID	Redundant Array of Independent Disks
RAIM	Receiver Autonomous Integrity Monitoring
RAM	Radiant Absorbent Material
RF	Radiofrequency
RFI	Radiofrequency Interference
RHCP	Right-Hand Circular Polarization
RINEX	Receiver Independent Exchange
RNAV	Area Navigation
RNSS	Radionavigation Satellite Service
RO	Radio Occultation
RTCA	Formerly Radio Technical Commission for Aeronautics (now RTCA, Inc)
Rx	Receiver
SARPS	Standards and Recommended Practices
SBAS	Satellite-Based Augmentation System
SC-OFDM	Sub-Carrier Orthogonal Frequency Division Multiplexing
SNR	Signal-to-Noise Ratio
SPB	Space-Based
SPIGAT	Software Programmable Interference Generator for ABC Testing
SWO	Space Weather Observation

SWOT	Surface Water and Ocean Topography
TAWS	Terrain Awareness Warning System
TEC	Total Electron Content
TIM	Timing
TSO	Technical Standard Order
Tx	Transmitter
μW	microwatt
UAS	Unmanned Aircraft System
USCG	U.S. Coast Guard
USG	U.S. Government
USGS	U.S. Geological Survey
VPOL	Vertical Polarization
VSG	Vector Signal Generator
WAAS	Wide Area Augmentation System
WGS	World Geodetic System
WP	Waypoint
WSMR	White Sands Missile Range

REFERENCES

[1] DOT GPS Adjacent Band Compatibility Assessment Plan December 2012.

[2] U.S. Air Force Background Paper on Use of 1-dB Decrease in C/No As GPS Interference Protection Criterion June 2017.

[3] ITU-R Report M.2292: Characteristics of Terrestrial IMT-Advanced systems for frequency sharing/interference Analyses.

[4] ITU Report ITU-R SA.2325-0: Sharing between space-to-space links in space research, space orientation and Earth exploration-satellite services and IMT systems in the frequency bands 2025-2110 MHz and 2200-2290 MHz.

[5] ICAO SARPs Annex 10 Volume I Appendix B.

[6] Report of the Tactical Operations Committee in Response to Tasking from the Federal Aviation Administration, December 2016.

[7] Status Report: Assessment of Compatibility of Planned LightSquared Ancillary Terrestrial Component Transmissions in the 1526-1536 MHz Band with Certified Aviation GPS Receivers, FAA Report PR 25, January 25, 2012.

[8] Final Report: A Generalized Statistical Model for Aggregate Radio Frequency Interference to Airborne GPS Receivers from Ground Based Emitters (DOT/FAA/TC-14/30, Rev. 1), August 7, 2017.

[9] Minimum Operational Performance Standards for GPS/Wide Area Augmentation System Airborne Equipment, RTCA/DO-229.

[10] FAA GPS Adjacent-Band Compatibility Study Methodology and Assumptions with RTCA SC-159 mark-ups, RTCA Paper No. 095-15/SC159-1040.

[11] Final Report: A Generalized Statistical Model for Aggregate Radio Frequency Interference to Airborne GPS Receivers from Ground Based Emitters (DOT/FAA/TC-14/30), September. 30, 2014.

[12] FAA GPS Adjacent-Band Compatibility Study Methodology and Assumptions with RTCA SC-159 mark-ups, RTCA Paper No. 095-15/SC159-1040.

[13] Global Positioning System Wide Area Augmentation System (WAAS) Performance Standard, October 31, 2008.

ACKNOWLEDGEMENTS

The authors would like to thank the following organizations for their contribution to the success of the testing and data collection efforts:

Aerospace Corporation
Army Research Laboratory (ARL), Electromagnetic Vulnerability Assessment Facility (EMVAF)
Federal Aviation Administration (FAA)
Federal Communication Commission (FCC)
General Motors (GM)
John Deere
MIT Lincoln Laboratory (MITLL)
MITRE Corporation
National Aeronautics and Space Administration (NASA)
National Oceanic and Atmospheric Administration (NOAA)
National Telecommunications and Information Administration (NTIA)
NovAtel
Trimble
U-Blox
UNAVCO
United States Air Force (USAF)
United States Coast Guard (USCG)
United States Geological Survey (USGS)
Zeta Associates